NUMERICAL STUDY ON INERTIAL MIGRATION OF PARTICLES IN MICROCHANNELS

Thesis

Submitted in partial fulfilment of the requirements for the degree of

DOCTOR OF PHILOSOPHY

By

NEERAJ M P

DEPARTMENT OF MECHANICAL ENGINEERING
NATIONAL INSTITUTE OF TECHNOLOGY KARNATAKA
SURATHKAL, MANGALORE-575 025, INDIA

January 2024

NUMERICAL STUDY ON INERTIAL MIGRATION OF PARTICLES IN MICROCHANNELS

Thesis

Submitted in partial fulfilment of the requirements for the

degree of

DOCTOR OF PHILOSOPHY

By

NEERAJ M P

DEPARTMENT OF MECHANICAL ENGINEERING
NATIONAL INSTITUTE OF TECHNOLOGY KARNATAKA
SURATHKAL, MANGALORE-575 025, INDIA

January 2024

Dedicated to my dear parents,
grandparents, family, teachers and friends
who stood by me at all my hard times

DECLARATION

I hereby declare that the Research Thesis entitled "**Numerical Study on Inertial Migration of Particles in Microchannels**" which is being submitted to the National Institute of Technology Karnataka, Surathkal in partial fulfillment of the requirements for the award of the Degree of Doctor of Philosophy in Mechanical Engineering is a bonafide report of the research work carried out by me. The material contained in this Research Thesis has not been submitted to any other Universities or Institutes for the award of any degree.

Register Number: 187102ME010

Name of the Research Scholar: NEERAJ M P

Signature of the Research Scholar:

Department of Mechanical Engineering
Place: NITK-Surathkal
Date:

CERTIFICATE

This is to certify that the Research Thesis entitled "**Numerical Study on Inertial Migration of Particles in Microchannels**" submitted by Mr. Neeraj M P (Register Number: 187102ME010) as the record of the research work carried out by him, is accepted as the Research Thesis submission in partial fulfilment of the requirements for the award of the Degree of Doctor of Philosophy.

Dr. RANJITH M
Research Guide

Chairman-DRPC
Date: 15.1.2024

राष्ट्रीय प्रौद्योगिकी संस्थान, कर्नाटक
यांत्रिकी अभियांत्रिकी विभाग
Dept. of Mechanical Engineering
National Institute of Technology

ACKNOWLEDGEMENT

It gives me immense pleasure to thank all the people who have helped, motivated and stood with me during my Ph.D. journey at NITK Surathkal. First of all, I would bestow sincere thanks to my guide **Dr. Ranjith M**, Assistant Professor, Mechanical Engineering Department, National Institute of Technology Karnataka, Surathkal, Mangalore for his decisions and advices that has motivated and led me to the right path.

I would also like to thank RPAC members, **Dr. Parthasarathy P**, Assistant Professor, Department of Mechanical Engineering and **Dr. Krishnan C.M.C**, Assistant Professor, Department of Electrical and Electronics Engineering, and **Dr. Anish S**, Associate Professor, Department of Mechanical Engineering, National Institute of Technology Karnataka, Surathkal, Mangalore for providing valuable suggestions and extending support to me on aspects of completing this work.

I wish to express my sincere thanks to **Prof. Ravikiran Kadoli**, Professor and Head of the Department, Department of Mechanical Engineering, National Institute of Technology Karnataka, Surathkal, Mangalore for their help in providing the facilities. I would also express my deepest gratitude to **Prof. Narendranath S** and **Prof. Shrikantha S Rao**, Department of Mechanical Engineering, National Institute of Technology Karnataka, Surathkal, Mangalore for providing the necessary support.

I would like to express my deepest feelings for my parents **Bhavadasan M P** and **Mini K S**, who were always there for me. Whatever I have done so far is all because of them. Their belief in me to excel was the driving force for me to go ahead and face challenges. Life would have not been as adventurous and interesting without friends. I would like to thank all of my friends for their immense support. Last but not the least, I thank God for showering blessing on me and for giving me such a wonderful family and friends.

ABSTRACT

Inertial migration has emerged as an interesting area of study in the area of biofluid dynamics. The particles in fluid flow move towards the wall and attain equilibrium position due to this phenomenon. This technique can help in particle separation which is highly important in biomedical engineering. Numerical study on inertial migration of non-spherical particles is a class of problem which belongs to fluid-structure interaction. Development of good numerical model to study the inertial migration will be of keen interest.

The inertial migration of neutrally and non-neutrally buoyant non-spherical particles is studied with the aid of feedback forcing based immersed boundary method. The inertial migration of neutrally buoyant cylindrical particle in both Poiseuille and shear flow in straight channel are analysed first in this work. Inertial migration is characterised by equilibrium position and migration time. Particle is observed to attain equilibrium position close to 0.6 times half the channel height in case of Poiseuille flow while equilibrium position is attained at channel centre in shear flow. To understand the dependence of inertial migration dynamics on Reynolds number, particle diameter, channel height and initial position, detailed parametric study is carried out. It is observed that equilibrium position moves to lower wall with increase in Reynolds number and channel height and reduction in particle diameter in Poiseuille flow. However, it is only get affected by channel height and shear rate (shift towards channel centre) in case of shear flow. Equilibrium position stay unaffected with initial position in both flow cases. On the other hand, migration time reduces with increase in Reynolds number and particle diameter and reduction in channel height in case of Poiseuille flow. The same phenomena happen in case of shear flow except migration time increases with particle diameter rise. In the following stage, inertial migration in various non-straight channels such as backward facing stepped, stepped and constricted channel are investigated. The presence of recirculation zones in these types of channels can make significant changes in inertial migration dynamics. Equilibrium position shifts towards channel centre with increase in Reynolds number, particle diameter and blockage ratio (ratio of step height to channel height) in case of backward facing stepped channel. In case of stepped channel, equilibrium position is driven towards lower wall with increase

in depth of step whereas it remains unchanged with variation in length of step. When particle migration in constricted channel comes into picture, it is noticed that equilibrium position is unaffected by Reynolds number and constriction clearance and only slightly influenced by particle diameter. Out of all non-straight channels a common behaviour observed is that equilibrium position shifts with respect to initial position of release. Moving on, inertial migration dynamics in straight, backward facing stepped and constricted channel is compared and it is concluded that constricted channel is better for separation since equilibrium position is more predictable in the same compared to other channel configurations. Motivated by the parametric study results, artificial neural network algorithm is utilised to create a prediction model for predicting equilibrium position, and migration time of particle in both straight and constricted channel.

Mass and shape of particle is another two properties which can play important part in inertial migration dynamics. Hence, in the following stage, lateral migration of various shaped particles such as circular, elliptical, square, rectangular and biconcave is addressed. It is observed that biconcave particle has equilibrium position closest to lower wall. The simulations are repeated for non-neutrally buoyant particles and it is observed that equilibrium position shifts towards lower wall when buoyancy force is taken into consideration.

The model is further extended to analyse the effect of application of control force to alter the equilibrium position to centre of channel in both Poiseuille and pulsatile flows. The control force in both flows is applied in such a way that particle equilibrium position is moved to centre of channel. Magnitude of control force increases with rise in Reynolds number and reduction in particle diameter in both flow cases. However, when density ratio (particle to fluid) is increased, magnitude of control force initially rises and then reduces in both flow cases. In case of pulsatile flow, frequency of oscillation is also taken into consideration for parametric study. Control force magnitude increases with frequency of oscillation. Gaining inspiration from the parametric study results, suitable correlations are proposed for control force with the aid of linear regression algorithm in both flow cases. It is concluded that, the control of

equilibrium position with application of external force can make significant advance in particle separation technology.

The current computational model is then utilised to simulate inertial migration of multiple particles in straight, stepped and slit channels. Two particle migration in straight channel is analysed first, and it is found that equilibrium positions of both particles come closer to channel centre compared to that in single particle migration. This may be due to the reverse lift force created by secondary flow vortices interaction between the particles. This interaction can reduce with increase in initial centre-to-centre distance and hence reduce migration time since time required for balancing of lifts decreases. The effect of initial orientation (horizontal, vertical and offset) is also studied and it is observed that migration time is higher for particle 2 in offset condition since it is released closer to channel centre. In the following stage, two particle migration in a stepped channel is simulated and the effect of density ratio and depth of step is studied. Equilibrium position is driven to lower wall first and then towards channel centre with increase in density ratio which can be due to the action of Saffman lift force. However, the strength of secondary flow vortices increases with depth of step and hence, equilibrium position shifts towards lower wall with it. In final step, migration of three particles in a slit channel is studied. It seems that equilibrium position stays constant with all parameters such as slit clearance, slit angle and initial orientation and only changes with initial position. The residence time increases with slit clearance and it is highest for a slit angle of $\pi/2$. For triangular orientation case, equilibrium position of particle 2 changes since its initial position is away from channel centre.

Keywords: Control force, Equilibrium position, Immersed boundary method, Inertial migration, Feedback forcing scheme, Migration time

TABLE OF CONTENTS

DECLARATION i

CERTIFICATE iii

ACKNOWLEDGEMENT v

ABSTRACT vii

TABLE OF CONTENTS xi

LIST OF FIGURES xv

LIST OF TABLES xxv

NOMENCLATURE xxvii

ABBREVIATIONS xxxi

CHAPTER 1. INTRODUCTION 1

1.1 Inertial migration 1

1.2 Immersed boundary method 5

1.3 Feedback forcing scheme-based IBM 6

1.4 Artificial neural network (ANN) 7

1.5 Linear regression (LR) 8

1.6 Outline of the thesis 8

CHAPTER 2. LITERATURE REVIEW 11

2.1 Theoretical studies 11

2.2 Experimental studies 12

2.3 Computational studies 13

2.3.1 Immersed boundary method 14

2.4 Research gap and critical review 16

2.5 Objectives 18

CHAPTER 3. INERTIAL MIGRATION OF PARTICLE IN STRAIGHT CHANNEL 19

3.1 Background 19

3.2 Methodology 21

3.3 Results and discussion 25

3.3.1 Migration of particle in Poiseuille flow 25
3.3.1.1 Effect of Re 30
3.3.1.2 Effect of initial position 31
3.3.1.3 Effect of diameter of particle 32
3.3.1.4 Effect of height of channel 33
3.3.2 Migration of particle in shear flow 34
3.3.2.1 Effect of Re 35
3.3.2.2 Effect of initial position 37
3.3.2.3 Effect of diameter 38
3.3.2.4 Effect of height of channel 39
3.3.2.5 Effect of shear rate 40
3.3.3 Comparison between the migration of particle in Poiseuille flow and shear flow 42
3.3.4 Artificial Neural Network (ANN) prediction model for inertial migration in Poiseuille flow in straight channel 43
CHAPTER 4. INERTIAL MIGRATION OF PARTICLE IN NON-STRAIGHT CHANNELS 47
4.1 Background 47
4.2 Methodology 48
4.3 Results and discussion 49
4.3.1 Migration of particle in backward facing stepped channel 49
4.3.1.1 Influence of Re 51
4.3.1.2 Influence of initial position 52
4.3.1.3 Influence of diameter 53
4.3.1.4 Influence of blockage ratio 54
4.3.2 Migration of particle in stepped channel 55
4.3.2.1 Effect of initial position 57
4.3.2.2 Effect of H_S 57
4.3.2.3 Effect of L_S 58
4.3.3 Migration of particle in constricted channel 59
4.3.3.1 Dependence of inertial migration dynamics on Re 65

4.3.3.2 Dependence of initial position 68
4.3.3.3 Dependence of diameter 69
4.3.3.4 Dependence of constriction clearance 71
4.3.3.5 Prediction model development for inertial migration in constricted channel 74
4.3.3.6 Critical Reynolds number 76
4.3.4 Comparison of inertial migration dynamics in different channel configurations 80
CHAPTER 5. INERTIAL MIGRATION OF VARIOUS SHAPED PARTICLES 83
5.1 Background 83
5.2 Methodology 84
5.3 Results and discussion 84
5.3.1 Migration of neutrally buoyant particle 85
5.3.2 Migration of non-neutrally buoyant particle 89
CHAPTER 6. CONTROL FORCE AND INERTIAL MIGRATION IN POISEUILLE AND PULSATILE FLOWS 91
6.1 Background 91
6.2 Methodology 92
6.3 Results and discussion 93
6.3.1 Control force in Poiseuille flow 93
6.3.1.1 Control force and Reynolds number 97
6.3.1.2 Control force and particle diameter 99
6.3.1.3 Control force and density ratio 102
6.3.1.4 Development of prediction model for control force in Poiseuille flow 105
6.3.2 Control force in pulsatile flow 107
6.3.2.1. Effect of Reynolds number on control force 111
6.3.2.2. Effect of particle diameter on control force 113
6.3.2.3. Effect of density ratio on control force 115
6.3.2.4. Effect of frequency on control force 117
6.3.2.5 Prediction model for control force in pulsatile flow 118

CHAPTER 7. INERTIAL MIGRATION OF MULTIPLE PARTICLES 123

7.1 Background 123

7.2 Methodology 123

7.3 Results and discussion 125

7.3.1 Inertial migration of two particles in straight channel 125

7.3.1.1 Effect of initial centre-to-centre distance 128

7.3.1.2 Effect of initial orientation 130

7.3.2 Inertial migration of two particles in stepped channel 132

7.3.2.1 Influence of density ratio 133

7.3.2.2 Influence of depth of step 135

7.3.3 Inertial migration of three particles in a slit channel 136

7.3.3.1 Effect of slit clearance 137

7.3.3.2 Effect of slit angle 138

7.3.3.3 Effect of initial position 140

7.3.3.4 Initial orientation and inertial migration 141

CHAPTER 8. CONCLUSIONS 145

8.1 Inertial migration of particle in straight channel 145

8.2 Inertial migration of particle in non-straight channels 146

8.3 Inertial migration of various shaped particles 148

8.4 Control force and inertial migration 148

8.5 Inertial migration of multiple particles 150

REFERENCES 153

List of Publications based on Ph.D. Research Work 161

BIODATA 165

LIST OF FIGURES

Figure 1.1	a) Illustration of wall and shear induced lifts (Tohme et al. 2021) b) Particle migration in straight channel (Qian et al. 2021)	2
Figure 1.2	a) Separation of bacteria and RBC using inertial microfluidics (Mach and Carlo 2010) b) isolation of adrenal cortical progenitor cells c) rapid inertial solution exchange (Zhang et al. 2016)	4
Figure 1.3	Eulerian and Lagrangian points of a structure immersed in a fluid	5
Figure 1.4	Schematic diagram for comparison of Peskin's and feedback forcing IBM schemes: a) Peskin's IBM b) feedback forcing IBM (Shin et al. 2008)	7
Figure 3.1	Physical model of migration of particle in Poiseuille flow	22
Figure 3.2	Physical model of migration of particle in shear flow	22
Figure 3.3	Flowchart of computational procedure	26
Figure 3.4	The grid independence test (Re=12.786, d=0.25). The midline fluid velocity(x-component) after particle attained equilibrium position is plotted against y	27
Figure 3.5	a) The initial position (1.0, 0.4) b) final position with u velocity contour of particle (48.45, 0.297)	28
Figure 3.6	a) The variation of lift force, F_l with y coordinate of particle centre, Y_C at Re=12.786 b) the variation of drag force, F_d with x coordinate of particle centre, X_C at Re=12.786	29
Figure 3.7	Particle trajectory for two different diameters 0.25 and 0.35 (Re=50.0)	29
Figure 3.8	The trajectory of particle centre with time for Re= 12.786, 27.727 and 96.74 for the initial position (1.0, 0.4) and d=0.25	30
Figure 3.9	The trajectory of particle centre with time for three different initial positions at re=12.786 and d=0.25	31

Figure 3.10	The trajectory of particle centre with time for various diameters of particle at Re=12.786 for the initial position of release (1.0, 0.4)	32
Figure 3.11	Variation of normalised equilibrium position with height of channel for Re=12.786 and d=0.25	33
Figure 3.12	a) The initial (25.0, 0.4) and b) final position with u velocity contour (24.121, 0.529) of particle at Re=12.786 and d=0.25	35
Figure 3.13	a) The variation of lift force with y coordinate of centre of particle for shear flow at Re=12.786 and d=0.25 b) The variation of drag force with x coordinate of centre of particle for shear flow at Re=12.786 and d=0.25	35
Figure 3.14	The variation of y coordinate of centre of cylinder with time for Re=1.0, 2.5, 5.0 and 12.786	36
Figure 3.15	The trajectory of particle centre with time for three different initial positions of release at Re=12.786 and d=0.25	37
Figure 3.16	The trajectory of particle centre with time for various diameters of particle at Re=12.786 and initial position = (25.0, 0.4) in shear flow	38
Figure 3.17	Variation of normalised equilibrium position with height of channel for Re=12.786 and d=0.25	39
Figure 3.18	Trajectory of particle centre with time for various shear rates for Re=12.786 and d=0.25	41
Figure 3.19	Variation of centre of particle with time in three conditions for Re=12.786, d=0.25	42
Figure 3.20	Schematic diagram of ANN prediction model	43
Figure 3.21	Performance plot of neural network training	44
Figure 3.22	Regression plot obtained for both predicted and observed values of Y_{EQN} and t_m	45

Figure 3.23	Behaviour of predicted values with that of observed values a) normalized equilibrium position Y_{EQN} b) Behaviour of predicted values with that of observed values of migration time t_m	45
Figure 4.1	Physical model of migration of particle in a backward facing stepped channel	49
Figure 4.2	Streamline patterns and u velocity contour of flow through a backward facing stepped channel without particle for three Re a) Re=12.786, b) Re=27.727, c) Re=96.74	50
Figure 4.3	Variation of center of particle with time for different Re with d=0.25	51
Figure 4.4	The trajectory particle center with time for three initial positions of release for Re=12.786 and d=0.25	52
Figure 4.5	The trajectory of particle with time for different diameter for Re=12.786	53
Figure 4.6	Trajectory of center of particle for different blockage ratios for Re=12.786, d=0.25	54
Figure 4.7	Physical model (stepped channel)	55
Figure 4.8	a) The initial position of the cylindrical particle in stepped channel (2.5, 0.5), b) final position with u velocity contour (8.401, 0.5171) (Re=12.786, d=0.2)	56
Figure 4.9	The variation of lift coefficient with lateral position of centre of cylinder for Re=12.786	56
Figure 4.10	Trajectory of centre of particle for three initial positions of release (Re=12.786)	57
Figure 4.11	The trajectory of particle with time for different height of contraction region (Re=12.786, initial position=0.5)	58
Figure 4.12	The trajectory of particle with time for different length of contraction region (Re=12.786, initial position=0.5)	58

Figure 4.13	Particle migration under fluid flow in constricted channel (physical model)	59
Figure 4.14	Streamline plot for flow through constricted channel (Re=125.0) obtained by a) Pitt et al. (2005) b) present work	61
Figure 4.15	The positions of particle at different time instances with u velocity contour (Re=10,d=0.25, Cc=0.5) a)t=0 (5.0,0.5)(initial position), b) t=0.5 (6.97,0.5003), c)t=1.0 (9.1,0.499)(enters the constricted region), d)t=1.1 (9.7,0.490) (resides in constricted region), e)t=1.5 (12. .109,0.50) (after attaining equilibrium position)	61
Figure 4.16	Trajectory of particle center with time (re=10, d=0.25, cc=0.5)	63
Figure 4.17	Trajectory of x and y coordinates of particle center (re=10, d=0.25, cc=0.5)	64
Figure 4.18	Behaviour of lift force with horizontal coordinate of particle center (re=10, d=0.25, cc=0.5)	64
Figure 4.19	a) Characteristics of lift force over with particle center (Y coordinate) b) characteristics of drag force with particle center (X coordinate) (Re=10, d=0.25, Cc=0.5)	65
Figure 4.20	Trajectory of particle center for Re =10, 20, 40 and 100 (d=0.25, cc=0.5)	
Figure 4.21	Streamline plot with **u velocity contour** for flow in constricted channel at t=1.5 a) Re=10, b) Re=20, c) Re=40, d) Re=100 (d=0.25)	67
Figure 4.22	a) Variation of lift force with horizontal position of particle for different Re a) Variation of lift force with horizontal position of particle for different Re b) Variation of lift force with time for different Re (d=0.25, Cc=0.5)	67
Figure 4.23	a) Variation of shortest equilibrium distance (D_S) with Reynolds number b) Variation of migration time (t_m) with Reynolds number (Re) (d=0.25, Cc=0.5)	68

Figure 4.24	Trajectory of center of particle for initial release positions 0.4, 0.5 and 0.6 (Re=10, d=0.25, C_C=0.5)	68
Figure 4.25	Particle trajectory for different diameters 0.2, 0.25 and 0.3 (Re=10.0, C_C=0.5)	69
Figure 4.26	a) Characteristics of lift force with horizontal position of particle for its different diameter b) Characteristics of lift force with time for its different diameter of particle (Re=10, Cc=0.5)	70
Figure 4.27	a) Variation of shortest equilibrium distance with diameter of particle b) Variation of migration time with diameter of particle (Re=10, Cc=0.5)	71
Figure 4.28	Particle trajectory for Cc =0.5, 0.6 and 0.7 (Re=10, d=0.25)	72
Figure 4.29	a) Characteristics of lift force with horizontal position of particle for different constriction clearances b) characteristics of lift force with time for various constriction clearances (Re=10, d=0.25)	73
Figure 4.30	a) Variation of shortest equilibrium distance (D_S) with constriction clearance (Cc) b) variation of migration time (t_m) with constriction clearance (Cc) (Re=10, d=0.25)	73
Figure 4.31	Architecture of ANN prediction model	74
Figure 4.32	Performance plot of neural network training	75
Figure 4.33	Regression plot obtained for both predicted and observed values of Y_{EQ}, t_m and D_S	76
Figure 4.34	Comparison between predicted values and observed values a) equilibrium position Y_{EQ} b) shortest equilibrium distance D_S c) migration time t_m	76
Figure 4.35	a) Variation of shortest equilibrium distance with Reynolds number for different diameters 0.2, 0.25 and 0.3 b) variation of migration time with Re for different diameters 0.2, 0.25 and 0.3 (C_C=0.5)	78

Figure 4.36	a) Variation of shortest equilibrium distance with Re for different Cc 0.5, 0.6 and 0.7 b) Variation of migration time with Re for different Cc 0.5, 0.6 and 0.7 (d=0.25)	78
Figure 4.37	Variation of Re_{cr} with C_C (d=0.25)	79
Figure 5.1	a) Initial position, b) final position of circular particle	86
Figure 5.2	a) Initial position, b) final position of elliptical particle	87
Figure 5.3	a) Initial position, b) final position of square particle	87
Figure 5.4	a) Initial position, b) final position of rectangular particle	87
Figure 5.5	a) Initial position, b) final position of biconcave particle	88
Figure 5.6	Figure 5.6 Vorticity plot over a) Biconcave particle, b) rectangular particle	88
Figure 5.7	Particle trajectory of different shaped particle with time (re=100.0, density ratio=1.0)	89
Figure 5.8	Particle trajectory of different shaped particle with time (re=100.0, density ratio=100.0)	90
Figure 6.1	Physical model a) Poiseuille flow, b) pulsatile flow	92
Figure 6.2	Particle trajectory for different magnitude of control forces (re=10.0, d=0.25, ρ=100.0)	94
Figure 6.3	The u velocity contours for particle migration in the absence and presence of external controlling force a) t=0.1 without $\mathbf{f}_{ctrl}$ b) t=1.0 without $\mathbf{f}_{ctrl}$, c) t=0.1 with $\mathbf{f}_{ctrl}$ =-26.0, d) t=1.0 with $\mathbf{f}_{ctrl}$ =-26.0 (Re=10.0, d=0.25)	95
Figure 6.4	Saffman lift force trajectory with particle lateral position in the presence and absence of control force (Re=10, d=0.25)	96
Figure 6.5	Lift force trajectory with particle lateral position	96
Figure 6.6	Particle centre trajectory with horizontal position for different Re in the absence of $\mathbf{f}_{ctrl}$ (d=0.25, ρ=100.0)	97

Figure 6.7	Particle centre trajectory in presence of $\mathbf{f}_{ctrl}$ with horizontal position (d=0.25, ρ=100.0)	98
Figure 6.8	The variation of control force ($\mathbf{f}_{ctrl}$) with re (d=0.25, ρ=100.0)	99
Figure 6.9	Particle trajectory in the absence of control force for different diameters with horizontal position of particle centre (ρ=100.0, Re=10.0)	100
Figure 6.10	Particle trajectory for different diameters in the presence of $\mathbf{f}_{ctrl}$ with horizontal position (Re=10.0, ρ=100.0)	101
Figure 6.11	the control force variation with d (Re=10.0, ρ=100.0)	102
Figure 6.12	Particle trajectory in the absence of control force for different density ratios with horizontal position of particle centre (d=0.25, Re=10.0)	103
Figure 6.13	Particle trajectory in the presence of control force for different density ratios with horizontal position of particle centre, (d=0.25, Re=10.0)	104
Figure 6.14	Trajectory of control force with density ratio (Re=10.0, d=0.25)	104
Figure 6.15	Network diagram of linear regression	106
Figure 6.16	The variation of predicted and observed values of $\log_e \mathbf{f}_{ctrl}$	107
Figure 6.17	The predicted and observed values of control force (test of correlation)	107
Figure 6.18	Particle trajectory for different control forces (Re=10.0, d=0.25, ρ=100.0, υ=2.5π)	108
Figure 6.19	The u velocity contours for particle migration in both absence and presence of external controlling force a) t=0.1 without $\mathbf{f}_{ctrl}$ b) t=15.0 without $\mathbf{f}_{ctrl}$, c) t=0.1 with $\mathbf{f}_{ctrl}$ =-20.0, d) t=15.0 with $\mathbf{f}_{ctrl}$ =-20.0 (Re=10.0, d=0.25, υ=2.5π)	109
Figure 6.20	Saffman lift force variation with particle lateral position in presence and absence of control force (Re=10.0, d=0.25, υ=2.5π)	110
Figure 6.21	Lift force trajectory with particle lateral position	110

Figure 6.22 particle center trajectory with horizontal position in absence of $\mathbf{f}_{ctrl}$ (d=0.25, ρ=100.0, υ=2.5π) 111

Figure 6.23 Particle centre trajectory in presence of $\mathbf{f}_{ctrl}$ with horizontal position (d=0.25, ρ=100.0, υ=2.5π) 112

Figure 6.24 The variation of control force ($\mathbf{f}_{ctrl}$) with Re (d=0.25, ρ=100.0, υ=2.5π) 112

Figure 6.25 Particle trajectory in absence of control force for different diameters of particle with horizontal position of centre of particle (ρ=100.0, re=10.0, υ=2.5π) 113

Figure 6.26 Particle trajectory in presence of control force for different diameters of particle with horizontal position of centre of particle (ρ=100.0, re=10.0, υ=2.5π) 114

Figure 6.27 The variation of control force with d (ρ=100.0, re=10.0, υ=2.5π) 114

Figure 6.28 Particle trajectory in absence of control force for different density ratios of particle to fluid with horizontal position of centre of particle, (d=0.25, Re=10.0, υ=2.5π) 115

Figure 6.29 Particle trajectory in presence of control force for different density ratios of particle to fluid with horizontal position of centre of particle (d=0.25, Re=10.0, υ=2.5π) 116

Figure 6.30 Variation of control force with density ratio (d=0.25, re=10.0, υ=2.5π) 117

Figure 6.31 Particle trajectory for different frequencies of oscillation in the absence of control force (Re=10.0, d=0.25, ρ=100.0) 118

Figure 6.32 Particle trajectory for different frequencies of oscillation in presence of control force (Re=10.0, d=0.25, ρ=100.0) 119

Figure 6.33 Variation of control force with frequency (d=0.25, Re=10.0, ρ=100.0) 119

Figure 6.34 The variation of predicted and observed values of loge $\mathbf{f}_{ctrl}$ in pulsatile flow 120

Figure 6.35	The predicted and observed values of control force in pulsatile flow (test of correlation)	121
Figure 7.1	Physical models of multiple particles in different channels a) two particles in straight channel, b) two particles in stepped channel and c) three particles in slit channel	124
Figure 7.2	Initial and final positions of particles with u velocity contour a) Initial position, b) Final position (Re=10.0, d=0.2)	126
Figure 7.3	Particle trajectory	127
Figure 7.4	Variation of D_C with X_C	127
Figure 7.5	Particle trajectory for different D_{Ci}	128
Figure 7.6	Variation D_C with time for different D_{Ci}	129
Figure 7.7	Initial orientation of particles a) horizontal, b) vertical, c) offset	130
Figure 7.8	particle trajectory for different initial orientations	131
Figure 7.9	Variation of D_C with time for different initial orientation	132
Figure 7.10	a) Initial position of particles ((5.0, 0.6) and (5.5, 0.6) b) Final position of particles with u velocity contour ((14.15, 0.586), (14.61, 0.586)) (Re=50.0, d=0.2, ρ=100.0, H_C=0.25)	133
Figure 7.11	a) Particle 1 trajectory against time b) particle 2 trajectory against time for different density ratios (Re=50.0, d=0.2 H_C=0.25)	134
Figure 7.12	Variation of migration time with density ratio (Re=50.0, d=0.2 H_C=0.25)	134
Figure 7.13	a) Particle 1 trajectory against time b) particle 2 trajectory against time for different depths of step (Re=50.0, d=0.2 ρ=100.0)	135
Figure 7.14	Variation of migration time with depth of step (Re=50.0, d=0.2, ρ=100.0)	136
Figure 7.15	a) Initial positions of three particles b) final position of particles with u velocity contour (d=0.2, Re=50.0, S_g=0.5 and Θ= π/2, ρ=100.0)	137

Figure 7.16 Variation of lateral positions of particles with a) horizontal position b) time (Re=50.0, d=0.2, ρ=100.0 and Θ=π/2) 138

Figure 7.17 Particle trajectory with time for different S_g (Re=50.0, d=0.2, ρ=100.0 and Θ=π/2) 139

Figure 7.18 Particle trajectory with time for different Θ (Re=50.0, d= 0.2, S_g=0.5, ρ=100.0) 140

Figure 7.19 Particle trajectory with time for different initial positions (Re=50.0, d= 0.2, S_g=0.5, ρ=100.0 and Θ=π/2) 141

Figure 7.20 Particle positions when migrating through slit for triangle orientation a) initial, b) when passing through slit and c) final position 142

Figure 7.21 Particle 3 trajectory with time for different orientations (Re=50.0, d= 0.2, S_g=0.5, ρ=100.0 and Θ=π/2) 143

Figure 7.22 Particle 2 trajectory with time for different orientations (Re=50.0, d= 0.2, S_g =0.5, ρ=100.0 and Θ=π/2) 143

LIST OF TABLES

Table 3.1	Boundary conditions	22
Table 3.2	Comparison of equilibrium positions Y_{EQ} of particle in Poiseuille flow for two diameters observed in the present work with that of (Huang et al.2021) (Re=50.0)	29
Table 3.3	Time taken to attain equilibrium position for three Re for d=0.25	31
Table 3.4	Migration time for different diameters of particle at Re=12.786	33
Table 3.5	Migration time for different height of channel for Re=12.786 and d=0.25	34
Table 3.6	Validation of results for shear flow for d=0.25	37
Table 3.7	Time taken to attain equilibrium position for d=0.25	37
Table 3.8	Migration time for different diameter of particle at Re=12.786	39
Table 3.9	Migration time for different height of channel for Re=12.786 and d=0.25	40
Table 3.10	Migration time for various shear rates	41
Table 3.11	Migration time for different flow conditions for Re=12.786, d=0.25	42
Table 4.1	Boundary conditions (backward facing stepped channel)	50
Table 4.2	Migration time for different diameter (d) of particle for Re=12.786	54
Table 4.3	Migration time for different blockage ratio of stepped channel for Re=12.786 and d=0.25	55
Table 4.4	Variation of migration time with length of contraction region	59
Table 4.5	a) Equilibrium position variation for different channel configurations b) migration time variation for different channel configurations	82
Table 5.1	Equilibrium position and migration time of different shaped particles	89
Table 5.2	Equilibrium position and migration time of different shaped particles (Re=100, density ratio=100)	90
Table 6.1	Migration time (t_m) for different Re in the absence and presence of $\mathbf{f}_{ctrl}$ (d=0.25, ρ=100.0)	99

Table 6.2	Migration time (t_m) for different d in the absence and presence of $\mathbf{f}_{ctrl}$ (Re=10.0, ρ=100.0)	101
Table 6.3	Migration time (t_m) for different ρ in absence and presence of $\mathbf{f}_{ctrl}$ (Re=10.0, d=0.25)	104
Table 6.4	Migration time (t_m) for different Re in absence and presence of $\mathbf{f}_{ctrl}$ (d=0.25, ρ=100.0, υ=2.5π)	112
Table 6.5	Migration time (t_m) for different d in absence and presence of $\mathbf{f}_{ctrl}$ (Re=10.0, ρ=100.0, υ=2.5π)	115
Table 6.6	Migration time (t_m) for different ρ in absence and presence of $\mathbf{f}_{ctrl}$ (Re=10.0, d=0.25, υ=2.5π)	117
Table 6.7	Migration time (t_m) for different υ in absence and presence of $\mathbf{f}_{ctrl}$ (Re=10.0, d=0.25, ρ=100.0)	120
Table 7.1	Migration time for different D_{Ci}	129
Table 7.2	Migration time for different Initial orientations	132
Table 7.3	Variation of migration time with density ratio (Re=50.0, d=0.2, H_C=0.25)	134
Table 7.4	Variation of migration time with depth of step (Re=50.0, d=0.2, ρ=100.0)	136
Table 7.5	Residence time (t_r) for different S_g) (Re=50.0, d=0.2, Θ=π/2)	139
Table 7.6	Residence time (t_r) for different Θ (Re=50.0, d=0.2, S_g=0.5)	140
Table 7.7	Residence time (t_r) for different initial position (Re=50.0, d=0.2, S_g=0.5 and Θ=π/2)	141
Table 7.8	Residence time ($_{tr}$) of particle 2 for different initial orientation (Re=50.0, d=0.2, S_g=0.5 and Θ=π/2)	143

NOMENCLATURE

b	Blockage ratio
C_C	Constriction clearance
d	Particle diameter
D_C	Centre-to-centre distance between particles
D_{Ci}	Initial centre-to-centre distance between particles
ds	Lagrangian grid size
D_S	Shortest equilibrium distance
d**x**	Eulerian grid size
F (s, t)	Lagrangian force
f (**x**, t)	Eulerian force
$\mathbf{F}_a$	Lagrangian force of constricted/ step/slit
$\mathbf{f}_a$	Eulerian force of constricted arc/ step/slit
$\mathbf{f}_{ctrl}$	Control force
F_d	Drag force
F_l	Lift force
$\mathbf{F}_P$	Lagrangian force of particle
$\mathbf{f}_P$	Eulerian force of particle
F_S	Shear induced lift
F_{SA}	Saffman lift force
F_W	Wall induced lift

g	Gravitational acceleration
H	Channel height
h	Eulerian grid spacing
H_C	Depth of step
H_S	Height of step
I_P	Mass moment of inertia of particle
k	Shear rate
L	Channel length
L_C	Length of constriction
L_S	Length of of step
m_P	Mass of particle
n	Current time step
$N(\mathbf{u}^n)$	Non-linear convection term
$p(\mathbf{x}, t)$	Fluid pressure
P_S	Pseudo pressure
Re	Reynolds number
Re_{cr}	Critical Reynolds number
Re_P	Particle Reynolds number
s	Material point
s_a	Material point of constricted arc/step/slit
S_g	Slit clearance
s_P	Material point of particle
t	time
t_0, t_1, t_2 and t_3	Time intervals of pulsatile flow

t_m	Migration time
t_r	Residence time
$\mathbf{U}$	Velocity of particle
$\mathbf{u}$ ($\mathbf{x}$, t)	Fluid velocity
$\mathbf{U}_a$	Velocity of constricted arc/step/slit
$\mathbf{U}_{ib}$ (s, t)	Interpolated immersed boundary velocity
$\mathbf{U}_{iba}$	Interpolated immersed boundary velocity of constricted arc/step/slit
$\mathbf{U}_{ibP}$	Interpolated immersed boundary velocity of particle
$\mathbf{U}_P$	Translational velocity of particle
$\mathbf{U}_P$	Velocity of particle
u_{ref}	Maximum channel velocty
$\mathbf{X}$ (s, t)	Lagrangian coordinates
$\mathbf{x}$ (x, y)	Cartesian coordinates
$\mathbf{X}_C$	Centre of particle
X_C	X coordinate of centre of particle
X_{CON}	x coordinate of point on constriction arc
Y_C	Y coordinate of centre of particle
Y_{CON}	y coordinate of point on constriction arc
Y_{EQ}	Equilibrium position
Y_{EQN}	Normalised equilibrium position

Y_{inin}	Normalised initial position

Greek Symbols

α, β	Large negative constants
δ	Dirac Delta function
Δt	Time step size
Θ	Slit angle
μ	Dynamic viscosity of fluid
ρ	Density ratio
ρ_f	Density of fluid
ρ_p	Density of particle
υ	Frequency of oscillation of pulsatile flow
ω_p	Angular velocity of particle

Superscripts

*	Dimensional value

ABBREVIATIONS

RBC	Red blood corpuscles
WBC	White blood corpuscles
FSI	Fluid structure interaction
IBM	Immersed boundary method
ANN	Artificial neural network
LR	Linear regression
ALE	Arbitrary Lagrangian Eulerain
LBM	Lattice Boltzmann method
FEM	Finite element method
N-S	Navier Stokes
FVM	Finite volume method
ICCG	Incomplete Cholesky conjugate gradient
MSE	Mean square error

CHAPTER 1. INTRODUCTION

Microfluidics is an interdisciplinary field that combines the principles of nanotechnology, biotechnology, chemistry, physics and engineering and it deals with the precise control, and manipulation of fluids that are geometrically constrained in the microscale. Microfluidics has emerged in the early 1980's and currently become one of the most promising technology that can be used in many applications such as development of inkjet print heads, DNA chips, lab-on-a-chip technology, micro-propulsion, and micro-thermal technologies. Typically, fluids are moved, mixed, separated or otherwise processed in microfluidic processes.

The bio-particles such as red and white blood corpuscles (RBC and WBC), platelets, thromboses can be isolated, fractionalized, purified or separated with the aid of various techniques in microfluidics. The separation of particles is highly important in biomedical field. The diseased cells and tissues have to be separated from the human body to examine the depth of infection. The microfluidic separation is mainly classified into two types namely active and passive. Active separation is achieved with the help of external forces like electric and magnetic field, acoustic etc. whereas, the passive techniques fully rely on channel geometry, particle size and hydrodynamic forces. The passive separation techniques include pinched flow fractionalization, deterministic lateral displacement and inertial migration. Recently, inertial migration has become a remarkable approach for the separation of bio-particles (Bazaz et al., 2020).

1.1 Inertial migration

Inertial migration is a lateral movement experienced by particle released in fluid due to pure fluid inertia forces. The inertial migration characteristics of a particle depends upon the fluid velocity, viscosity, channel and particle dimensions etc. In other words, the inertial migration arises due to pure hydrodynamic forces. The inertial migration is contributed by two forces such as wall and the shear induced lift. The wall induced lift (F_W) emerges due to flow of bulk shear which drives the particle towards the center of channel while, the shear induced lift (F_S) arises due to the curvature of the profile of velocity which pushes the particle to the channel wall (Figure 1.1 a) and b)).

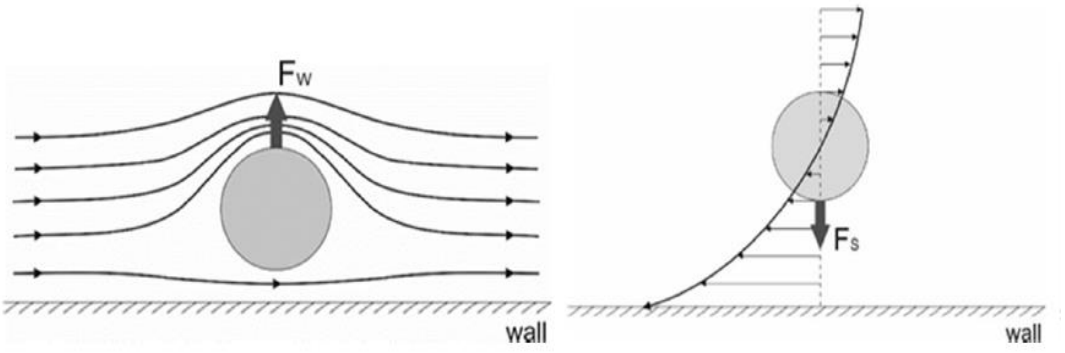

a)

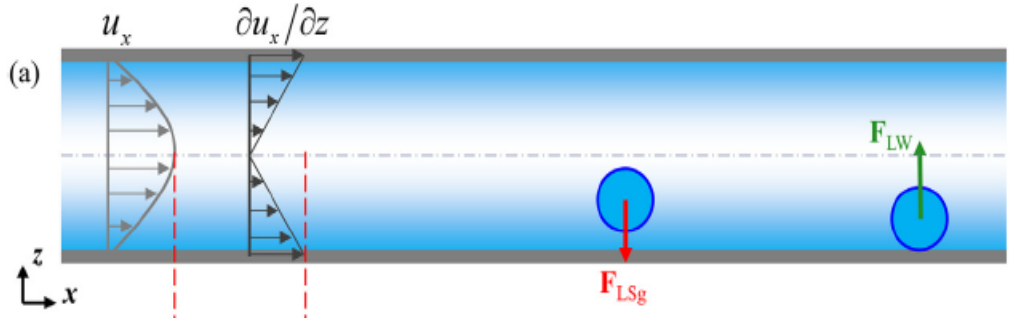

b)

Figure 1.1 a) Illustration of wall and shear induced lifts (Tohme et al. 2021), b) Particle migration in straight channel (Qian et al. 2021)

The particle will stop lateral migration at equilibrium position where the shear and wall induced lifts are balanced which results in zero lift force. This equilibrium position has a major role in separation of particles. The time taken to reach the equilibrium position is called migration time. The segregation of bio-particles will become easier by predicting their equilibrium position. Therefore, inertial migration of particles will play a pivotal role in biomedical field **(**Examples of separation of pathogenic bacteria and RBC, isolation of adrenal cortical progenitor cells and rapid inertial solution exchange are shown in figure 1.2**)**. The separation of diseased cells, pathogenic bacteria from the human blood and drug delivery can be aided with the technique of inertial migration. It should be also noted that, inertial migration has applications in the chemical process industries and pollution control which involves handling of particles suspended in moving fluid. For example, the movement of sugar fragments in sugar industry, migration of airborne particles in air and waste particle flow in polluted water can

acquire equilibrium position according to their size and other flow conditions. Hence, inertial migration techniques can be applied for separation of these particles and may be purification of the parent fluid.

Due to complex nature of fluid-structure interaction (FSI) involved with moving deformable/rigid particles in fluid flow, numerical modeling of inertial migration of particles in channel flow is challenging. Hence suitable numerical schemes are required to model such problem. The approach to study FSI can be classified into two which are monolithic approach and partitioned approach.

The monolithic approach uses single solver to solve governing equations of fluid and displacement of the structure. This approach needs developed code which incorporates the physical properties. In partitioned approach separate solvers are used to solve governing equations of fluid flow and displacement of the structure. Hence, the flow solver and displacement solver are coupled in the case of partitioned approach. Software with good coupling algorithm can be used in partitioned approach.

FSI can again be classified into two types based on the type of treatment on the grid. They are known as conforming mesh methods and non-conforming mesh method. The researcher who use conforming mesh method consider the interphase conditions as the physical boundary conditions. It considers interphase as a part of the solution and it needs remeshing as the structure moves. Hence, grid should move according to the structure movement or deformation. Whereas the non-conforming meshes treat the interface conditions and boundary locations as constraints imposed on the governing equations. Hence, the remeshing can be avoided in non-conforming meshes. A methodology of FSI problems utilizing computational mesh based numerical methods with the aid of immersed boundary method (IBM) has become popular in recent years. The advantage of IBM is that it is monolithic and it incorporates non-conforming mesh and hence the complexity of remeshing can be avoided which is suitable for simulation of inertial migration. Elaborate discussion on IBM is given below.

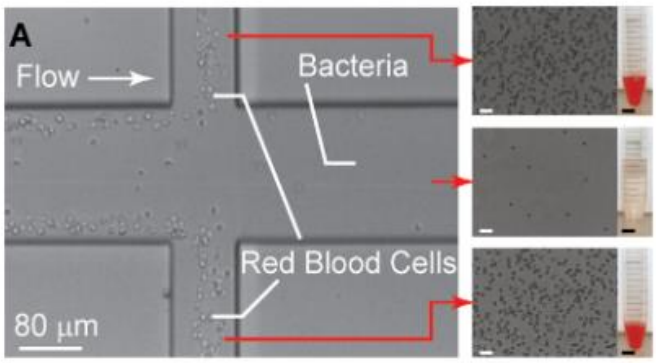

a)

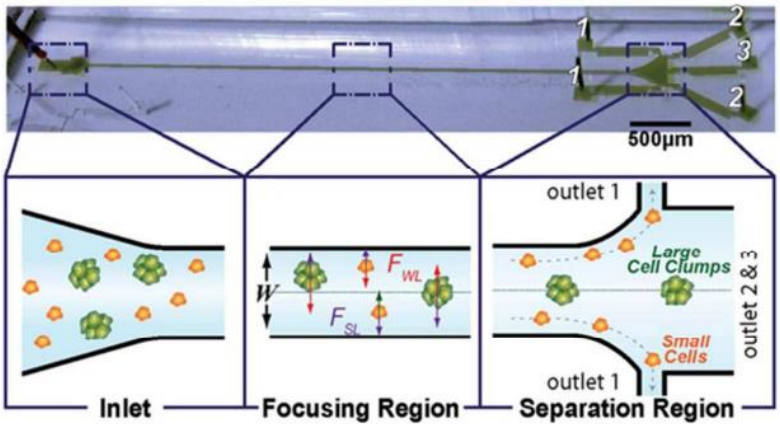

b)

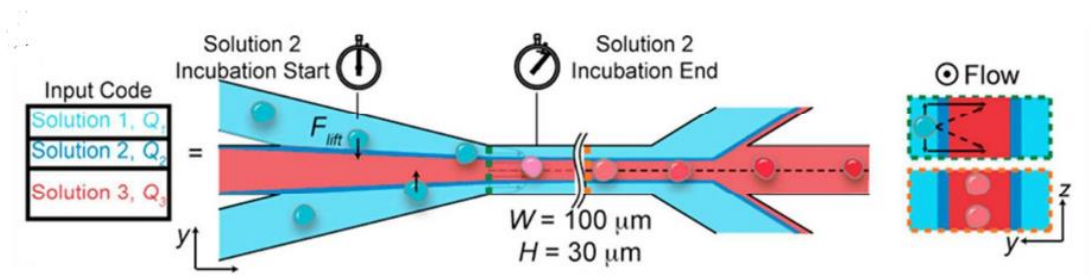

c)

Figure 1.2 a) Separation of bacteria and RBC using inertial microfluidics (Mach and Carlo 2010) b) isolation of adrenal cortical progenitor cells c) rapid inertial solution exchange (Zhang et al. 2016)

1.2 Immersed boundary method

Immersed boundary method (IBM) was proposed by (Peskin, 1977). He simulated blood flow through the heart using this method. It is a monolithic method which uses non-conforming mesh as the grid technique. In this method the structure is said to be immersed in the fluid. This immersed part can be boundary of the structure or an area or volume inside the grid. IBM calculates the momentum force from the equations of the displacement of the structure and add as an additional term (body forcing term) to the governing equations of the fluid. Those equations are then solved to obtain the fluid velocity. Figure 1.3 illustrates the Eulerian and Lagrangian grid points in IBM.

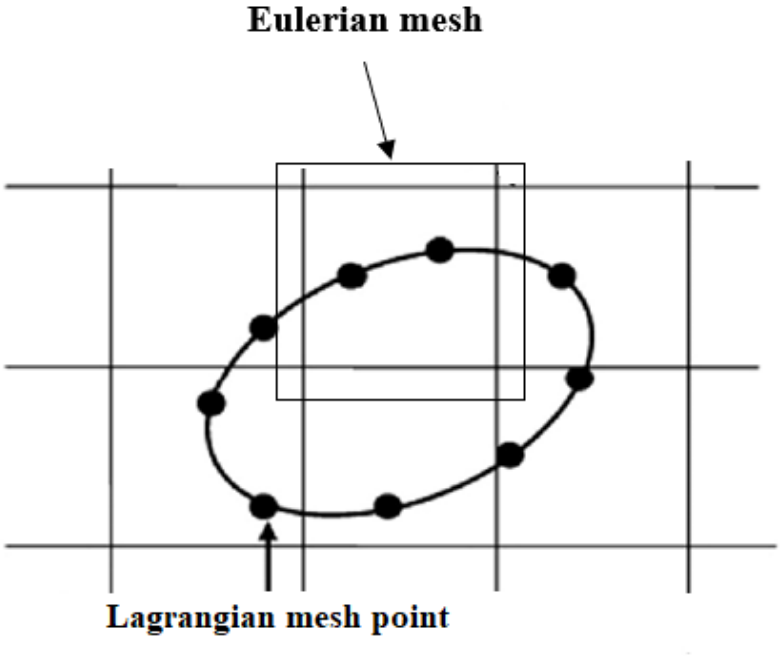

Figure 1.3 Eulerian and Lagrangian points of a structure immersed in a fluid

IBM can be classified based on the approach of taking momentum forcing into the governing equations of fluid. If the momentum forcing term is united into the governing equation of fluid before discretization then the approach is called continuous forcing approach. Dirac delta function is used in this approach for the interpolation of fluid velocity and structural velocity. This function was first introduced by (Dirac, 1930). It is used to model an idealized point mass. The main characteristic of this function is that it has zero value at every position except at zero. In case of discrete forcing approach, the momentum force comes discretely after discretization of governing equations of

fluid. This allows better control over conservativeness, stability and accuracy of the numerical solver.

Feedback forcing scheme is a type of continuous forcing type IBM. The Lagrangian force calculation in feedback forcing based IBM is different from Peskin's IBM scheme. The detailed discussion on feedback forcing based IBM is given below.

1.3 Feedback forcing scheme-based IBM

Huang et al. (2007) introduced a different type of continuous forcing IBM scheme by combining the virtual boundary method which was proposed by (Goldstein et al. 1993) with Peskin's regularized delta function. This method is called feedback forcing scheme. The main difference between Peskin's IBM and feedback forcing scheme is that, in this method the momentum force on the immersed boundary is calculated by using a feedback law. The Peskin's scheme uses position of the immersed boundary to calculate the momentum force whereas the feedback forcing scheme uses velocity of the immersed boundary points for calculation of momentum force (The difference between both of these schemes can be visualized in figure 1.4 a) and b)). One additional term which contain the velocity is added to this equation to control the unwanted oscillation and converge the problem faster. Unwanted oscillation is defined as the oscillation of numerical solution without being converged during the iterative process. Another advantage of this scheme over Peskin's IBM is that it can employ a larger time step for simulations. Thus, the current study incorporates feedback forcing based immersed boundary method for the analysis of inertial migration dynamics of particles.

The feedback forcing based IBM can be employed to simulate inertial migration for different parametric cases. These simulation results can be utilized to develop empirical models for prediction of inertial migration dynamics related parameters like equilibrium position and migration time. Various machine learning techniques such as artificial neural network (ANN), linear regression (LR) can become suitable for this procedure. These empirical models can predict the inertial migration characteristic under different parametric cases.

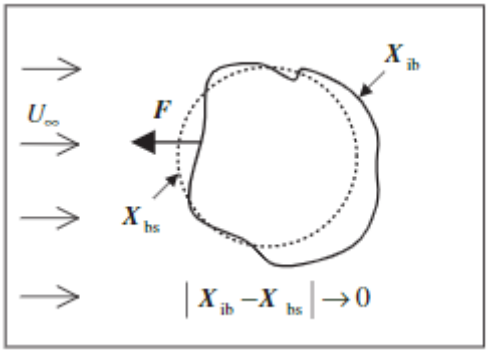

a)

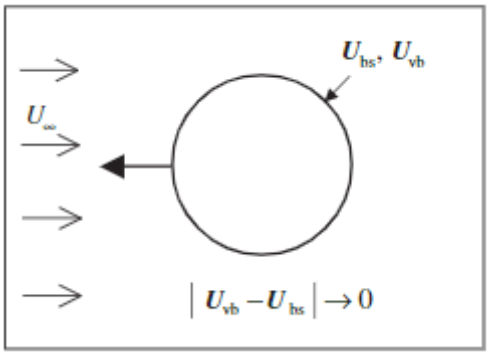

b)

Figure 1.4 Schematic diagram for comparison of Peskin's and feedback forcing IBM schemes: (a) Peskin's IBM and(b) feedback forcing IBM (Shin et al. 2008)

1.4 Artificial neural network (ANN)

The output of numerical simulations can be used to build empirical models for the prediction in other parametric cases. Artificial neural network (ANN) is such a tool which gains inspiration from the human brain system. A set of random data can be assessed, learned, memorized by ANN algorithm. By using these set of random data, it can build a relationship in between them also. This gives it an ability to solve new problems based on the information obtained from past experience. ANN comprises of three components i.e., network architecture, training method and transfer functions. The input and output layers and hidden layers are the parts of network architecture. The hidden layers are constructed with neurons (parallel processing elements) with each being interconnected to the proceeding layer by weights (w). The process in which interconnected weights are tuned for obtaining the expected output is known as training.

For training back-propagation algorithm is employed. The key idea of back-propagation algorithm is to reduce the error between output and hidden layers and network training. Initially, arbitrarily valued weights are assigned and continuously modified until the minimization criteria are achieved by incorporating Levenberg-Marquardt algorithm. Ultimately, a transfer function is utilized that converts the output of the neural network to the desired structure. This transfer function can be either logistic sigmoid or tangent sigmoid and linear type is taken for output layer (Kanchan and Maniyeri 2020c).

1.5 Linear regression (LR)

Linear regression (LR) is one of the common prediction models in machine learning in which a relation can be established between a scalar and one or more explanatory variables. The interpretation and training of data are easier in linear regression than in other machine learning algorithms and is also easy to implement. Linear regression is normally applied to single input-output pairs. If output is y and input is x then $y=px+q$, where q is the intercept and p is the slope. If the number of inputs is more than one, then the natural log will come into picture. The advantage of LR is that an empirical correlation can be obtained which connects the single output and multiple inputs. This correlation can be utilised in future studies for prediction of the desired outputs based on different parametric cases.

1.6 Outline of the thesis

The remaining chapters of the thesis is organized as shown below.

Chapter 2- A vast literature review is presented which discuss various previous works that studied inertial migration. The theoretical, experimental and computational studies on inertial migration have reviewed in this session. It also presents a brief review on immersed boundary method and feedback forcing based IBM. The research gap, critical review and objectives of the thesis are included at the end of chapter 2.

Chapter 3- The inertial migration of single rigid neutrally-buoyant particle in straight channel (both Poiseuille and shear flow) is discussed here. The detailed methodology and results are discussed in this chapter.

Chapter 4- The lateral migration dynamics of single rigid neutrally-buoyant particle in non-straight channels such as stepped and constricted channels are analysed in this chapter. Also, development of prediction model for equilibrium position and migration time using ANN is presented.

Chapter 5- The inertial migration of various shaped particles such as circular, elliptical, rectangular, square and biconcave is discussed in this chapter. The cases of both neutrally and non-neutrally buoyant particles are discussed in this chapter.

Chapter 6- The implementation of control force for controlling the equilibrium position of massive particles under Poiseuille and pulsatile flows is explored here. Along with that, development of empirical correlation for control force using linear regression is presented.

Chapter 7- The migration of two and three particles in straight, stepped and slit channel are analysed in this chapter.

Chapter 8- The key findings of all simulations and prediction models are summarized and concluding remarks are given in this chapter.

CHAPTER 2. LITERATURE REVIEW

A vast literature review on inertial migration is presented in this session. The analytical studies are presented first which is followed by experimental works and in the third part numerical literatures are presented.

2.1 Theoretical studies

The phenomena of inertial migration were first observed by Segre and Silberberg (1961) while conducting an experiment in which polymethyl methacrylate spherical particles were suspended in fluid medium having mixtures of glycerol, butanediol and water. The rigid spheres were found to be shifted towards 0.6 times the radius of channel which is independent of the initial position of release of particle. This was termed as Segre-Silberberg effect which is known as the foundation of inertial migration phenomena. The analytical methods with different perturbation theories were used to study the inertial migration dynamics and Segre-Silberberg effect. Rubinow and Keller (1961) computed both lift and drag forces by using relative velocity between fluid and particle. This calculation involved Stokes and Oseen expansions. The transverse force over an elastic sphere which is migrating in steady inertia-less flow was determined by Tam and Hyman (1973) with the use of linear elastic theory. It was observed that the particle reached the same equilibrium position independent of its initial position of release. The expression for lateral force on the rigid sphere which is migrating in Poiseuille flow was put forward by Ho and Leal (1974). The importance of this formula is that it connected the size of particle and velocity gradient of the flow. This study was extended to migration of rigid sphere in viscoelastic fluid (Ho and Leal 1976). Schonberg and Hinch (1989) utilized singular perturbation theory for the determination of lift force in inertial migration dynamics of a particle in which the flow Reynolds number is in the order of unity. Most of the above studies dealt with migration of particles in low and intermediate Reynolds number (Re) flows. Asmolov (1999) computed the lift force over the sphere for a wide range of Re values with the help of the method called matched asymptotic expansions. It was observed that two equilibrium positions existed for neutrally buoyant particle at large slip velocities of particle. (Matas et al. 2009) also used matched asymptotic expansions methodology and analyzed the inertial migration of spherical particle in three-dimensional pipe through

which laminar flow takes place. This was one of the first studies of inertial migration in three-dimensional flow. It was observed that after a critical Re of 700, one additional equilibrium position exist for the particle (Matas et al. 2004). In the previous studies, the particle size was assumed to be small enough that it does not disturb the fluid flow. However, if we consider the physical facts, the particle size can play an important role in inertial migration. Hood et al. (2015) considered the above fact and suggested new correlation to compute the exerted force over the particle in three-dimensional square microchannel using regular perturbation analysis. They studied the balancing forces inside the domain numerically and developed an analytical model for the computation of lift forces on the particle. They analysed the lift force up to Re of 80. The lift forces were found to be zero at eight different positions out of which four were stable. It is a known fact that theoretical studies are based on a number of assumptions which can be different from real scenarios. Hence, experimental methods with the aid of different visualisation techniques were also carried out to assess inertial migration dynamics.

2.2 Experimental studies

Frank et al. (2003) visualized the particle migration with the aid of confocal microscopy in Brownian suspension. It was observed that as the Peclet number (Pe) increases the equilibrium position shifted more towards the wall. Abbas et al. (2014) used In-situ microscope to find the trajectory of microspheres in shear flow and it was noticed that the spheres aligned to the centre of the channel for low Re values. Liu et al. (2015) suggested critical Re for good inertial focusing of a large number of spherical particles. The spherical particles were visualized using fluorescent light in this work. The lift coefficients was calculated experimentally by Zhou and Papautsky (2013) using particle streak velocimetry. Koh et al. (2014) developed a prism-embedded microfluidic device for 3D imaging of inertial microfluidics. Zhou et al. (2020) utilized high speed imaging for inertial migration of particles and they observed that two metastable position arise before reaching equilibrium position while particles undergo a long migration path. The experimental methods require high precision equipment to capture the trajectory of particles in fluid flow. Also, the data collection using computational methods is far easier compared to experimental methods such as PIV and confocal

microscopy. Hence, computational studies are considered to be a better option for the analysis of inertial migration.

2.3 Computational studies

Hu et al. (1992) used Arbitrary Lagrangian Eulerain (ALE) method to simulate the fluid-particle interactions. Huang et al. (1997) also made use of ALE for studying lateral migration of a particle in shear flow. The surface velocity is calculated from the translational and angular speed and the radial distance from the centre. Each of these parameters are updated at every iteration.

Lattice Boltzmann method (LBM) is efficient in case of tracking particle dynamics in domains where solid-fluid interphases are present (Aidun and Clausen 2010b). Ladd (1994) investigated about the equilibrium position of spherical particle in square channel at Re range of 100-1000 with the aid of LBM. Inamuro et al. (2000) used LBM to simulate the migration of neutrally buoyant cylinders. The nine-point model was used in this work and they noticed that for a particular aspect ratio and diametrical ratio the equilibrium positions of all cylindrical particles were in line. Chun and Ladd (2006) simulated the migration of non-spherical particles using LBM and found that at high Reynolds number greater than 750, the equilibrium position obtained is very much close to the wall and it does not change with increase of Reynolds number further.

Another numerical scheme called overlapping grid method was chosen by Su et al. (2018) for simulating the lateral migration of cylindrical particles and special disk like particles. The characteristic of this method is that it uses an overlapped grid which consists of four types of grids. They are the general Cartesian grid system, body fitted grids for the particles and fine grids at the poles of the particles. They found that the surface stresses at the ends of the particles play an important role in migration. It was also observed that the equivalent diameter of the particle was seen to be increasing as Reynolds number increases.

Immersed boundary method (IBM) are suited for handling complex FSI problems. It incorporates non-conforming mesh and Cartesian grid. The use of Cartesian grid makes it easy to solve problems with topologically complex boundaries. For instance, generation of a body-conformal grid for solving particle migration is quite tedious but

the problem can be tackled quite easily using a Cartesian grid based immersed boundary method. For problems with moving boundaries, the use of IB method also eliminates the added complexity associated with remeshing, which usually accompanies other body conformal grid methods (e.g., Arbitrary Lagrangian-Eulerian method) (Mittal and Bhardwaj 2022). Since the inertial migration of particles involves fluid-structure interaction the IBM is an efficient tool to simulate and study these phenomena.

2.3.1 Immersed boundary method

The immersed boundary method (IBM) was proposed by Peskin (1977) to simulate the behaviour of heart with blood flow. IBM has been used effectively in the field of computational fluid dynamics to simulate stationary and moving boundaries(structures). The locomotion of jellyfish was simulated with the aid of IBM (Huang and Sung 2009). Following this the movement of an oblate (Park et al. 2014) and prolate jellyfish (Park et al. 2015) was simulated with the use of IBM. The bacteria are one of the other organisms present abundantly in water and other fluids and its interaction with fluid is an important topic of interest. The bacterial flagellum propulsion was analysed by Maniyeri et al. (2012) by using IBM. This study was further extended to simulate the rotational dynamics of an elastic rod inspired by bacterial flagella (Maniyeri and Kang 2012) and bacterial flagellar bundling (Maniyeri and Kang 2014). The dynamics of flexible filaments in flow is another area of interest to biologists and engineers in a wide variety of applications involving folding and unfolding sequence of long-chain biomolecules like DNA, non-motile sperm and microalgae. The buckling and recuperation dynamics of a single filament was examined with the aid of IBM by (Kanchan and Maniyeri 2019). The same was further extended to study the filament dynamics in an oscillating flow (Kanchan and Maniyeri 2020). The speciality of this work is that the authors employed a temporal second order IBM scheme for the simulation. Along with those, the working of a valve less pump (Shin and Sung 2010) was simulated by using IBM. Kim et al. (2012) explored the dynamics of a flexible ring in fluid flow with the help of IBM.

Navidbakhsh and Rezazadeh (2012) used LBM-IBM method in which LBM is employed to solve the fluid equations and IBM for the structural equations to conduct a study on malaria affected red blood cells. The fluid-structure coupling was done using

IBM. They found that the deformation of eukaryotic cell is larger than that of a prokaryotic cell. The sedimentation of denser particles was simulated by using IBM (Ghosh and Stockie 2015). Sun and Bo (2015) made use of combined IBM-LBM approach along with finite element method (FEM) to study the migration of spherical particle of different sizes. Jiang et al. (2016) simulated the inertial migration of single spherical particle in a symmetric serpentine channel with the aid of combined LBM-IBM-FEM approach. In high sufficient Re (more than 250) the particle overcame the inertial lift by the dominant drag force. The equilibrium position shifted towards the centre at that scenario. Banaei et al. (2017) presented a study which focused on motion of elastic capsule in fluid flow with stiff nucleus in it. It was modelled as a eukaryotic cell. The fluid-structure coupling was done using IBM. They found that the deformation of eukaryotic cell is larger than that of a prokaryotic cell. Lashgari et al. (2017) used IBM to study the inertial migration of single ellipsoidal particle in straight duct in which the particle is released from a position which is far away from the centre of the duct where velocity is low. Yuan et al. (2018) combined IBM with LBM and simulated the inertial migration of single spherical particle in three-dimensional rectangular microchannel. It was noticed that as Re increased, the equilibrium position shifted towards the wall. But when Re is greater than 200, the equilibrium position is shifted gradually away from the wall. This is due to the formation of secondary vortices around the particle at that Re value. These vortices tend to drive the particle away from the wall. The IBM scheme was developed and some of its other versions were proposed by some authors. The feedback forcing based IBM is such a scheme which was developed in 2007.

Huang et al. (2007) made use of feedback forcing based IBM to study the characteristics of flexible filaments in uniform flow. The bi-stable properties of the filaments were also observed in this work. Shin et al. (2008) compared both Peskin's and feedback forcing based IBM schemes and tabulated their advantages and disadvantages over one another. The stability regime of different type of Dirac delta functions with feedback forcing based IBM were also studied in this work. Uddin et al. (2015) made use of feedback forcing based IBM for the simulation of flexible tandem filaments in a viscous flow. It was mainly focused on studying the interaction between the wings and the

vortices. The upstream flapping went on uniform flow whereas the downstream flapping went on according to the heaving and pitching motion of the wings.

Song et al. (2011) studied the migration of two-dimensional elastic circular capsule in moderate Re (1-40) viscous shear flow. The swinging and tumbling motion of particle was captured in this work. Shin and Sung (2012) simulated the lateral migration of elastic capsule in two-dimensional domain with the help of feedback forcing based IBM for Re range of 10-100. The inclination angle of the capsule became small as Re increased and the equilibrium position of particle is unaffected by initial position of release of particle. The inertial migration of three-dimensional elastic capsule was simulated by Kim et al. (2015) with the aid of penalty IBM with feedback forcing scheme. They confirmed the fact that initial behaviour of the capsule depends on the initial position of release of particle whereas the equilibrium position does not depend upon the same.

2.4 Research gap and critical review

The literature review shows that, majority of the works are addressed on spherical particle lateral migration in straight channels. However, the emergence of inertial microfluidics has put forward some non-straight channel configurations like serpentine (Liu et al. 2018) and spiral (Wu et al. 2012). The behaviour of lateral migration in straight and non-straight channels are different. The presence of recirculation zones in the non-straight channels should be the reason behind this phenomenon. The secondary flows inside non-straight channels can alter the symmetry of lift forces exerted on the particle by the addition of more viscous drag force on it and by the virtue of that modified equilibrium positions can be attained (Warkiani et al. 2014). Still, instead of constructing complex shaped channels the secondary flows can be generated in a channel by adding grooves or projections inside (Jiang et al. 2016). Mao and Alexeev (2011) simulated single spherical particle (rigid) migration in microchannel with added ridges in it (with help of LBM).

It should be also reminded that, most of the previous research concentrated on neutrally buoyant particle migration. It is interesting to see the effect of the mass of the particle in the inertial migration dynamics and equilibrium position. (Akhatov et al. 2008) implemented theoretical analysis on the migration of massive aerosol particles in

straight channels. Qian, et al. (2021) simulated the migration of aerosol particles whose densities were very much higher than the air through which they were moving. When the particles became neutrally non-buoyant, the effect of the buoyant force also came into play. Hence, along with shear and wall lift forces, the buoyancy force will also significantly affect the equilibrium position. The buoyancy force acts against the induced wall lift. However, the emergence of another force, called the Saffman lift, acts as a reactive force against the buoyancy force. The Saffman lift force depends on the relative velocity of the particle with respect to the fluid and it increases when the (particle to fluid) density ratio becomes higher. Hence, the equilibrium position shifts to the top wall when density ratio increases beyond a particular value.

It also shows that, there are large number of works in migration of circular and spherical particles in fluid flow. However, very few studies are reported on inertial migration of different shaped particles other than circular and elliptical.

The previous works already been stated that the equilibrium position depends on flow velocity, particle size and channel dimensions. However, if it is possible to direct the particles towards an equilibrium position at a particular desired location in the channel, irrespective of all other flow parameters, then it can lead to significant advances in the design of separation devices. (Schaaf and Stark 2017) applied an axial force in the flow, in such a way that deformable particles attained equilibrium positions at the lower end of the channel. The same was later achieved for neutrally buoyant rigid particles (Prohm and Stark 2014). (Prohm et al. 2014) utilised external torque to drive the particles and attain an equilibrium position at a particular location. The common characteristic in these works is that all researchers tried to apply the control force in such a manner that the particles attained an equilibrium position at the extreme ends of the channel. Also, the particles considered were neutrally buoyant. The centre of the channel is another important location where separation can take place. However, until now, no works have been reported on the application of control force to bring non-neutrally buoyant rigid particles to the channel centre in inertial migration.

The interaction of multiple particles in inertial migration is not much studied yet in previous works. It will be interesting to see what changes will be brought by interaction of multiple particles in inertial migration dynamics.

Instead of running numerical simulations for a large number of test cases, suitable prediction models can be created with the aid of algorithms like artificial neural network (ANN) and linear regression (LR). Kanchan and Maniyeri (2020) combined IBM simulation data with ANN algorithm to generate a prediction model for flowrate pass a flexible membrane. Hence, it was proved that IBM data can be easily coupled with ANN and other type of machine learning algorithms (linear regression (LR)) for development of prediction models. These prediction models can have large impact on future design of suitable inertial migration aided separation devices. Gaining motivation from the above points the following objectives are formulated and presented below.

2.5 Objectives

The objective of the present thesis is divided into five parts and they are given below.

- To study the inertial migration of rigid neutrally buoyant cylindrical particle in a straight channel in both Poiseuille and shear flows using feedback forcing based IBM model.
- To analyse the inertial migration dynamics of single neutrally buoyant cylindrical particle in non-straight channels such as constricted and stepped channel.
- To study the lateral migration of various shaped particles (neutrally buoyant and massive) in straight channel.
- To analyse the effect of control force over inertial migration dynamics related parameters of single massive particle migrating in Poiseuille and pulsatile flows.
- To study the multiple particle migration in straight and non-straight (stepped and slit) channels.

Additionally, suitable prediction models will be developed with the help of ANN and LR coupled with IBM simulation data to assess the inertial migration dynamics.

CHAPTER 3. INERTIAL MIGRATION OF PARTICLE IN STRAIGHT CHANNEL

In this chapter, inertial migration of single neutrally buoyant rigid cylindrical particle in a straight channel is discussed. Two flow conditions such as Poiseuille and shear flow are considered. More details are given below.

3.1 Background

Inertial migration is a type of movement experienced by particles suspended in flowing fluid. The inertial migration occurs by two lift forces which are exerted by fluid on a particle that migrates in flow. The parabolic velocity profile of fluid creates induced shear lift which drags the particle close to nearer channel wall. On the flip side, induced wall lift appears because of bulk flow of shear adjacent to the wall which acts in opposite direction to the former force. The particle flows in lateral direction up to a particular point called equilibrium position at which these two forces get canceled each other. The time taken by particle to acquire equilibrium position is termed as migration time. These two parameters are dependent on channel dimension, particle size, and conditions of flow. The inertial migration depends completely upon the conditions of fluid flow and dimensions of channel and particle. Hence, it can be adopted as a passive separation technique (separation category which does not require any external forces like electricity, acoustics, magnetic force, etc.) for various particles in the fields of biomedical engineering and microfluidics. This includes separation of red blood corpuscles, platelets, bioaerosol, pathogenic bacteria, viruses and non-motile cells (Bazaz et al. 2020). For effective particle separation which is aided by inertial migration, knowledge of equilibrium position and migration time is a necessary criterion.

Direct numerical simulations were carried out on inertial migration of spherical particle by determination of the lift force and velocity at a specific point (Carlo et al. 2009). The advantage of this method is that it could avoid problems aroused during re-meshing at each step. Newton's second law was used to obtain both the translational and angular velocity of particle. Hu et al. (1992) used Arbitrary Lagrangian Eulerain (ALE) method to simulate the fluid-particle interactions. The surface velocity is calculated from translational and angular speed and radial distance from center. Each of these

parameters are updated at every iteration. Yang et al. (2005) made use of ALE method to find the lift force over spheres in fluid flow. Pan and Glowinski utilized fictitious domain method to imitate the lateral migration of neutrally buoyant cylinders (Pan and Glowinski 2002). The domain inside particle is included in the mesh unlike ALE method and a force is applied to it to conserve rigidity of particle.

Lattice Boltzmann method (LBM) is efficient in case of tracking particle dynamics in domains where solid-fluid interphases are present (Aidun and Clausen 2010). Ladd (1994) investigated about equilibrium position of spherical particle in square channel at Re range of 100-1000 with the aid of LBM. Inamuro et al. (2000) used LBM to simulate the migration of neutrally buoyant cylinders. The nine-point model was used in this work and they noticed that for a particular aspect ratio and diametrical ratio equilibrium positions of all cylindrical particles were in line. Chun and Ladd (2006) simulated the migration of non-spherical particles using LBM and found that at high Re greater than 750 equilibrium position obtained is very much close to wall and it does not change with increase of Re further. Fox et al. (2020) studied the inertial bifurcation of circular cylindrical particle in shear flow with aid of LBM. A critical particle Re was determined above which particle will undergo a pitching bifurcation or in other words equilibrium position shifts away from center of channel.

The overlapping grid method was chosen for simulating lateral migration of cylindrical particles and special disk like particles (Su et al. 2018). The characteristic of this method is that it uses an overlapped grid which consists of four types of grids. They are, general Cartesian grid system, body fitted grids for particles and fine grids at the poles of particles. They found that surface stresses at the ends of particles play an important role in migration. It was also observed that equivalent diameter of particle was seen to be increasing as Re increases. Direct numerical simulations are carried out on inertial migration of both neutrally and non-neutrally buoyant cylindrical particles in shear flow and it was observed that equilibrium position of particles was seen to be at the center of channel for the shear flow case (Huang et al. 1997). The migration of spherical particle in a serpentine channel was examined by Liu et al. (2018). It was observed that for high Re, equilibrium position did not change with the variation in initial position of release of particle.

From the literature review, it is evident that most of studies pertinent to inertial migration are done for rigid spherical particles. Only limited number of works have been reported for non-spherical rigid particles. Further, numerical simulations are essential in understanding the migration dynamics under different fluid flow conditions and channel configurations to explore phenomena of inertial migration which will assist in development of efficient microfluidic separation devices. Since the underlying physics behind inertial migration mainly involves fluid-structure interaction, as stated in chapter 2 (section 2.3), immersed boundary method (IBM) will be an efficient numerical tool to investigate this problem. In most of the literatures, three-dimensional numerical models are reported for simulation of inertial migration which demands large computational time and associated complexities. In addition, the time taken to reach equilibrium position (migration time) which plays an important role in separation of particles is not much taken into consideration by previous authors. It is observed that an immersed boundary model which is frequently used in computational fluid dynamics to capture the fluid-structure interaction to investigate inertial migration of cylindrical particle in straight channel has not been reported so far in literatures.

Deriving motivation from these, in this chapter, a two-dimensional computational model based on feedback forcing IBM is proposed to investigate inertial migration dynamics of rigid neutrally buoyant cylindrical particle under Poiseuille and shear flow in a straight channel. Using the developed model, inertial migration will be explored for case of initial position of release and diameter of particle, height of channel and Re. Finally, a prediction model for equilibrium position and migration time of cylindrical particle residing in Poiseuille flow in a straight channel is developed using ANN algorithm. The methodology and governing equations are given in section 3.2. The simulation results are discussed in section 3.3.

3.2 Methodology

The physical domain contains a neutrally buoyant cylindrical particle of diameter d which is released in two types of flow conditions namely Poiseuille and shear flow (figures. 3.1 and 3.2 respectively).

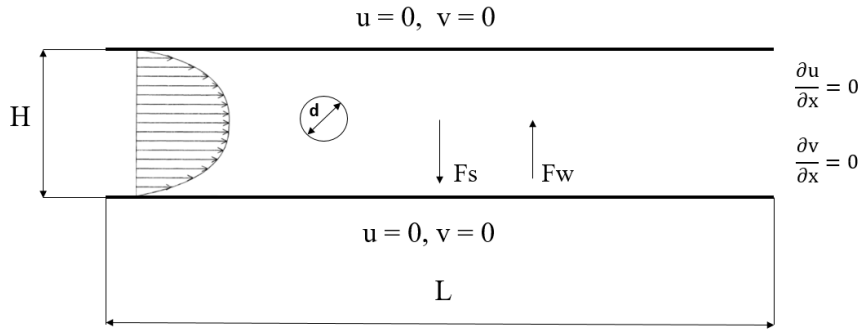

Figure 3.1 Physical model of migration of particle in Poiseuille flow

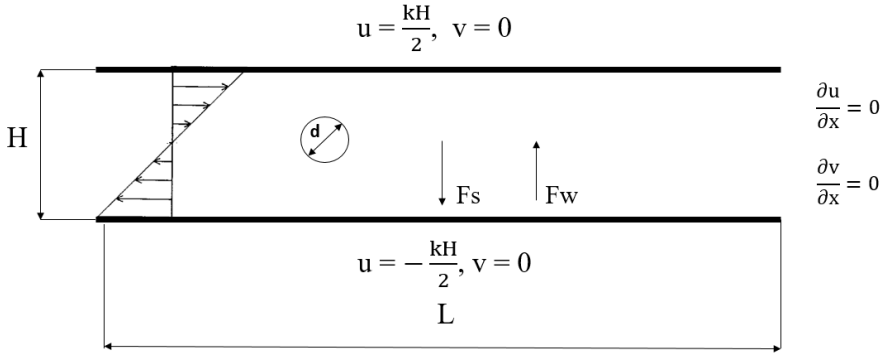

Figure 3.2 Physical model of migration of particle in shear flow

In figure 3.2, k is the shear rate and it is double of ratio of velocity of wall and height of channel H.

The boundary conditions for above three flow conditions are shown in table 3.1.

Table 3.1 Boundary conditions

Type of flow	Inlet	Outlet	Top wall	Bottom wall
Poiseuille flow	6.0(y/H)(1-(y/H)) y=0 to H	$\frac{\partial u}{\partial x} = 0, \frac{\partial v}{\partial x} = 0$	u=0, v=0	u=0, v=0
Shear flow	k(y-H/2) y=0 to H	$\frac{\partial u}{\partial x} = 0, \frac{\partial v}{\partial x} = 0$	u=kH/2, v=0	u=-kH/2, v=0

There are two grid systems in immersed boundary framework. The fluid grid system is represented by Cartesian coordinates **x*** = (x*, y*). On the other hand, Lagrangian coordinate system **X***(s*, t*) is used to represent particle (structure), where, s* and t* represent material point and time respectively. The superscript * is used to indicate

dimensional quantity. The fluid velocity $\mathbf{u}^*(\mathbf{x}^*, t^*)$, pressure $p^*(\mathbf{x}^*, t^*)$ and Eulerian force density $\mathbf{f}^*(\mathbf{x}^*, t^*)$ are flow variables whereas, Lagrangian force density $\mathbf{F}^*(s^*, t^*)$ is structural variable. The continuity and Navier-Stokes (N-S) equations for fluid flow are given by,

$$\nabla^*.\mathbf{u}^* = 0 \tag{3.1}$$

$$\rho_f \frac{\partial \mathbf{u}^*}{\partial t^*} + \mathbf{u}^*.\nabla^*\mathbf{u}^* = -\nabla^* p^* + \mu\nabla^{*2}\mathbf{u}^* + \mathbf{f}^*(\mathbf{x}^*, t^*) \tag{3.2}$$

where, ρ_f and μ are the density and dynamic viscosity of fluid. Equations (3.1) and (3.2) are non-dimensionalized with respect to the characteristic length (height of channel) and characteristic velocity (maximum channel velocity).

The dimensionless continuity and N-S equations are given by,

$$\nabla.\mathbf{u} = 0 \tag{3.3}$$

$$\frac{\partial \mathbf{u}}{\partial t} + \mathbf{u}.\nabla\mathbf{u} = -\nabla p + \frac{1}{Re}\nabla^2\mathbf{u} + \mathbf{f}(\mathbf{x}, t) \tag{3.4}$$

where $Re = \rho_f u_{ref} H/\mu$, where u_{ref} is the maximum channel velocity and particle Reynolds number $Re_P = Re\,(d/H)^2$ (Choi and Kim, 2010). The non-dimensionalized N-S equations are discretized by finite volume method (FVM) on a staggered Cartesian grid system and semi-implicit scheme is used for time marching as given below.

$$\frac{\mathbf{u}_{i,j}^{n+1} - \mathbf{u}_{i,j}^{n}}{\Delta t} + N(\mathbf{u}^n) = -\left(\frac{\partial p}{\partial x_i}\right)^n + \frac{1}{2Re}(\nabla^2\mathbf{u}^{n+1} + \nabla^2\mathbf{u}^n) + \mathbf{f}(\mathbf{x}, t) \tag{3.5}$$

where, $N(\mathbf{u}^n)$ is the nonlinear convection term.

The Eulerian force density $\mathbf{f}(\mathbf{x}, t)$ is calculated by the interpolation of Lagrangian force with Dirac delta function δ (Shin et al. 2008).

$$\mathbf{f}(\mathbf{x}, t) = \int \mathbf{F}(s, t)\,\delta(\mathbf{x} - \mathbf{X}(s, t))\,ds \tag{3.6}$$

where, size of Lagrangian grid is represented by ds.

The feedback forcing scheme is utilized to compute the Lagrangian force (Huang et al. 2007).

$$\mathbf{F}(s, t) = \alpha \int (\mathbf{U}_{ib} - \mathbf{U})\Delta t + \beta(\mathbf{U}_{ib} - \mathbf{U}) \tag{3.7}$$

Where $\mathbf{U}_{ib}$ is the interpolated immersed boundary velocity from fluid velocity according to equation (3.8), α and β are large negative constants and **U** denotes velocity of particle (Shin et al. 2008).

$$\mathbf{U}_{ib}(s, t) = \int \mathbf{u}(\mathbf{x}, t)\, \delta(\mathbf{x} - \mathbf{X}(s, t))\, d\mathbf{x} \tag{3.8}$$

where, Eulerian grid size is represented by d**x**.

The four-point Dirac delta function is used here for the interpolation and it is given by (Peskin 2002),

$$\delta(\mathbf{x}) = \frac{1}{h^2}\, \emptyset\left(\frac{x}{h}\right)\, \emptyset\left(\frac{y}{h}\right) \tag{3.9}$$

where, h is the Eulerian grid spacing and ∅ is given by,

$$\emptyset(r) = \begin{cases} \frac{1}{8}(3 - 2|r| + \sqrt{1 + 4|r| - 4r^2} & \text{for } 0 \leq |r| \leq 1 \\ \frac{1}{8}(5 - 2|r| + \sqrt{-7 + 12|r| - 4r^2} & \text{for } 1 \leq |r| \leq 2 \\ 0 & \text{for } |r| > 2 \end{cases} \tag{3.10}$$

The four-point Dirac delta function is selected because it has larger stability regime compared with two, three and six. The velocity of particle **U** is composed of translational ($\mathbf{U}_p$) and angular ($\boldsymbol{\omega}_p$) velocities as given below,

$$\mathbf{U} = \mathbf{U}_p + \boldsymbol{\omega}_p\, (\mathbf{X} - \mathbf{X}_C) \tag{3.11}$$

where, $\mathbf{X}_C$ is the center of particle.

$\mathbf{U}_p$ and $\boldsymbol{\omega}_p$ are calculated from Newton's equations of motion in the dimensionless form (Feng and Michaelides 2004, 2009).

$$\mathbf{U}_p{}^{n+1} = \mathbf{U}_p{}^{n} + \frac{1}{m_p}[\sum(-\mathbf{F}(s,t)ds)]\Delta t + \frac{\rho_f}{\rho_p}\left(\mathbf{U}_p{}^{n} - \mathbf{U}_p{}^{n-1}\right) + \left(1 - \frac{\rho_f}{\rho_p}\right)\mathbf{g}\Delta t \tag{3.12}$$

$$\boldsymbol{\omega}_p{}^{n+1} = \boldsymbol{\omega}_p{}^{n} + \frac{1}{I_p}[\sum(-\mathbf{F}(s,t)(\mathbf{X}(s) - X_c)ds)]\Delta t + \frac{\rho_f}{\rho_p}(\boldsymbol{\omega}_p{}^{n} - \boldsymbol{\omega}_p{}^{n-1}) \tag{3.13}$$

where, I_p and m_p are the dimensionless mass moment of inertia and mass of particle respectively. In the present work, neutrally buoyant particle is considered and hence $\frac{\rho_f}{\rho_p}$ is set to 1.0. The position of particle is updated by (Huang et al. 2007),

$$\mathbf{X}^{n+1}(s) = \mathbf{X}^{n}(s) + \mathbf{U}\Delta t \tag{3.14}$$

This will give trajectory of particle in fluid flow. The discretized equations are solved using semi-implicit fractional step-based algorithm (Maniyeri and Kang 2014; Maniyeri and Kang 2012). The Eulerian force density **f** (x, t) is calculated from equation (3.6) and then equation (3.5) is solved using incomplete Cholesky conjugate gradient (ICCG) method to obtain the intermediate velocity. The pseudo-pressure is calculated from intermediate velocity by equation (3.15) by ICCG method.

$$\nabla^2 {P_S}^{n+1} = \frac{1}{\Delta t}(\nabla . \mathbf{u}^{n+1}) \tag{3.15}$$

where P_S is the pseudo-pressure. The pseudo-pressure is then utilized to obtain actual velocity and pressure of fluid as shown in equations (3.16) and (3.17).

$$\mathbf{u}_a{}^{n+1} = \mathbf{u}^{n+1} - \Delta t \, \nabla {P_S}^{n+1} \tag{3.16}$$

$$P^{n+1} = P^n + {P_S}^{n+1} - \frac{1}{2} \nabla^2 {P_S}^{n+1} \tag{3.17}$$

where $\mathbf{u}_a$ represents actual velocity of fluid. A FORTRAN code is developed to solve the resulting system of equations. The algorithm is shown in figure 3.3.

3.3 Results and discussion

The inertial migration of single rigid neutrally buoyant cylindrical particle in both Poiseuille and shear flow are simulated and the results are discussed in following sections.

3.3.1 Migration of particle in Poiseuille flow

A two-dimensional numerical model is developed with the use of immersed boundary finite volume method based on feedback forcing scheme to investigate the migration of a neutrally buoyant rigid cylindrical particle in straight channel as shown in figure. 3.1. A dimensionless domain of 50 x 1 is selected in which a cylindrical particle of diameter 0.25 is released. The time step taken is 0.001 and value of α and β are taken as -4000.0 and -40.0 respectively (Shin et al. 2008).

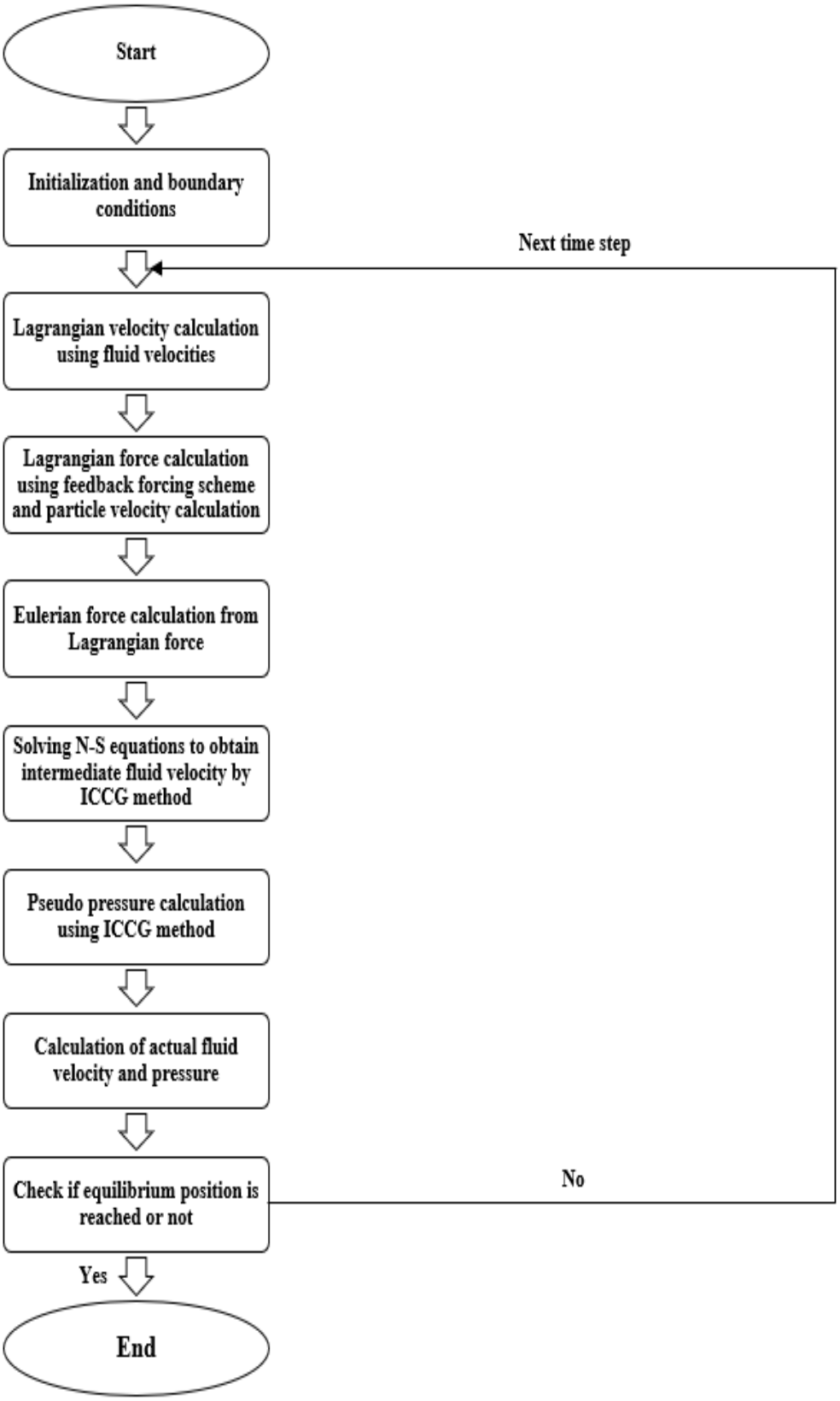

Figure 3.3 Flowchart of computational procedure

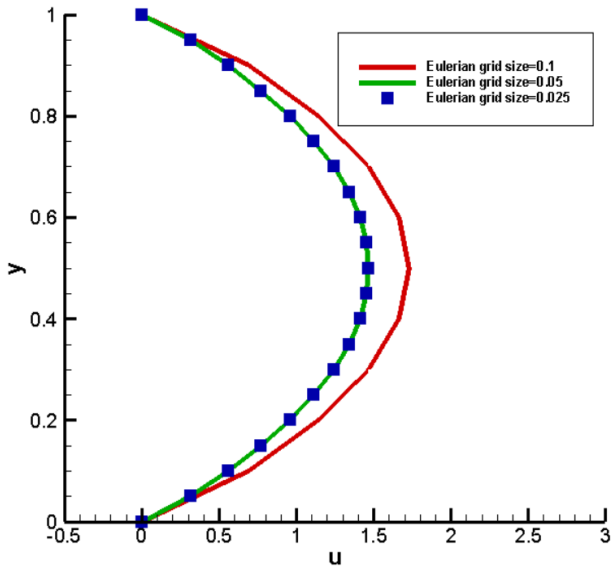

Figure 3.4 The grid independence test (Re=12.786, d=0.25). The midline fluid velocity(x-component) after particle attained equilibrium position is plotted against y

First of all, grid independence test is carried out for three different uniform Eulerian grid sizes 0.1, 0.05 and 0.025 for Re=12.786. The x-component of fluid velocity at the centreline of channel is plotted against height of channel in figure 3.4 when particle reached equilibrium position for the case of inertial migration in the straight channel under Poiseuille flow (refer to figure 3.1). It can be depicted from figure 3.4 that the centreline velocity pattern coincides for grid sizes 0.05 and 0.025. Hence 0.05 is chosen as the optimum Eulerian grid size due to reduced computational cost compared with 0.025.

In the next phase, numerical simulations are performed to explore particle migration when it is released from a position of (1.0, 0.4) (position of centre of particle) in channel. The particle stops lateral migration at equilibrium position. The shear induced and wall induced lifts are balanced at this position. The lateral coordinate of centre of particle is taken as equilibrium position when it reaches a position where lift forces are balanced. Through numerical simulations using the developed model, initial and final positions of particle for Re=12.786 is captured and are shown in figure 3.5. Further, the lift and drag forces (F_l and F_d respectively) are calculated and plotted against the lateral

and horizontal (Y_C and X_C respectively) positions of particle respectively in Figures 3.6a) and 3.6b).

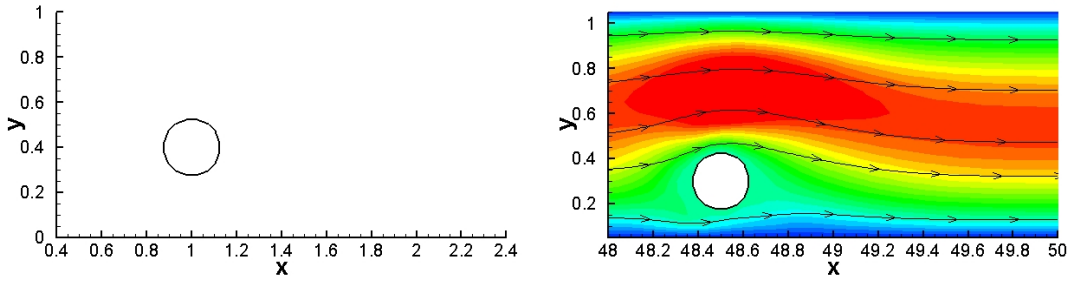

Figure 3.5 a) The initial position (1.0, 0.4) b) final position with u velocity contour of particle (48.45, 0.297)

The lateral coordinate of particle where lift forces are balanced is used to represent equilibrium position of particle. The lift force reaches zero at a position around 0.297 which is almost 0.6 times half of the height of channel. This indicates that the lift forces are balanced at this point and hence Segre-Silberberg effect is satisfied (Inamuro et al. 2000). However, the drag force does not approach zero and this indicates that even after particle attains equilibrium position it still moves in the horizontal direction in the case of Poiseuille flow. It is to be noted that equilibrium position is indicated by Y_{EQ}. The migration time is represented by t_m.

In the next step, trajectory of neutrally buoyant particle is traced for two different particle diameters (0.25 and 0.35) as shown in figure 3.7. The initial position of particle remains the same in all cases: (1.0, 0.4).

The particle lateral position becomes constant after a particular horizontal position. The particle stops lateral movement after this point and it is known as equilibrium position (Y_{EQ}). The values of equilibrium positions for two diameters are given in Table 3.2 and compared with those in Huang et al. (2021). The values are in good agreement.

Moving forward, the effect of different parameters like Re, initial position and diameter of particle and height of channel on equilibrium position and migration time are investigated.

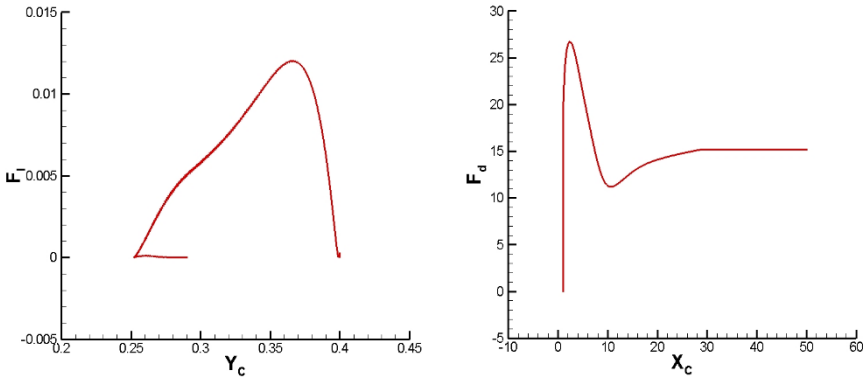

Figure 3.6 a) The variation of lift force, F_l with y coordinate of particle centre, Y_C at Re=12.786 b) The variation of drag force, F_d with x coordinate of particle centre, X_C at Re=12.786

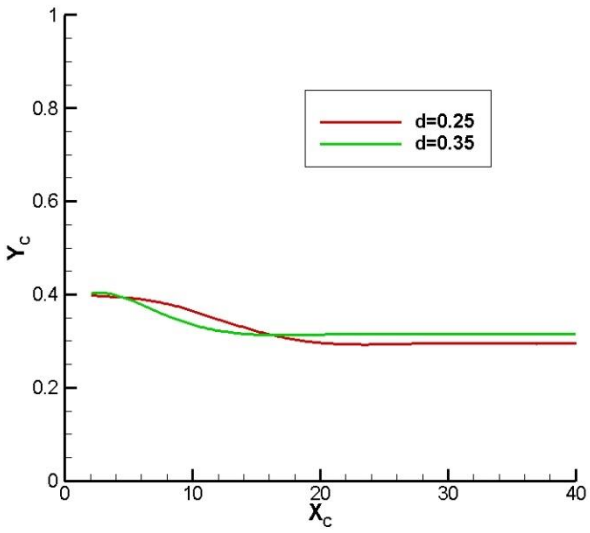

Figure 3.7 Particle trajectory for two different diameters 0.25 and 0.35 (Re=50.0)

Table 3.2 Comparison of equilibrium positions Y_{EQ} of particle in Poiseuille flow for two diameters observed in the present work with that of (Huang et al.2021) (Re=50.0)

d	**Y_{EQ}** (Huang et al. 2021)	**Y_{EQ} (Present study)**
0.25	0.291	0.293
0.35	0.313	0.316

3.3.1.1 Effect of Re

The particle migration is simulated for three different Re 12.786, 27.727 and 96.74. The particle is released from an initial position of (1.0, 0.4) and the diameter of particle is fixed as 0.25 in each case. The height of channel is kept constant as 1.0. The particle trajectory for the corresponding Reynolds numbers are shown in figure 3.8.

The trajectory of y coordinate of centre of particle which is released from the initial position (1.0, 0.4) with time is shown in figure 3.8 for three different Re (12.786, 27.727 and 96.74). From figure 3.8 it can be understood that equilibrium position of particle is shifted towards the bottom wall as Re increases. This may be due to the fact that high Re (high velocity) create a rise in shear induced lift and hence it becomes more dominant force than wall induced lift. Also, it should be noted that as Re increases the resistance between fluid layers will decrease hence it will result in a rise in slip velocity (relative velocity of particle with fluid), so equilibrium position goes downward to the bottom wall as Re increases. In table 3.3, migration time t_m of particle under three Re considered, is presented. As mentioned before, increase in slip velocity of particle becomes reason for reduction in migration time for case of high Re=96.74.

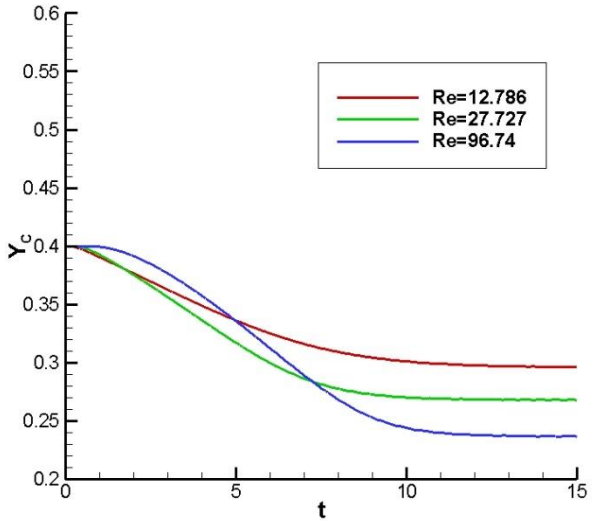

Figure 3.8 The trajectory of particle centre with time for Re= 12.786, 27.727 and 96.74 for the initial position (1.0, 0.4) and d=0.25

Table 3.3 Time taken to attain equilibrium position for three Re for d=0.25

Re	t_m
12.786	**13.768**
27.727	**12.891**
96.74	**12.358**

3.3.1.2 Effect of initial position

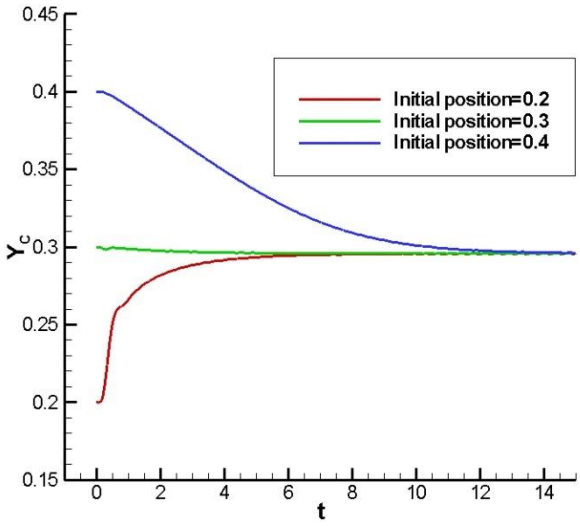

Figure 3.9 The trajectory of particle centre with time for three different initial positions at Re=12.786 and d=0.25

Further, numerical simulations are employed to investigate the influence of initial positions of particle release. The particle (diameter 0.25) starts from three separate initial positions (1.0, 0.2), (1.0, 0.3) and (1.0, 0.4) for Re=12.786. The height of channel is kept constant as 1.0. Figure 3.9 depicts the trajectory of particle with time for three initial positions. For the three initial positions considered, particle migrates to the same equilibrium position. The shear and wall induced lifts depends upon flow and channel parameters mainly such as flow Reynolds number, particle diameter and channel height. The particles will migrate to the same equilibrium position independent of the initial position of release. Hence, it can be concluded that the initial position of release of

particle do not have much significance in particle migration. The above results are in accordance with the findings of (Inamuro et al. 2000; Pan and Glowinski 2002).

3.3.1.3 Effect of diameter of particle

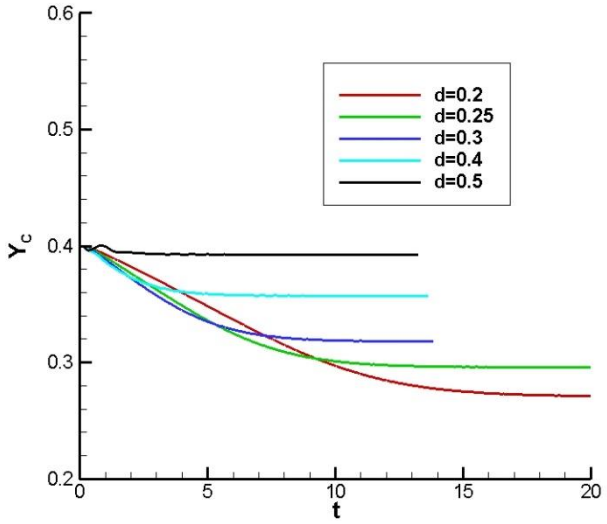

Figure 3.10 The trajectory of particle centre with time for various diameters of particle at Re=12.786 for the initial position of release (1.0, 0.4)

The effect of diameter of particle on equilibrium position and migration time is analysed by varying the diameter from 0.2 to 0.5. The Re is taken as 12.786 and the height of channel is 1.0 for all sizes of particle. The particle is released from (1.0, 0.4) in all cases. The particle trajectories can be observed from figure 3.10. It can be noticed from figure 3.10 that equilibrium position shifts towards the bottom wall with the decrease in diameter of particle. The dimensionless mass of particle is directly proportional to its diameter. Hence, the reduction in particle diameter will also reduce its mass. The particle velocity on the other hand increases with reduction in mass of particle (equation (3.12)). The increase in particle velocity will rise the effect of shear induced lift and it will drive equilibrium position towards lower wall. The variation of migration time with diameter is shown in table 3.4. The migration time reduces as diameter of particle increases. As the diameter of particle increases the distance between channel wall and particle decreases. This leads to increase in effect of wall induced lift. Hence, the balance of shear and wall induced lifts occur at a faster rate as diameter becomes larger and equilibrium position is attained faster.

Table 3.4 Migration time for different diameters of particle at Re=12.786

d	t_m
0.2	**19.781**
0.25	**13.768**
0.3	**10.409**
0.4	**6.107**
0.5	**3.290**

3.3.1.4 Effect of height of channel

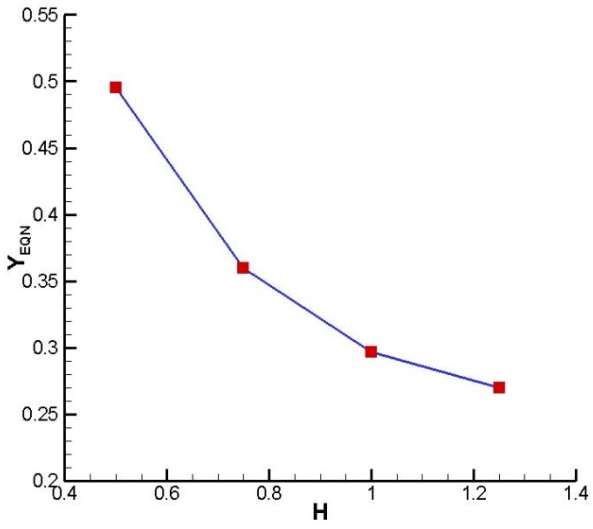

Figure 3.11 Variation of normalised equilibrium position with height of channel for Re=12.786 and d=0.25

The effect of height of channel wall (H) on inertial migration of particle is studied and the results obtained through numerical simulations are shown in figure 3.11. In this case, particle of diameter 0.25 is released from initial position of (1.0. 0.4) in channel and Re remains as 12.786 in all cases. The height of channel is varied from 0.5 to 1.25. For the comparison of equilibrium position in channels of different heights a new parameter called normalised equilibrium position Y_{EQN} is introduced. It is the ratio of equilibrium position Y_{EQN} and height of channel H. As height of channel increases

equilibrium position shifts towards the bottom wall. The height of channel changes while the diameter of particle remains constant. Hence, as height of channel increases the distance between channel wall and particle increases which in turn increases effect of shear induced lift and equilibrium position shifts towards lower wall. However, the increase in height of channel lags time for balancing of induced lifts because of increase in distance of particle from wall. Hence, migration time increases as height of channel increases which can be observed from table 3.5.

Table 3.5 Migration time for different height of channel for Re=12.786 and d=0.25

H	t_m
0.5	**6.012**
0.75	**7.283**
1.0	**13.768**
1.25	**20.112**

3.3.2 Migration of particle in shear flow

In the next stage, developed computational model is employed to study inertial migration of single rigid neutrally buoyant cylindrical particle in simple shear flow as shown in figure 3.2. The particle is released from an initial position of (25.0, 0.4) in a dimensionless channel of 50 x 1 for Re= 12.786 and equilibrium position achieved by particle at the end of simulation is shown in figure 3.12. The shear rate used is 1.0 and diameter of particle is taken as 0.25.

The particle reaches an equilibrium position around the centre of channel. A similar observation was reported in the works of Huang et al. (1997). Figure 3.13 a) exhibits the variation of lift force with y coordinate of centre of particle and it can be inferred that the lift force becomes zero at equilibrium position of 0.529. It is also to be noted that the drag force also become zero at equilibrium position (Fig. 3.13 b)). In case of shear flow, the velocity of flow is zero at channel centre. Due to zero-flow velocity particle will also stop moving when it reaches channel centre. It implies that particle attains equilibrium position close to the centre of channel when it is released in shear flow. This may be the reason for zero drag and lift forces at channel centre as shown in

figure 3.13 a) and b). In the next stage, effect of parameters like Re, initial position of release and diameter of particle, height of channel and shear rate on equilibrium position and migration time is analysed.

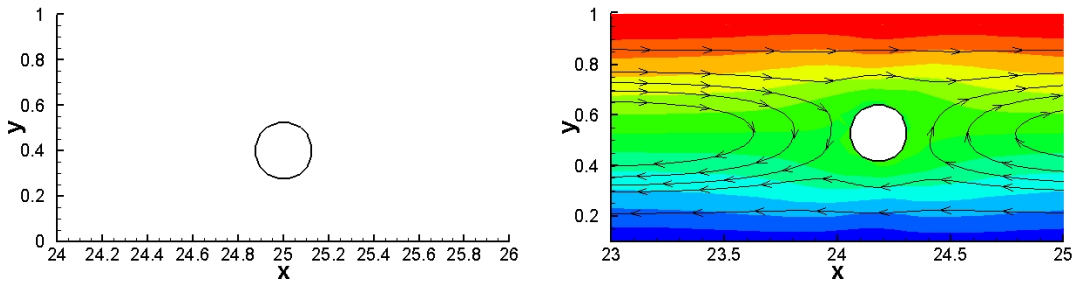

a) b)

Figure 3.12 a) The initial (25.0, 0.4) and b) final position with u velocity contour (24.121, 0.529) of particle at Re=12.786 and d=0.25

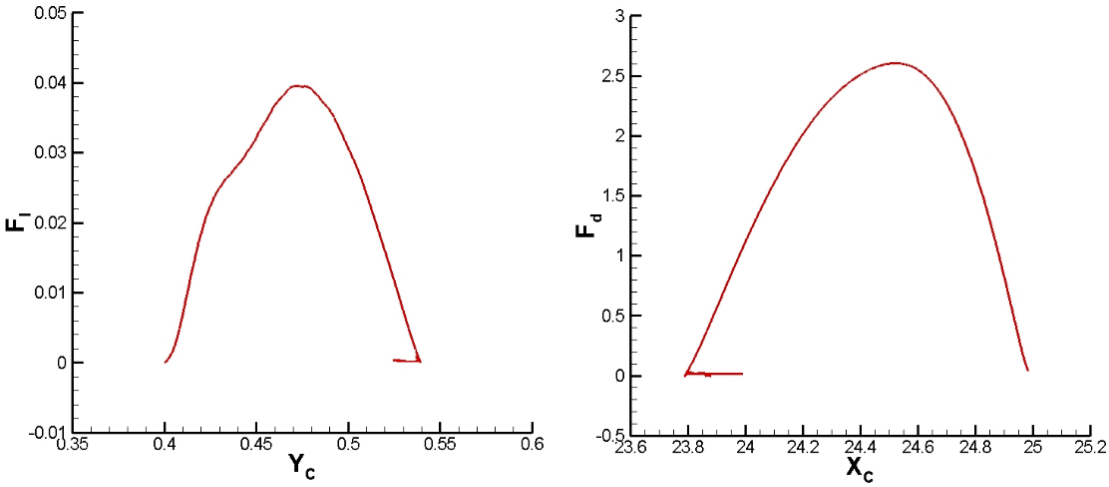

a) b)

Figure 3.13 a) The variation of lift force with y coordinate of centre of particle for shear flow b) The variation of drag force with x coordinate of centre of particle for shear flow at Re=12.786 and d=0.25

3.3.2.1 Effect of Re

The particle migration in shear flow is simulated for four Re 1.0, 2.5, 5.0 and 12.786. The particle is released from an initial position of (25.0, 0.4) and the diameter of particle

is taken as 0.25 in all cases. The height of channel is kept constant as 1.0. The trajectory of centre of particle is captured and is shown in figure 3.14.

Numerical simulations are performed to predict the effect of Re under imposed shear flow. It is interesting to see that equilibrium position of particle does not vary much when Reynolds number increases and it is always close to the centre. Similar observation was presented by Huang et al. (1997). In shear flow, stable position for a particle is at centre. The upper and lower walls move in opposite direction with same magnitude of velocity in shear flow. Due to this action, velocity of flow become zero at centre. Hence, drag and lift forces over particle by the fluid will become zero at channel centre. It will make shear and wall induced lifts negligible and particle will stop moving in either vertical or horizontal directions in channel. Hence, equilibrium position is found to be observed at centre of channel. The results are tabulated and compared with that of Huang et al. (1997) in Table 3.6. The results are found to be in good agreement. The migration time is computed for different Re and is tabulated in table 3.7. Because of a rise in slip velocity with increase in Re of particle, migration time decreases with increase in Re and it is clear from table 3.7.

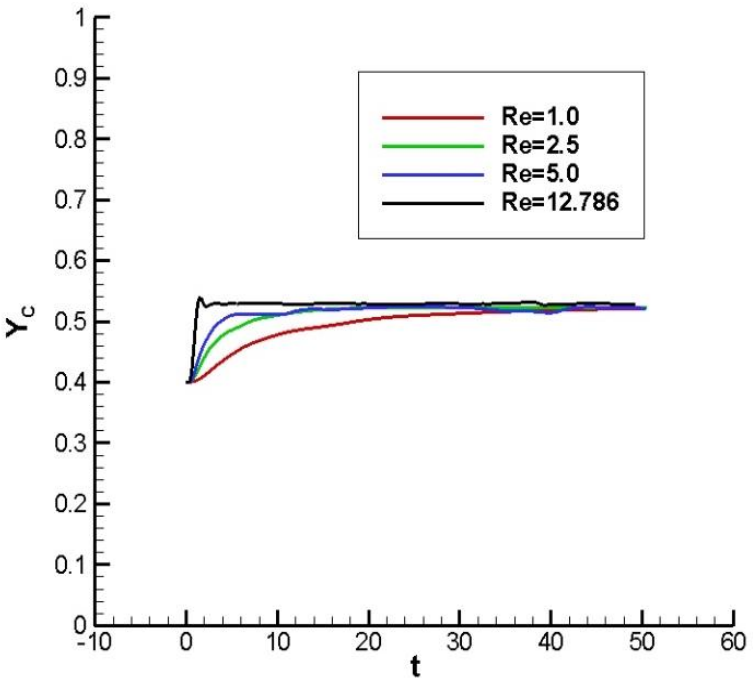

Figure 3.14 The variation of y coordinate of centre of cylinder with time for Re= 1.0, 2.5, 5.0 and 12.786

Table 3.6 Validation of results for shear flow for d=0.25

Re	Y_{EQ} (Huang et al. 1997)	Y_{EQ} (Current work)
1.0	0.496	**0.519**
2.5	0.498	**0.523**
5.0	0.500	**0.524**

Table 3.7 Time taken to attain equilibrium position for d=0.25

Re	t_m
1.0	**42.150**
2.5	**24.510**
5.0	**15.426**
12.786	**9.975**

3.3.2.2 Effect of initial position

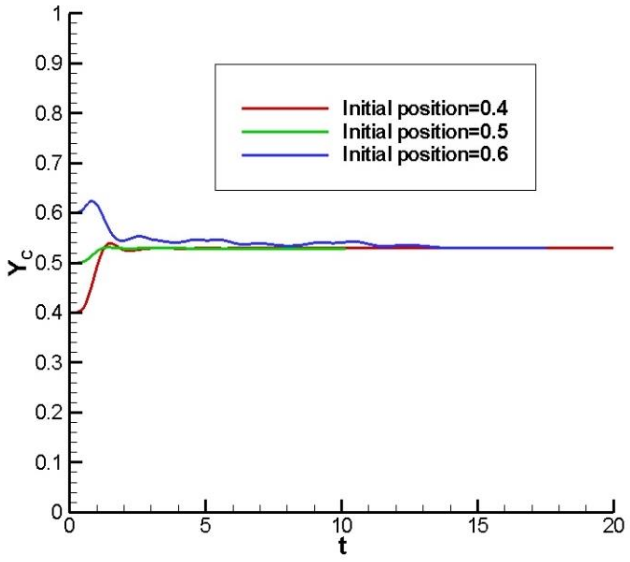

Figure 3.15 The trajectory of particle centre with time for three different initial positions of release at Re=12.786 and d=0.25

To analyse the effect of initial position of release of particle under shear flow, simulations are carried out for three different initial positions at Re=12.786. The particle diameter is 0.25 and height of channel is taken as 1.0. Three different initial position of particle is considered ((25.0 0.4), (25.0, 0.5) and (25.0, 0.6)). Figure 3.15 shows the trajectory of particle centre with time for three initial positions of release. From figure 3.15, it can be observed that for all the initial position of release considered, particle finally migrates to same equilibrium position. These findings are in accordance with those of Huang et al. (1997).

3.3.2.3 Effect of diameter

The influence of diameter of particle on the inertial migration is studied and illustrated in figure 3.16. The particle diameter is changed from 0.2 to 0.5. Re is kept same in all cases (12.786) and the initial position of release of particle is (25.0, 0.4). The height of channel is kept as 1.0.

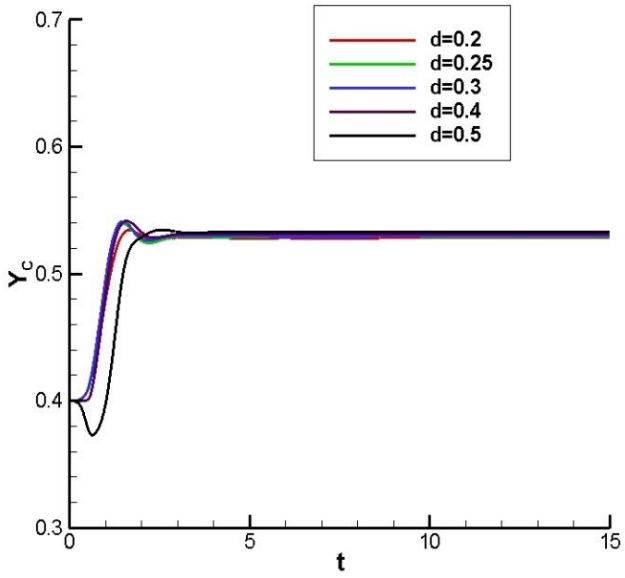

Figure 3.16 The trajectory of particle centre with time for various diameters of particle at Re=12.786 and initial position = (25.0, 0.4) in shear flow

From figure 3.16 it is evident that, equilibrium position stays close to the centre of channel with change in diameter. This implies that equilibrium position stays close to the centre of channel and it is almost independent of particle size in case of shear flow. This may be due to the reason that velocity is zero at channel centre for shear flow and

it will create zero lift force over particle while it reaches channel centre. Hence, particle will attain equilibrium position at channel centre independent of its size in case of shear flow. Table 3.8 shows migration time for particle for different diameters. The particle velocity becomes higher due to decrease in diameter which leads to reduction in time taken to attain equilibrium position.

Table 3.8 Migration time for different diameter of particle at Re=12.786

d	t_m
0.2	**9.845**
0.25	**9.975**
0.3	**10.024**
0.4	**10.058**
0.5	**10.072**

3.3.2.4 Effect of height of channel

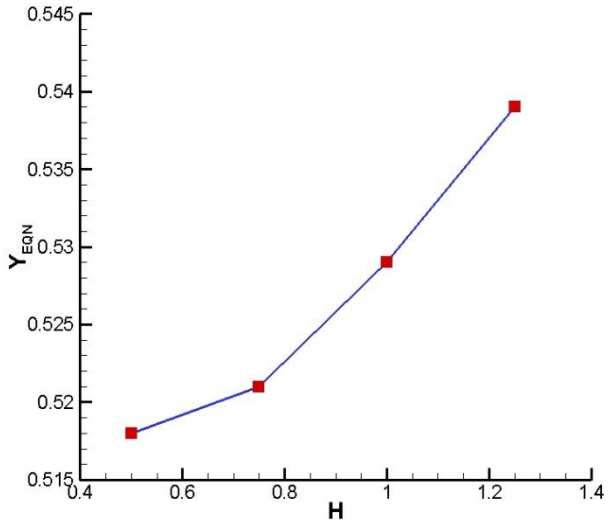

Figure 3.17 Variation of normalised equilibrium position with height of channel for Re=12.786 and d=0.25

The influence of height of channel on inertial migration of particle is investigated in this section. The channel height is changed from 0.5 to 1.25 and other parameters like Re (12.786), diameter of particle (0.25) remain unchanged. The normalised equilibrium position is taken into consideration for comparing equilibrium position of particles in channels of different heights. Figure 3.17 shows the variation of normalised equilibrium position with height of channel.

From figure 3.17 it is clear that as height of channel increases equilibrium position shifts towards the upper wall slightly. The raise in channel height by keeping particle diameter same increases the distance between particle and wall. As distance to wall increases the effect of wall induced lift on particle become less. Hence, the dominant shear induced lift pushes particle towards wall as height of channel increases. However, due to the reduction in effect of wall induced lift with raise in channel height, migration time increases. So, migration time increases with increase in height of channel as depicted in table 3.9.

Table 3.9 Migration time for different height of channel for Re=12.786 and d=0.25

H	t_m
0.5	**5.881**
0.75	**6.930**
1.0	**9.975**
1.25	**10.552**

3.3.2.5 Effect of shear rate

The shear rate of flow is varied from 0.25 to 1 and the change in characteristics of inertial migration is studied further. The flow is simulated at Re= 12.786 and diameter of particle is taken as 0.25. The particle is released from an initial position of (1.0, 0.4) and the height of channel is kept as 1.0. Figure 3.18 shows the trajectory of particle with time for different shear rates.

From figure 3.18, it can be seen that particle equilibrium shifts upward as shear rate increases but equilibrium position for shear rates of 0.75 and 1.0 are almost same. As the velocity of flow increases with increase in shear rate shear induced lift increases

and particle equilibrium position shifts towards upper wall. But for higher shear rates 0.75 and 1.0 equilibrium positions are seen to be close. This may be due to the fact that velocity of flow is zero at centre of channel in a shear flow and hence shear induced lift will be less even after increasing the velocity of flow. Hence, after this point the increase in velocity of flow and shear rate does not contribute to shift in equilibrium position. Table 3.10 shows migration time for different shear rates. As shear rate increases the velocity of flow increases and the migration time reduces.

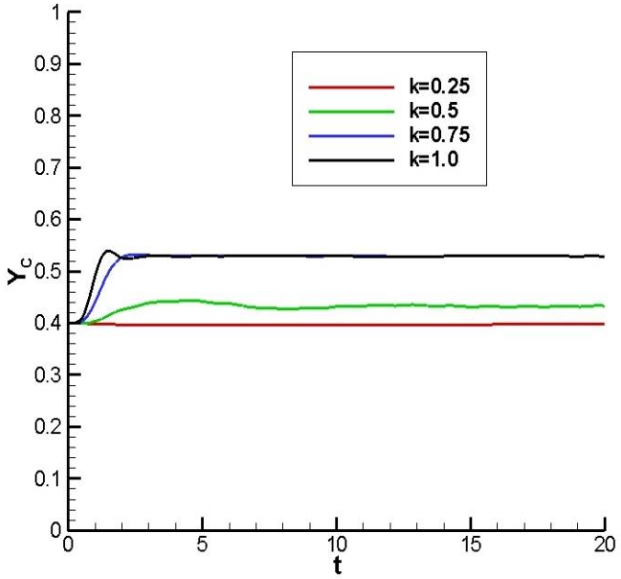

Figure 3.18 Trajectory of particle centre with time for various shear rates for Re=12.786 and d=0.25

Table 3.10 Migration time for various shear rates

k	t_m
0.25	**19.512**
0.5	**13.483**
0.75	**9.986**
1.0	**9.975**

3.3.3 Comparison between the migration of particle in Poiseuille flow and shear flow

In the next stage, particle migration behaviour in Poiseuille flow and shear flow are compared. The particle is released from same initial position (1.0, 0.4) and Re is taken as 12.786 for all cases. The particle diameter is taken as 0.25 and height of channel is taken as 1.0. The trajectory of particle with time is shown in figure 3.19.

It is clear from figure 3.19 that particle equilibrium position is closer to the lower wall in case of Poiseuille flow and closer to the centre of channel in case of shear flow.

The migration time is lower in case of shear flow, since the particle attain an equilibrium position near the centre of channel. Hence, the distance travelled in lateral direction to achieve equilibrium position is lower in case of shear flow compared to Poiseuille flow. The equilibrium position of particle in shear flow is near the centre of channel in case of shear flow and the initial position of release is (1.0, 0.4). Hence, the distance travelled in lateral direction to achieve equilibrium position is lower in case of shear flow compared to that of Poiseuille flow.

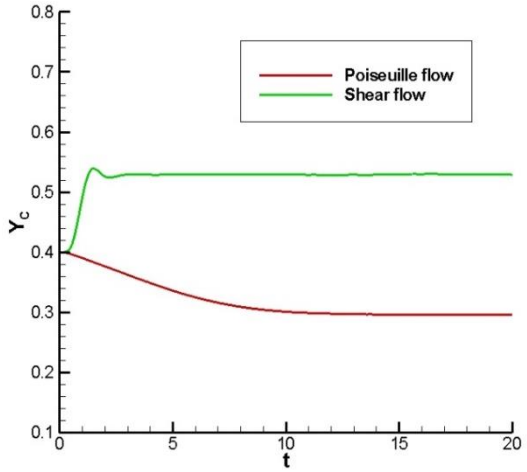

Figure 3.19 Variation of centre of particle with time in three conditions for Re=12.786, d=0.25

Table 3.11 Migration time for different flow conditions for Re=12.786, d=0.25

Flow type	t_m
Poiseuille flow	**13.768**
Shear flow	**9.975**

3.3.4 Artificial Neural Network (ANN) prediction model for inertial migration in Poiseuille flow in straight channel

The detailed parametric study is carried out on inertial migration of cylindrical particle in Poiseuille flow in a straight channel (section 3.3.1). It is interesting to see that equilibrium position (Y_{EQ}), migration time (t_m) are depended on Reynolds number (Re), diameter of particle (d) and height of channel (H). The initial position of release of particle (Y_{ini}) does not have any influence on equilibrium position. However, it has significant impact on migration time. Hence, taking these observations into consideration a prediction model is developed for normalized equilibrium position (Y_{EQN}) and migration time with Reynolds number, diameter of particle, channel height and normalized initial position (Y_{inin}) (The channel height H is varied and hence the initial position of particle release is divided by H to give the normalized initial position. This is used to compare initial position of particle in different channel heights) as inputs. Artificial neural network (ANN) algorithm is incorporated to construct a prediction model. The schematic network diagram of the ANN model is illustrated in figure 3.20.

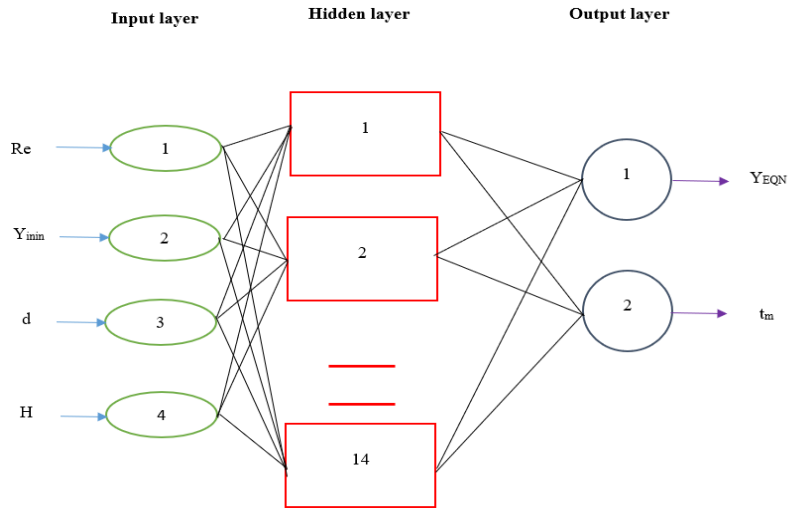

Figure 3.20 Schematic diagram of ANN prediction model

The prediction model consists of four input and two output layers as shown in figure 3.20. The number of hidden layers is chosen as 14. This is selected on the basis of minimum mean square error (MSE). The values of Reynolds numbers are 12.786, 27.727 and 96.74. The diameter varies from 0.2 to 0.3, height of channel changes from 0.5 to 1.25. Additionally, normalized initial position varies between 0.2 and 0.3. Before

entering into ANN algorithm, the normalization of all input and output values are carried out using equation 3.18.

$$\text{Normalised data} = \frac{\text{Data value-Minimum value}}{\text{Maximum value-Minimum value}} \tag{3.18}$$

The ANN algorithm utilizes 108 simulation data and logarithmic transfer function is used (Kanchan and Maniyeri 2020). Two-third of data is used for training and the rest is used for testing of model. Figure 3.21 shows the performance plot.

The training process stops when the MSE approaches minimum value. The regression plot which shows behaviour of predicted outputs with that of observed ones can be seen in figure 3.22.

The variance value of 0.993 seems to be close to 1.0. Also, it is clear from figure 3.22 that the predicted and observed values maintain a linear relationship. The following figures (figures 3.23 a)-b)) shows the characteristics of predicted values of normalized equilibrium position and migration time with their corresponding observed values.

The predicted and observed values are almost close at all test numbers as it is visible from figure 3.23 a) and b). This implies that the constructed ANN prediction model has good prediction capability and it can be easily combined with IBM simulation data. The developed ANN model can help to predict equilibrium position and migration time for a given channel and particle dimension which will be a great aid in inertial particle separation procedures.

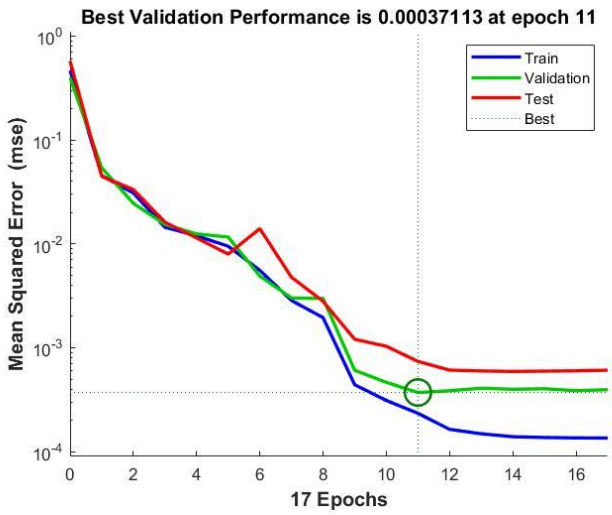

Figure 3.21 Performance plot of neural network training

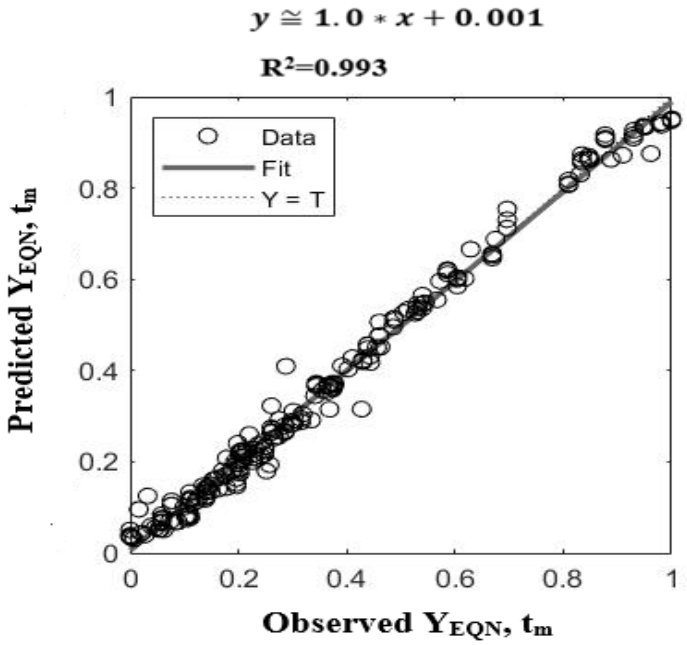

Figure 3.22 Regression plot obtained for both predicted and observed values of Y_{EQN} and t_m

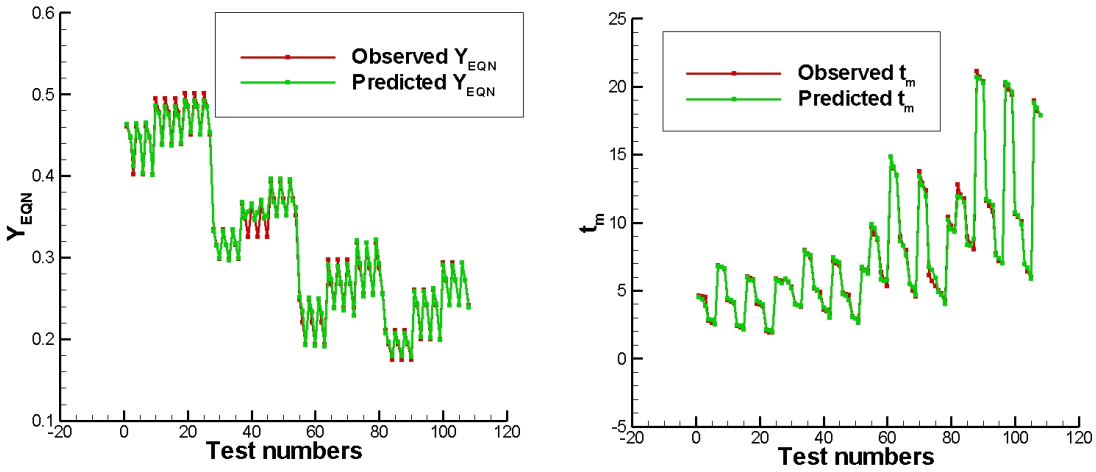

a) b)

Figure 3.23 Behaviour of predicted values with that of observed values a) normalized equilibrium position Y_{EQN}, b) migration time t_m

CHAPTER 4. INERTIAL MIGRATION OF PARTICLE IN NON-STRAIGHT CHANNELS

Inertial migration of single rigid cylindrical particle in non-straight channels is discussed in this chapter. The rigid cylindrical particle migration in backward facing stepped, stepped and constricted channels are simulated by using feedback forcing based IBM. More discussions are given below.

4.1 Background

The literature review in chapter 2 shows that majority of the works are addressed on spherical particle lateral migration in straight channels. However, the emergence of inertial microfluidics has put forward some non-straight channel configurations like serpentine (Liu et al. 2018b), trapezoidal (Wu et al. 2012a) and spiral (Warkiani et al. 2014a) for effective inertial migration particle separation. The behavior of lateral migration in straight and non-straight channels is different. The presence of recirculation zones in non-straight channels should be the reason behind this phenomenon. The secondary flows inside non-straight channels can alter the symmetry of lift forces exerted on particle. This happens by the addition of more viscous drag force on particle and by virtue of that modified equilibrium positions can be attained (Tang et al. 2020). Still, instead of constructing complex-shaped channels, secondary flows can be generated in a channel by adding grooves or projections inside. Mao and Alexeev simulated single spherical particle (rigid) migration in a microchannel with added ridges in it (with help of LBM) (Mao and Alexeev 2011a). Massive sample analysis was achieved in this work. Another interesting study came from Sollier et al. where they used pillars inside the microchannel for effective separation of biotin particles and 98% sorting was possible with this model (Sollier et al. 2015).

By analyzing previous works, it is inferred that the works on non-spherical particle inertial migration in non-straight channels are limited (Lin et al. 2007, 2011). Another fact which attracts is that most of the non-straight channels simulated in previous works are complex in construction.

By addressing these scenarios, a simple two-dimensional numerical model is developed to analyse rigid cylindrical particle (neutrally buoyant) migration in backward facing

stepped, stepped and constricted channels. The feedback forcing-based immersed boundary method is utilized to construct the numerical model. In backward facing stepped channel a step is present at the entrance of channel. The stepped channel consists of two steps from half-length of channel. Constricted microchannel is one of the important types of non-straight channel (Vahidkhah et al. 2016). Two curved arcs are present in the constricted microchannel at center in horizontal direction of channel. The presence of these additional structures in channel can play a pivotal part in inertial migration and separation of particle flowing inside it. The built model aims to characterize and study the separation of particle in terms of equilibrium position, migration time, and shortest equilibrium distance. The simulations are carried out for different Reynolds numbers, initial release position, particle diameter and constriction clearance. Moving on, an artificial neural network (ANN) prediction model is developed using the IBM simulation data. It can predict equilibrium position, migration time, and shortest equilibrium distance without further performing simulations. The methodology is given in section 4.2 and the results are discussed in 4.3.

4.2 Methodology

The feedback forcing based IBM methodology for simulation of inertial migration of particle is already explained in chapter 3 (section 3.2). The only difference is that the steps and constriction arcs are modelled as additional immersed boundaries. Hence, additional terms are introduced for both Eulerian and Lagrangian forces corresponding to constriction arcs and steps. The updated equations of Eulerian and Lagrangian forces are given below.

$$\mathbf{F}_a(s_a, t) = \alpha \int (\mathbf{U}_{iba} - \mathbf{U}_a)\Delta t + \beta(\mathbf{U}_{iba} - \mathbf{U}_a) \tag{4.1}$$

$$\mathbf{F}_p(s_p, t) = \alpha \int (\mathbf{U}_{ibp} - \mathbf{U}_p)\Delta t + \beta(\mathbf{U}_{ibp} - \mathbf{U}_p) \tag{4.2}$$

$\mathbf{U}_a$ and $\mathbf{U}_p$ indicate the velocity of constricted or stepped parts and particle respectively. Since constricted and stepped parts are stationary $\mathbf{U}_a$ is taken as zero throughout the simulation. The Eulerian force calculation is given in equations 4.3 and 4.4.

$$\mathbf{f}_a(\mathbf{x}, t) = \int \mathbf{F}_a(s_a, t)\, \delta(\mathbf{x} - \mathbf{X_a}(s_a, t))\, ds_a \tag{4.3}$$

$$\mathbf{f}_p(\mathbf{x}, t) = \int \mathbf{F}_p(s_p, t)\, \delta(\mathbf{x} - \mathbf{X_p}(s_p, t))\, ds_p \tag{4.4}$$

The calculated Eulerian forces are added to the N-S equations as follows.

$$\frac{\mathbf{u}_{i,j}^{n+1}-\mathbf{u}_{i,j}^{n}}{\Delta t} + N(\mathbf{u}^{n}) = -\left(\frac{\partial p}{\partial \mathbf{x}_i}\right)^{n} + \frac{1}{2Re}(\nabla^2\mathbf{u}^{n+1} + \nabla^2\mathbf{u}^{n}) + \mathbf{f}_a(\mathbf{x},t) + \mathbf{f}_p(\mathbf{x},t) \quad (4.5)$$

The remaining equations and methodology are same as discussed in chapter 3.

4.3 Results and discussion

The inertial migration characteristics of cylindrical particle in non-straight channels are shown and discussed in the following subsections.

4.3.1 Migration of particle in backward facing stepped channel

The physical model of particle migration in backward facing stepped channel is shown in figure 4.1.

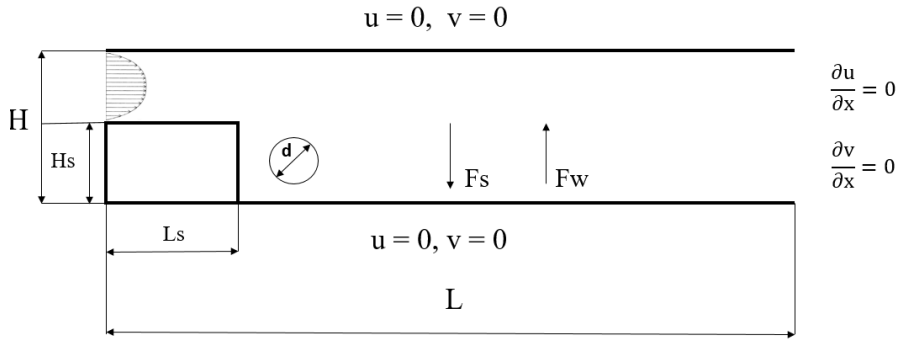

Figure 4.1 Physical model of migration of particle in a backward facing stepped channel

where Hs and Ls are the height and length of step. The boundary conditions are given in table 4.1.

A dimensionless domain of 50x1 in which particle of diameter 0.25 is released (refer to figure 4.1). The length and height of the step is chosen as 1 and 0.5 respectively. Here, the step is modelled as an additional immersed boundary with Lagrangian grid size of 0.01. The other numerical parameters related to modelling of step are taken as same as that of particle. As a preliminary work, flow over a backward facing stepped channel is simulated without particle for three different Re 12.786, 27.727 and 96.74 and the streamline patterns are shown in figure 4.2.

Table 4.1 Boundary conditions (backward facing stepped channel)

Type of flow	Inlet	Outlet	Top wall	Bottom wall
Backward facing stepped channel	6.0(y/(H-Hs))(1-(y/(H-Hs))) y=Hs to H	$\frac{\partial u}{\partial x}=0, \frac{\partial v}{\partial x}=0$	u=0, v=0	u=0, v=0

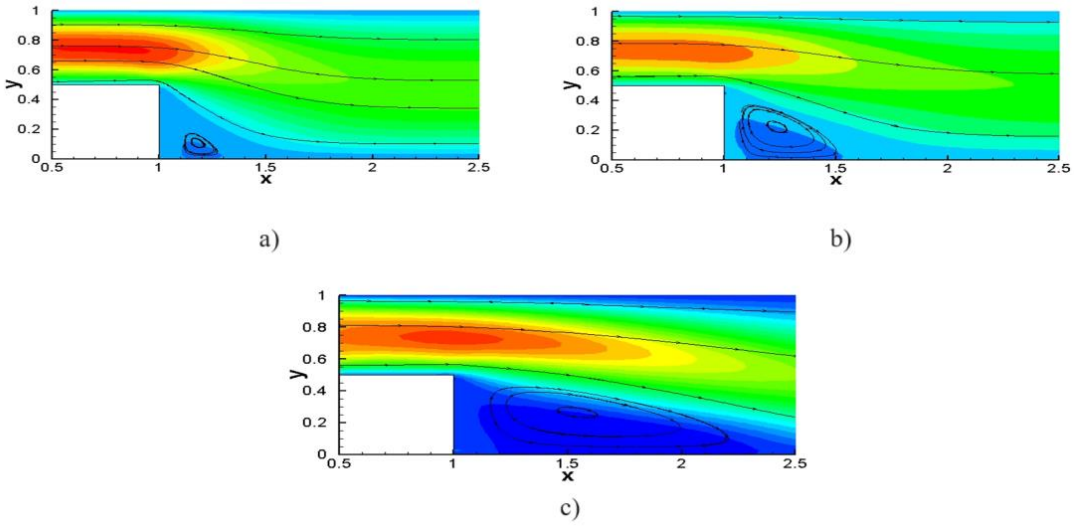

Figure 4.2 Streamline patterns and u velocity contour of flow through a backward facing stepped channel without particle for three Re a) Re=12.786, b) Re=27.727, c) Re=96.74

It is clear from figure 4.2 that the vortices are present at right side of step and its size increases as Re increases. It is to be noted that similar observations are reported by Biswas et al. (2004)for Re range of 10-100. The presence of vortices can play a key role in inertial migration of particle and it has to be explored. Accordingly, simulations are performed to study particle migration in a backward stepped channel as shown in figure 4.1. The effect of different parameters likes Re, initial position of release and diameter of particle on the inertial migration is analysed. One of another parameters which is taken into consideration is the blockage ratio, b. It is the ratio between height of step (H_S) and channel height (H).

4.3.1.1 Influence of Re

The flow Re is varied (12.786, 27.727 and 96.74) and the change in equilibrium position and migration time is studied. Particle is released from an initial position of (1.26, 0.4) and the diameter is taken as 0.25 in all three cases. The step height is chosen as 0.5 with blockage ratio as 0.5. The particle trajectory for three different Re can be seen from figure 4.3.

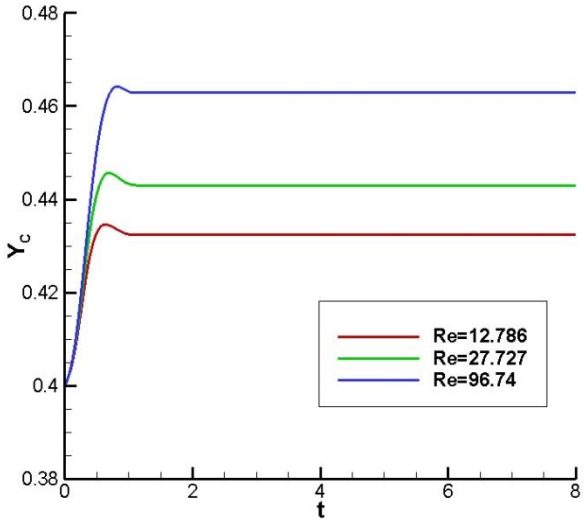

Figure 4.3 Variation of center of particle with time for different Re with d=0.25

It is clear from figure 4.3 that equilibrium position shifts towards upper wall as Re increases. As Re increases size of the vortices increases. These vortices act against shear induced lift and push back particle from bottom wall. Hence, particle equilibrium position shifts towards upper wall as Re increases. Another interesting point to be noted is that migration time is almost same for all three Re. The slip velocity of particle increases with Re and it should decrease migration time normally. However, in case of stepped channel since the vortices are present and its size increases with increase in Re, force acting against shear induced lift increases. Due to combined effect of increase in slip velocity of particle and opposite force against shear induced lift, migration time stay unaffected with variation in Re. In case of straight channel, equilibrium position seems to be shifting towards lower wall with increase in Re (section 3.3.1.1). However, in case of backward facing stepped channel equilibrium position moves towards upper wall. The migration time decreases with increase in Re in case of straight channel whereas it is independent of Re in case of backward facing stepped channel.

4.3.1.2 Influence of initial position

The influence of initial position of particle is analysed further. The particle is initially released from three various positions (1.26, 0.4), (1.26, 0.5) and (1.26, 0.6). Re, diameter of particle and height of channel are kept constant as 12.786, 0.25 and 1.0 respectively for all three cases. The blockage ratio is taken as 0.5 in all cases. The trajectory of particle for separate initial positions of release can be seen from figure 4.4.

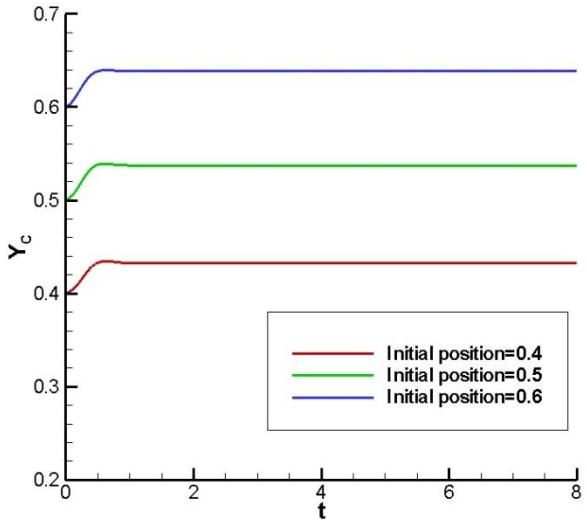

Figure 4.4 The trajectory particle centre with time for three initial positions of release for Re=12.786 and d=0.25

The study of inertial migration in straight channel showed that initial position of release does not have any effect on equilibrium position of particle in case of both Poiseuille flow and shear flow. But in case of a stepped channel it has significant effect. From figure 4.4 it can be seen that as initial position shifts towards upper wall equilibrium position of particle also follows the same behaviour. The presence of vortices may be the reason for this behaviour. As initial position shifts towards the upper wall distance between vortices and particle increases. Hence, shear induced lift becomes dominant and it pushes particle towards nearer wall. Hence, when particle is released from 0.5 and 0.6 it shifts towards the upper wall due to increased effect of shear induced lift because of increased gap between particle initial position and vortices.

4.3.1.3 Influence of diameter

The effect of size of particle is studied in the next stage. The particle diameter is changed from 0.2 to 0.5 and Re is kept as 12.786 throughout. The particle is released from an initial position of (1.26, 0.4) and height of channel is kept as 1.0. The blockage ratio is taken as 0.5. The particle trajectory with time for different diameter of particle is shown in figure 4.5.

The equilibrium position of particle shifts towards lower wall as diameter of particle decreases. This may be due to the increase in effect of shear induced lift because of rise in velocity of particle. The particle velocity increases and hence migration time decreases as diameter of particle decreases which is clear from Table 4.2.

The migration time decreases with increase in particle diameter in case of inertial migration in straight channel. On the other hand, it increases with particle diameter. The increase in particle diameter reduces distance between flow vortices and particle which creates more imbalances in lift forces. This will increase the time for balancing of forces and hence migration time also.

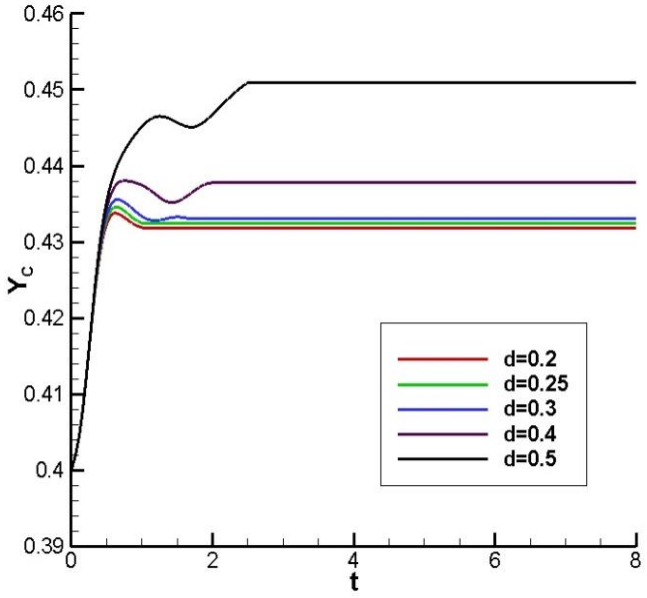

Figure 4.5 The trajectory of particle with time for different diameter for Re=12.786

Table 4.2 Migration time for different diameter (d) of particle for Re=12.786

d	t_m
0.2	**1.011**
0.25	**1.053**
0.3	**1.684**
0.4	**2.143**
0.5	**2.509**

4.3.1.4 Influence of blockage ratio

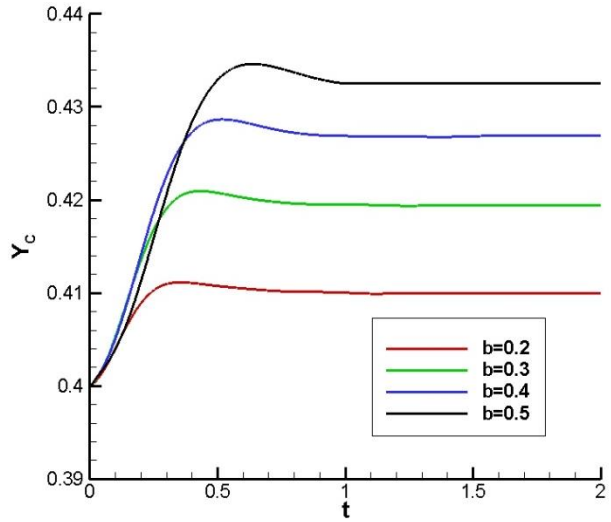

Figure 4.6 Trajectory of centre of particle for different blockage ratios for Re=12.786, d=0.25

The effect of blockage ratio on inertial migration of particle is addressed further. It is varied from 0.2 to 0.5 and other parameters like Re (12.786) and diameter of particle (0.25) are kept as constant. The particle is released from an initial position of (1.26, 0.4) in all cases. Figure 4.6 shows the trajectory of particle with time for different blockage ratios.

As blockage ratio increases particle equilibrium position shifts towards upper wall. This may be due to the increase in size of vortices as blockage ratio increases. The increase in height of step enlarges size of vortices and hence resistance to shear induced lift

becomes stronger and particle shifts more towards upper wall. The increase in blockage ratio contributes to increase in migration time also (table 4.3). As blockage ratio increases velocity of flow decreases and also the exposure of fluid velocity to particle decreases. Hence, migration time increases as blockage ratio increases.

Table 4.3 Migration time for different blockage ratio of stepped channel for Re=12.786 and d=0.25

b	t_m
0.2	**0.945**
0.3	**0.953**
0.4	**1.016**
0.5	**1.053**

4.3.2 Migration of particle in stepped channel

The particle migration in stepped channel is simulated and the related results are discussed in this section. The physical model of the problem is shown in figure 4.7.

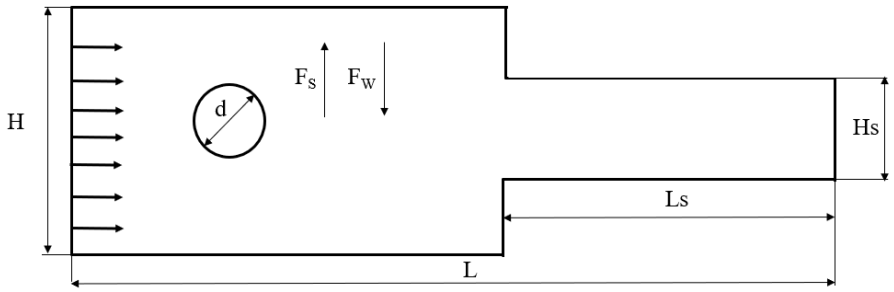

Figure 4.7 Physical model (Stepped channel)

Here, H is the height of channel, L is length of channel, H_S and L_S are height and length of contraction portion (step) in channel, and d is diameter of particle. The fluid enters from left boundary with parabolic velocity profile.

The particle is released from an initial position of (2.5, 0.5). The initial and equilibrium position of particle is shown in figure 4.8 a) and b) respectively. The diameter of particle is 0.2.

The particle attains equilibrium position at (8.401, 0.5171). The lift forces are balanced at equilibrium position and it can be seen from the variation of coefficient of lift force with respect to lateral position. The lift coefficient become zero at equilibrium position (figure 4.9). The y coordinate of the centre of particle is represented by Y_C.

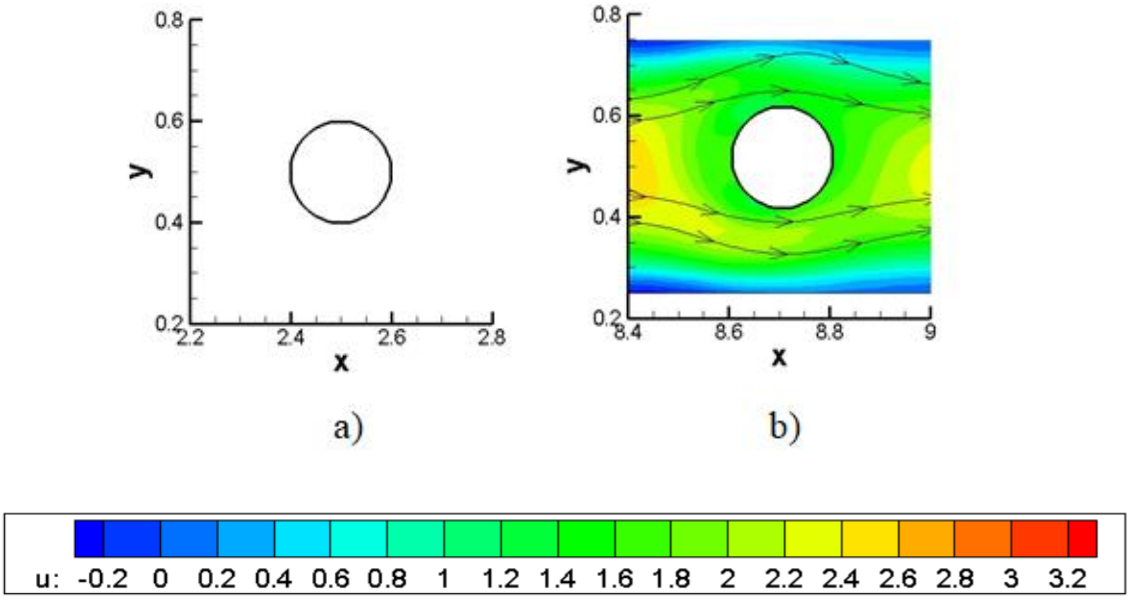

Figure 4.8 a) The initial position of the cylindrical particle in stepped channel (2.5, 0.5), b) final position with u velocity contour (8.401, 0.5171) (Re=12.786, d=0.2)

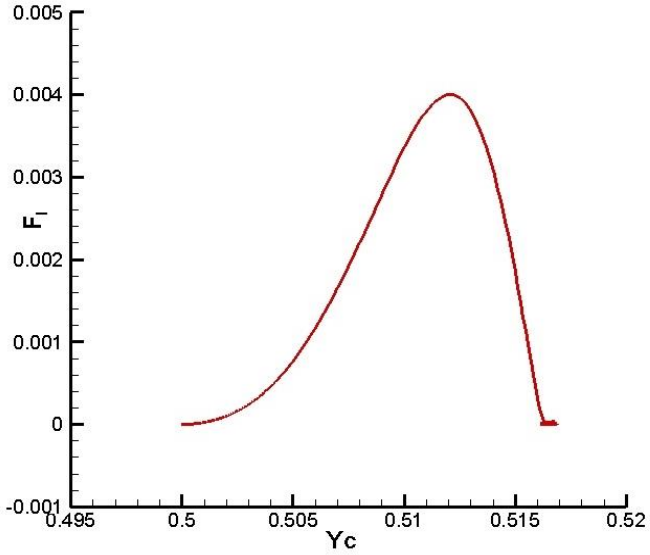

Figure 4.9 The variation of lift coefficient with lateral position of centre of cylinder for Re=12.786

4.3.2.1 Effect of initial position

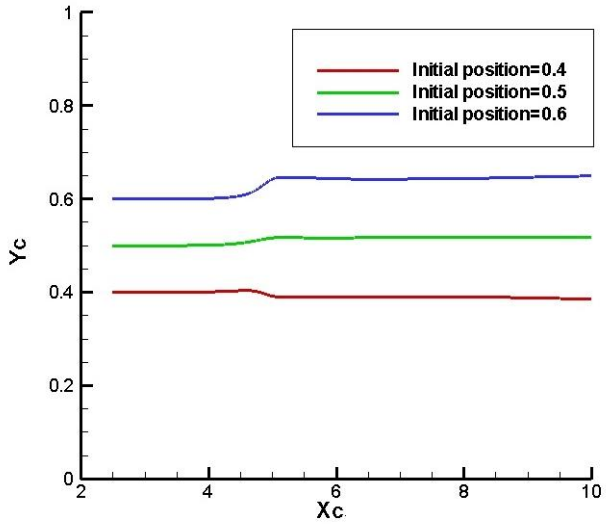

Figure 4.10 Trajectory of centre of particle for three initial positions of release (Re=12.786)

Further, the effect of initial position of release of particle on equilibrium position is analyzed and it is illustrated in figure 4.10 (Re=12.786). The diameter of particle is kept constant for all cases as 0.2. The x coordinate of centre of particle is denoted by X_C.

The equilibrium position shifts off-centre with respect to initial position. As stated in in section 4.3.1.2 initial position has significant effect on equilibrium position of particles in inertial migration. The presence of vortices may be the cause of this behaviour. The similar behaviour can be seen in section 4.3.1.2 (backward facing stepped channel).

4.3.2.2 Effect of Hs

In the next stage, effect of height of contraction portion on equilibrium position is analyzed and it is shown in figure 4.11.

The particle equilibrium position shifts slightly towards the upper wall when height of contraction portion is lowered. The velocity of flow increases when height of contraction portion decreases. Due to this fact the shear force on particle increases and shear induced lift become more dominant than wall induced lift. This may be the reason for particle to migrate towards top wall when height of contraction portion reduces.

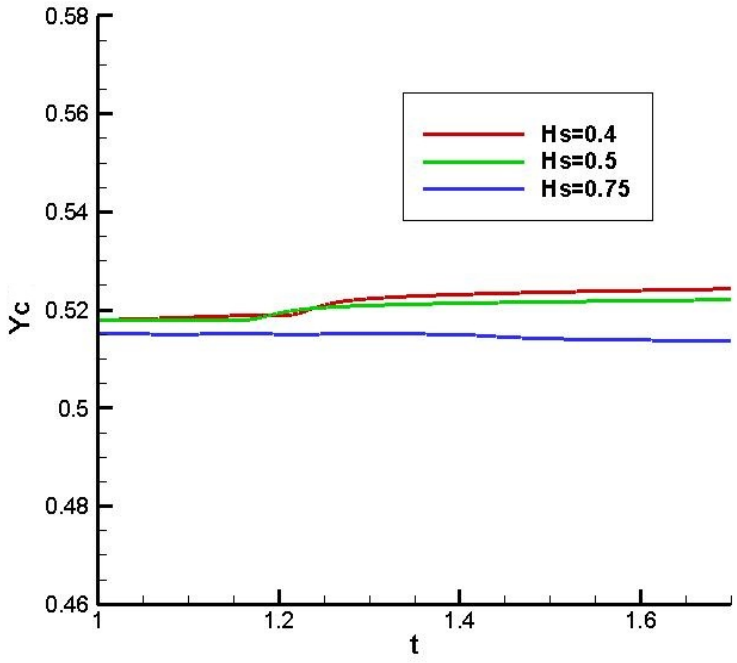

Figure 4.11 The trajectory of particle with time for different height of contraction region (Re=12.786, initial position=0.5)

4.3.2.3 Effect of Ls

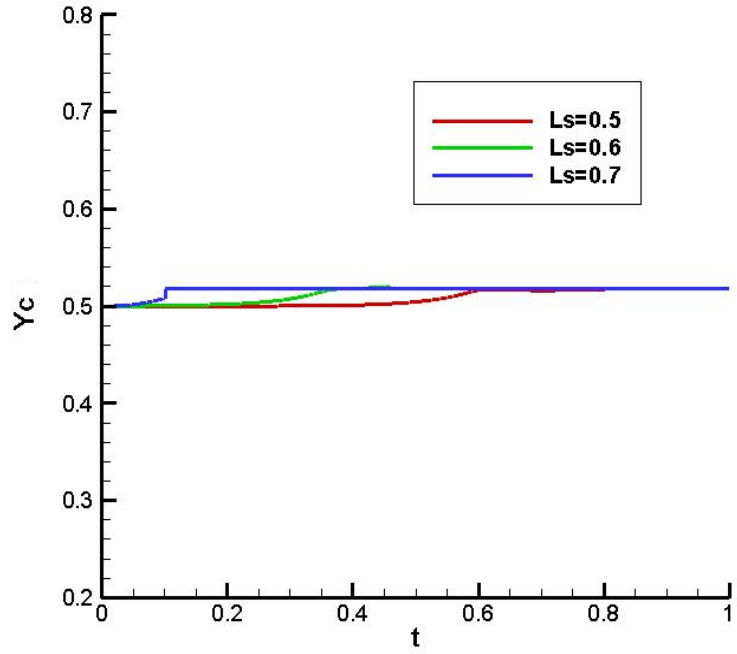

Figure 4.12 The trajectory of particle with time for different length of contraction region (Re=12.786, initial position=0.5)

Table 4.4 Variation of migration time with length of contraction region

Length of contraction region L_S	**Migration time t_m**
7.0	0.119
6.0	0.423
5.0	0.534

In this section, effect of length of contraction portion on lateral migration is addressed (figure 4.12). As it is observable from figure 4.12 that equilibrium position of particle does not change significantly with respect to variation in length of contraction portion. This may be due to the fact that velocity of flow remains unchanged with length of contraction portion. However, migration time decreases with increase in length of contraction portion (shown in table 4.4). The length of entrance region decreases with increase in length of contraction portion because the total length of channel remains unchanged and it may be the cause for reduction in migration time.

4.3.3 Migration of particle in constricted channel

The illustration of particle migration in constricted channel can be seen in figure 4.13 (physical model).

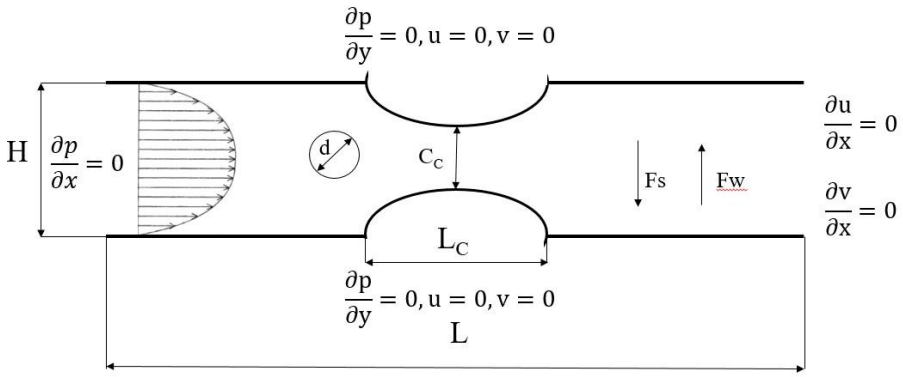

Figure 4.13 Particle migration under fluid flow in constricted channel (Physical model)

The term d represents particle diameter and Cc is the constriction clearance (minimum gap in constricted portion). Here, H and L indicate the height and length of channel whereas notations Fw and Fs represent the wall and shear induced lifts respectively. The constriction arcs are modelled as sin wave patterns (Y_{CON} = (C_C/L_C) (1.0 +

$\sin(((\pi/2) - \pi (X_{CON} - (L/2.0))$ where L_C is length of constricted region and X_{CON} and Y_{CON} are x and y coordinates of points on constricted arc). The rigid particle and the constriction part (varying gap portion in channel) are modelled as separate immersed boundaries. The fluid enters with parabolic velocity profile and leaves channel with zero velocity gradients. No-slip boundary conditions are assumed at both top and bottom walls.

The Eulerian and Lagrangian grid sizes are 0.05 and 0.01 respectively. The corresponding number of Eulerian grids in x and y directions in case of constricted channel of dimension 20x1 are 401 and 21. The number of Lagrangian grids on the surface of particle is 73 and that on the surface of constriction arcs are 316.

The fluid flow without particle through a constricted channel of length and height 20 and 1 is simulated. The length of constricted part is taken as 2 and constriction clearance is selected as 0.4. The streamline plot for Re=125.0 is shown in figure 4.14.

The streamlines and shape of recirculation zones close to the constricted part is observed to be similar to that of Pitt et al (Pitt et al. 2005).

In next step, movement of rigid neutrally buoyant cylindrical particle in constricted channel is simulated. Figure 4.15 shows the positions of particle at different time instances in the flow (along with horizontal velocity line contour) for Reynolds number, Re=10. The particle diameter (d) is 0.25. The constriction clearance (Cc) is 0.5 and the constriction part starts from 9 and ends at 11 in linear direction in channel of length (L) 20 and height (H) 1.

The particle is released from (5.0, 0.5) and it passes through the constriction part at t=1.1. At time t=1.5 a flow separation can be seen at both sides of particle. The particle attains equilibrium position as balance of lift forces reached and hence particle velocity in the vertical direction becomes zero and it will stop movement in the lateral direction. Hence particle may have attained equilibrium position at or before t=1.5. This can be clearer from particle center trajectory with time in figure 4.16. The terms Y_C and X_C are used to represent y and x coordinate of center of particle respectively.

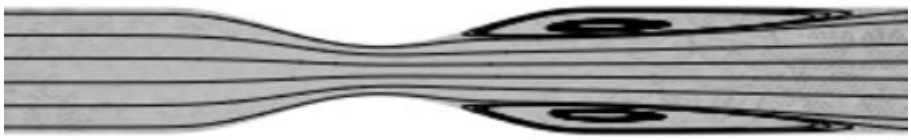

a)

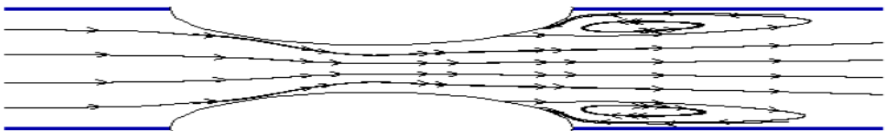

b)

Figure 4.14 Streamline plot for flow through constricted channel (Re=125.0) a) Obtained by Pitt et al. (2005) b) Present work

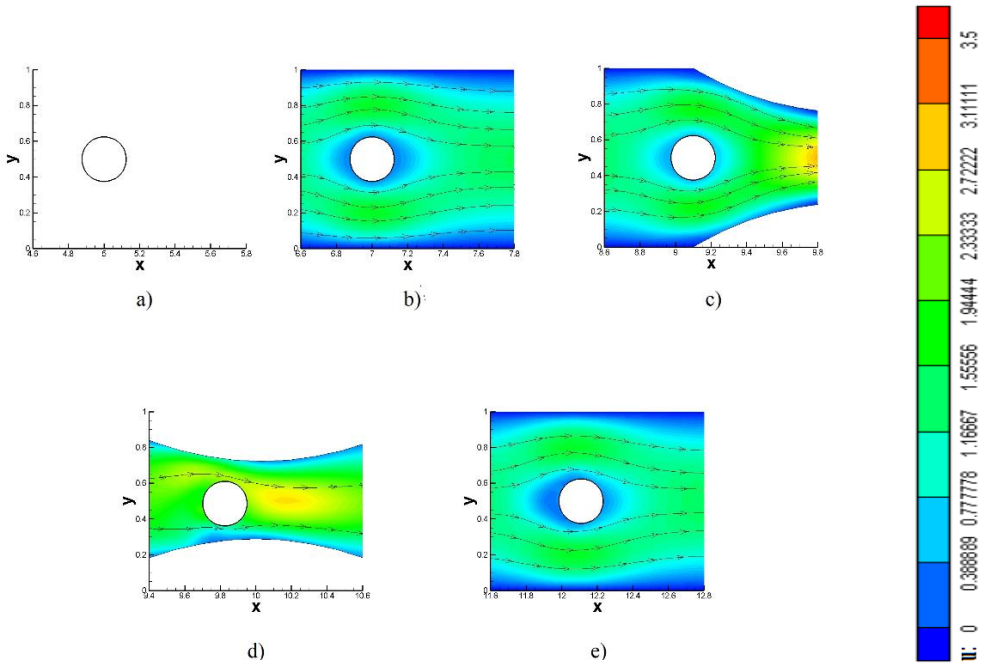

Figure 4.15 The positions of particle at different time instances with u velocity contour (Re=10,d=0.25, Cc=0.5) a)t=0 (5.0,0.5)(initial position), b) t=0.5 (6.97,0.5003), c)t=1.0 (9.1,0.499)(enters the constricted region), d)t=1.1 (9.7,0.490) (resides in constricted region), e)t=1.5 (12. .109,0.50) (after attaining equilibrium position)

The particle acquires equilibrium position at (11.591, 0.499) (from figure 4.16 it is clear that particle trajectory become parallel to t axis just before t=1.5). This implies that particle equilibrium position (represented by particle y coordinate of center) does not

change much from initial position in this case. But it is also interesting to notice that there is a sudden drop in the trajectory after t=0.9. It can be also observed from figure 4.15 d). This drop-in particle trajectory happens when it passes through the constriction part. It can be understood also from the plot where Y_C is mapped against X_C (figure 4.17).

When particle enters the constricted region first it travels down in lateral direction and then moves back to its original lateral position. The area of constricted region gradually decreases to the half (for Cc=0.5) and then increases. Since influence of wall lift force increases with drop-in distance between wall and particle, lift force F_l varies in the constricted part abruptly as shown in figure 4.18. The lift force is calculated by integrating Eulerian force in y-direction (f_y) over the domain as shown in equation (4.6) (Lai and Peskin 2000).

$$F_l = \int_\Omega \mathbf{f}_y(\mathbf{x}, t)d\mathbf{x}. \tag{4.6}$$

From figure 4.18 it is understandable that the lift force exerted on particle by fluid reaches its peak when it passes through constricted part. It is already mentioned that the wall lift force increases gradually up to channel center as particle passes through constricted region. Hence the lift force exerted on particle also raises. But the area of constricted region increases after channel center. Hence, as particle move from center to end of constricted region, the distance between it and the lower wall gradually increases from minimum. Therefore, wall lift force exerted on particle starts to decline down and the lift force also reach back to the minimum value as it moves past the constricted portion. This characteristic is clearly visible in figure 4.18. It is also understood from figure 4.18 that lift force approaches zero at a horizontal position of particle at 11.591. This implies that both wall and shear lift forces exerted on particle are cancelled each other at this point. Figure 4.19 a) plots the behaviour of lift force with lateral location of particle. The particle starts from a lateral position of 0.5 and the lift force over it reaches maximum at 0.49 which is noticed from figure 4.19 a). After that the lift force drops to zero at 0.485 and then travels back to maximum value when it reaches 0.49. Moving further the lift force is reached zero when particle moves back to 0.499. The lift force approaches zero at a lateral position of 0.499 which is very close to the y coordinate of initial release position. This value can be considered as

equilibrium position (The equilibrium position is denoted by the lateral coordinate of particle at balance point of lift forces). This can be stated as one main advantage of particle migration in constricted channel. When particle migrates in straight channel it attains an equilibrium close to 0.6 times of half the height of channel irrespective of its initial release position (Inamuro et al. 2000). But in a constricted channel geometry particle attains equilibrium position closer to initial position. When the constricted arcs are added in straight channel flow velocity near corner reduces which will create adverse pressure gradient and hence secondary flows are generated and it will act as an additional force on particle. This will oppose shear induced lift which in turn balance the lift forces at a position close to initial release point. Hence, equilibrium position of particle is seen near to the initial release point. Further, the variation of drag force over particle with its horizontal position is shown in Figure 4.19 b).

The drag force over particle (figure 4.19 b)) shows a sudden peak in the constricted part. The gradual change in fluid flow velocity (first increases, reaches a maximum and then decreases) in the constricted portion may be reason for this behaviour. It is essential to perform extensive study on the behavior of particle migration for other parameters like Reynolds number, diameter of particle, constriction clearance and initial release position.

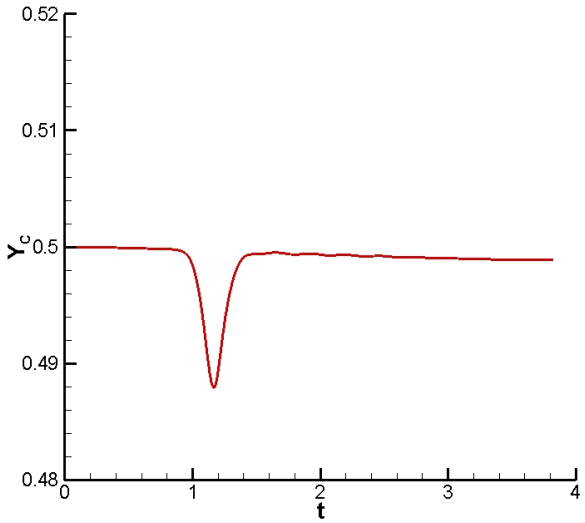

Figure 4.16 Trajectory of particle center with time (Re=10, d=0.25, Cc=0.5)

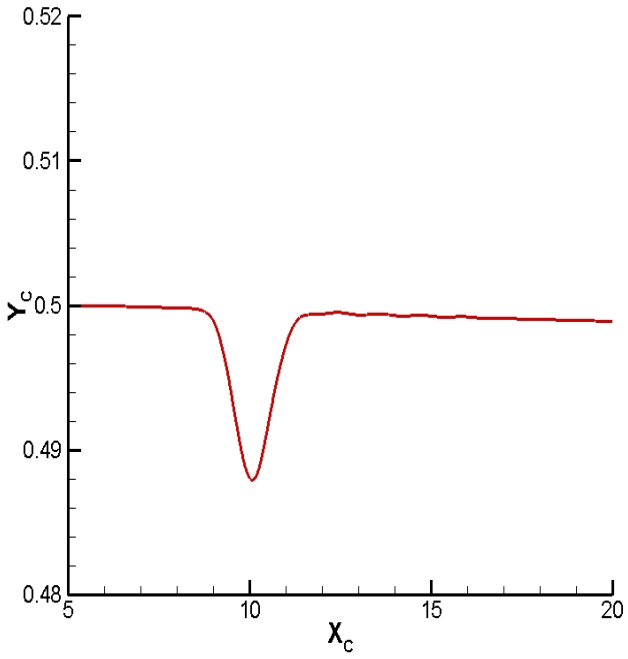

Figure 4.17 Trajectory of x and y coordinates of particle center (Re=10, d=0.25, Cc=0.5)

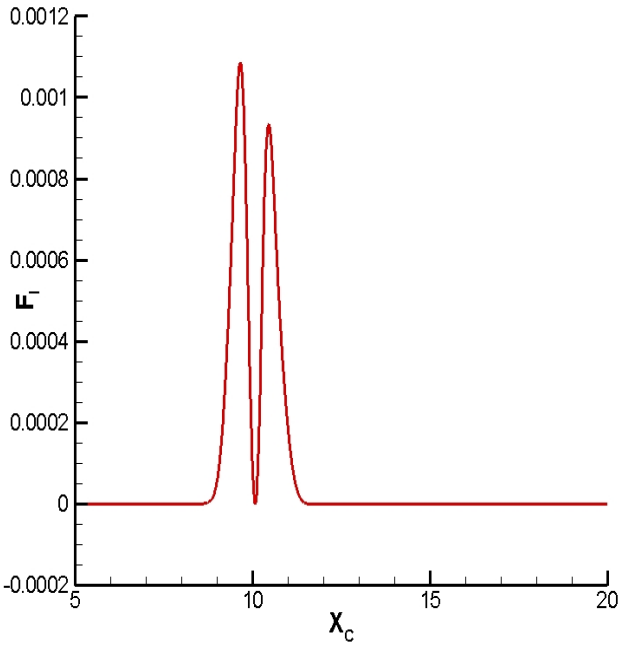

Figure 4.18 Behaviour of lift force with horizontal coordinate of particle center (Re=10, d=0.25, Cc=0.5)

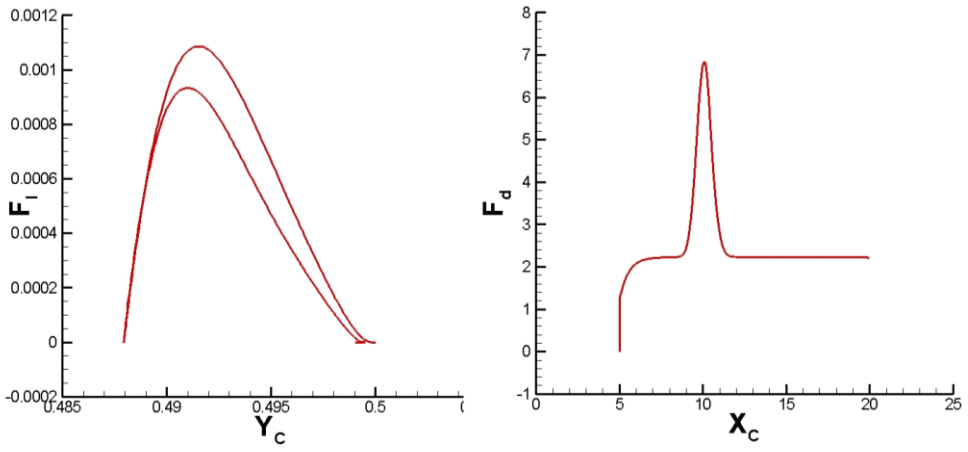

a) b)

Figure 4.19 a) Characteristics of lift force over with particle center (Y coordinate) b) characteristics of drag force with particle center (X coordinate) (Re=10, d=0.25, Cc=0.5)

4.3.3.1 Dependence of inertial migration dynamics on Re

The Reynolds number is an important parameter in case of inertial migration. The increase in Reynolds number makes a shift in equilibrium position of particle towards the nearby wall in case of migration in straight channel (chapter 3) and it shifts towards channel center in backward facing stepped channel (4.3.1.1). Hence, it is interesting to observe the influence of Reynolds number on equilibrium position and migration time in case of constricted channel. Figure 4.20 shows particle trajectory in the constricted channel for four Reynolds numbers 10, 20, 40 and 100. In all four cases particle is released from an initial position of (5.0, 0.5) and its diameter is 0.25. The constriction clearance is also kept same as 0.5 for all Reynolds numbers.

Figure 4.20 shows that particle center trajectory for all four Reynolds numbers almost coincides after the passage of constricted part. It means that equilibrium position attained by particle is almost equal for all Reynolds number ranging from 10 to 100. This is a different characteristic from that of particle migration in straight channel (chapter 3) and backward facing stepped channel (section 4.3.1.1). When particle migration takes place in straight channel, equilibrium position tends to shift towards the lower channel wall with raise in Reynolds number. On the other hand, equilibrium position is driven towards upper wall with increase in Re in case of particle migration

in backward facing stepped channel. But in the case of constricted channel Reynolds number does not significantly affect particle equilibrium position. The presence of constriction part may be the reason behind this. In constriction part the distance between wall and particle first decreases and then increases as particle passes constricted region. The change in this distance produces oscillation in the wall lift force as it reduces with raise in distance between wall and particle. With the increase in Reynolds number particle slip velocity raises as inertial forces become more dominant than viscous force. Hence, with that the shear lift will also increase. The presence of secondary flow vortices plays a pivotal role in case of particle migration in constricted channel. The size and strength of secondary flow vortices becomes larger with raise in Reynolds number (refer horizontal velocity contours in figure 4.21 a)-d) along with particle). Therefore, the additional strength of secondary flow cancels the raise in shear lift due to increase in Reynolds number. Hence, equilibrium position stays unaffected with change in Reynolds number. This can be considered as one main advantage of constricted channel. For a given range of Reynolds numbers, particle attains almost same equilibrium position unlike that in straight channel. Hence, the prediction of equilibrium position and separation of particle will become easier when constricted channel is used instead of straight channel for a range of Reynolds numbers 10-100.

Further, to study the separation possibilities a new term called shortest equilibrium distance (D_S) is introduced. D_S is the algebraic distance between initial position and equilibrium position. The behaviour of lift force with particle horizontal position and time are shown in figure 4.22 a) and b).

It is clear from figure 4.22 a) that the lift force over particle become zero at different linear distances from initial position for various Reynolds numbers. The distance from initial to the point of equilibrium position is calculated and termed as shortest equilibrium distance (D_S). Also, the variation of lift force with time is plotted in figure 4.22 b) for different Reynolds numbers. It is already observed that strength of secondary flow near constriction portion increases with raise in Reynolds number (figure 4.21 a)-d)). Hence particle travels more distance in the horizontal direction to escape from influence of secondary flow and attain equilibrium position. So, the shortest equilibrium distance increases with raise in Reynolds number (figure 4.23 a)).

Since particle covers more horizontal distance to acquire equilibrium position migration time also increases with Reynolds number (figure 4.23 b)). The migration time increases with Re in case of straight channel (section 3.3.1.1) and it remains constant with Re for migration in backward stepped channel.

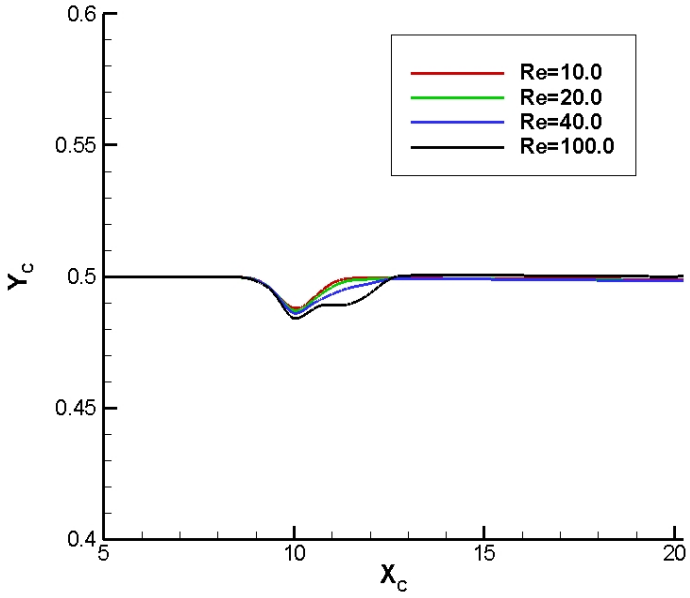

Figure 4.20 Trajectory of particle center for Re =10, 20, 40 and 100 (d=0.25, Cc=0.5)

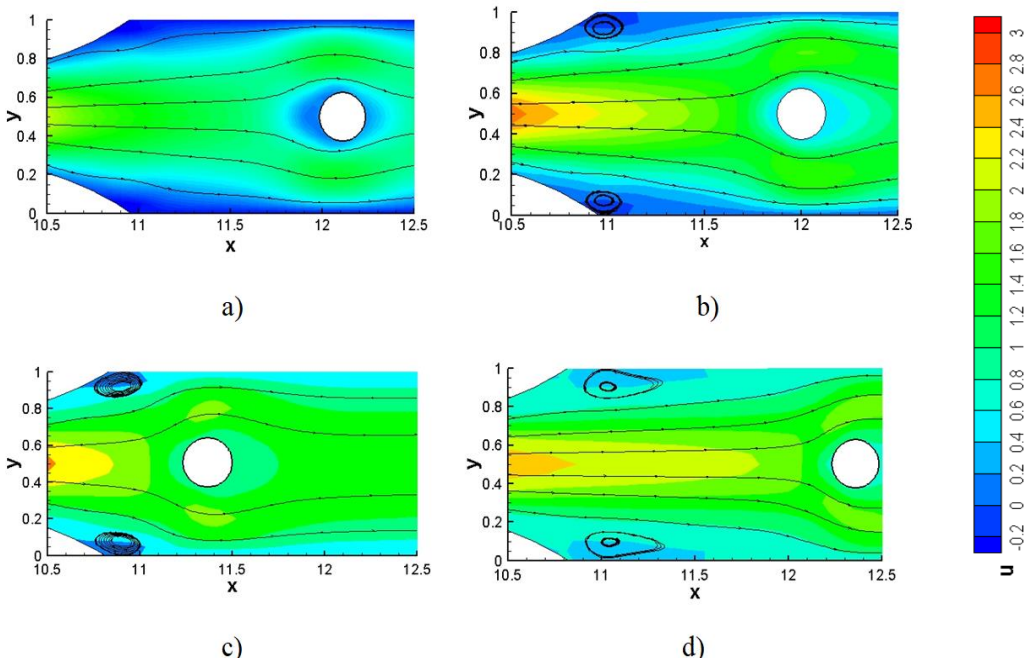

Figure 4.21 Streamline plot with u velocity contour for flow in constricted channel at t=1.5 a) Re=10, b) Re=20, c) Re=40, d) Re=100 (d=0.25)

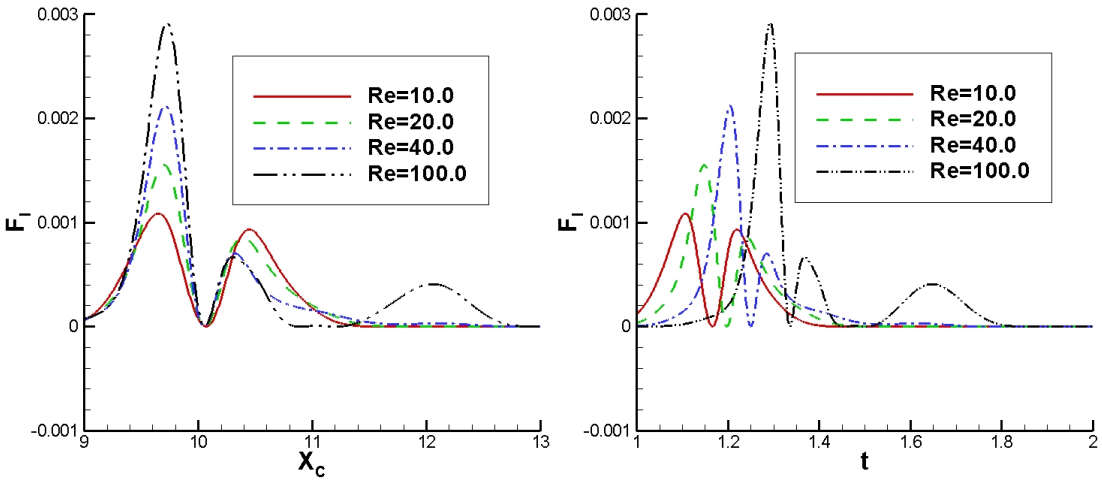

Figure 4.22 a) Variation of lift force with horizontal position of particle for different Re b) Variation of lift force with time for different Re (d=0.25, Cc=0.5)

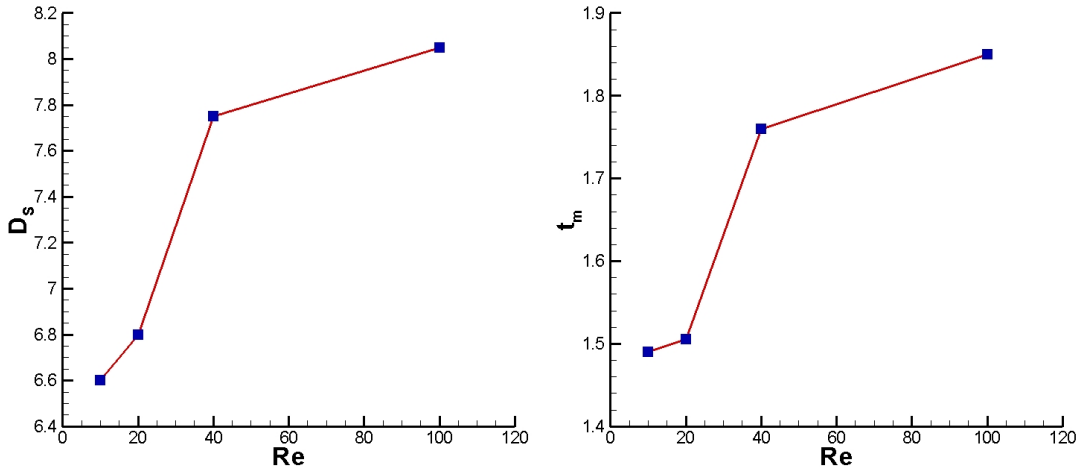

Figure 4.23 a) Variation of shortest equilibrium distance (D_S) with Reynolds number b) Variation of migration time (t_m) with Reynolds number (Re) (d=0.25, Cc=0.5)

4.3.3.2 Dependence of initial position

Moving on to the next step, initial release position of particle is varied from (5.0, 0.4) to (5.0, 0.6) and the migration is simulated. The Reynolds number, particle diameter and constriction clearance are kept as constant as 10.0, 0.25 and 0.5 respectively. The migration trajectory can be seen in figure 4.24.

The particle attains different equilibrium positions with respect to their initial release position. This is a different result from the case of particle migration in straight channel where irrespective of initial position particle aligned to same equilibrium position for similar flow conditions (chapter 3). This is believed to be due to presence of constricted part in channel. Due to the variation of wall induced and total lift forces in constricted part particle tends to attain an equilibrium position almost closer to its initial release position. Since the x coordinate of particle release position and other flow conditions are same the parameters like migration time and shortest equilibrium distance remain unchanged for all three cases. The equilibrium position remains unchanged with change in initial position in case of straight channel whereas it varies in case of both backward facing stepped and constricted channel.

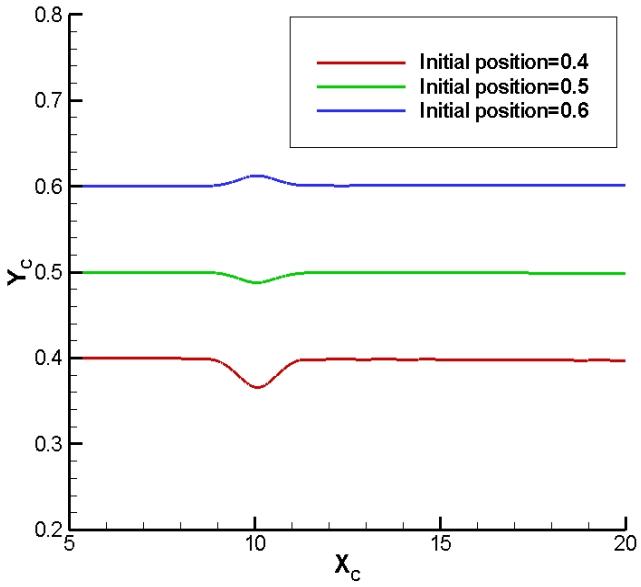

Figure 4.24 Trajectory of center of particle for initial release positions 0.4, 0.5 and 0.6 (Re=10, d=0.25, Cc=0.5)

4.3.3.3 Dependence of diameter

Further, the effect of particle diameter on inertial migration is analyzed. The simulations for three diameters of particle 0.2, 0.25 and 0.3 are carried out. The Reynolds number, constriction clearance is kept same as 10.0 and 0.5 respectively for each case. For all cases particle is released from (5.0, 0.5). The particle trajectory is illustrated in figure 4.25.

It is depicted from figure 4.25 particle equilibrium position moves slightly towards lower wall with reduction in diameter. There can be two reasons behind this. The particle velocity increases with the reduction in mass (equation (3.12)). The mass of particle decreases with its diameter reduction. Hence, increase in particle velocity contribute to rise in influence of shear lift which push equilibrium position to lower wall. On the flip side, as particle diameter decreases, distance between wall and outer surface of particle lowers. This will reduce the influence of wall lift over particle which in effect make particle attain its equilibrium position near to lower wall. The same behavior can be seen in case of straight channel and backward facing stepped channel. It is further interesting to observe the lift force variation with particle horizontal position and time (figure 4.26 a) and b)).

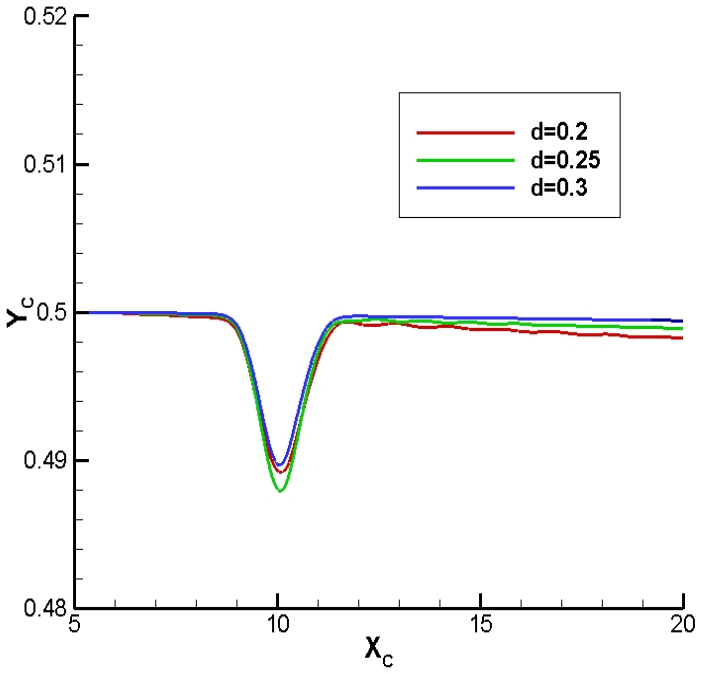

Figure 4.25 Particle trajectory for different diameters 0.2, 0.25 and 0.3 (Re=10.0, Cc=0.5)

From figure 4.26 a) it is evident that particle covers more distance in horizontal direction before the lift force approaches zero as its diameter increases. It is already mentioned that the wall lift effect escalates with expansion in diameter of particle. So,

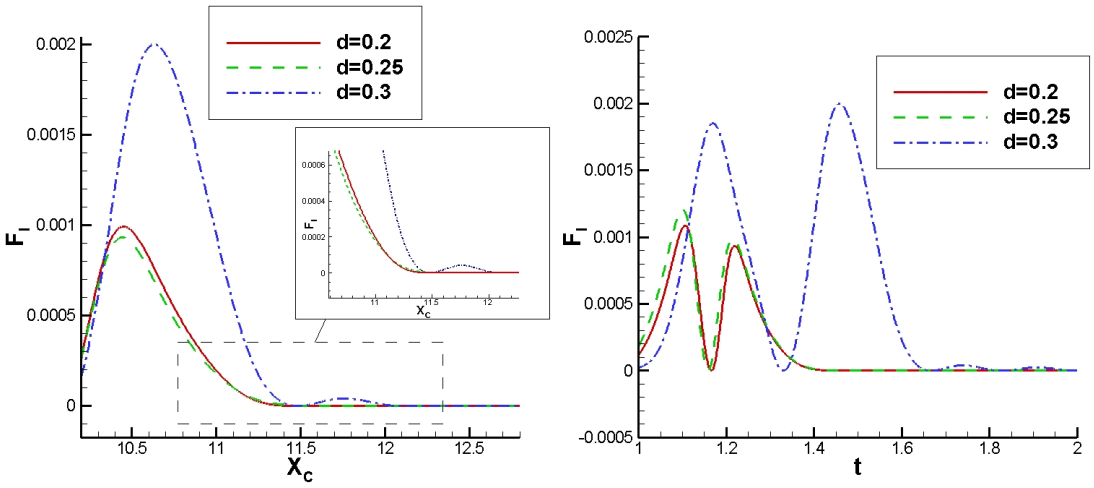

Figure 4.26 a) Characteristics of lift force with horizontal position of particle for its different diameter b) Characteristics of lift force with time for its different diameter of particle (Re=10, Cc=0.5)

to overcome the rise in wall induced lift particle tends to travel more distance in linear direction to acquire equilibrium position which will consume more time (figure 4.26 b)). Also, as particle diameter enlarges the distance between surface of it and secondary flow vortices near the constricted part reduces. Hence particle with higher diameter gets deflected from this secondary flow and travels more distance in linear direction. The raise in distance travelled to reach equilibrium position and reduction in particle velocity due to diameter increase helps to increase migration time also. This behavior can also be visible from the variation of shortest equilibrium distance and migration time against particle diameter (figure 4.27 a) and b)).

The figure 4.27 a) and b) clearly indicates that the shortest equilibrium distance and migration time increases with increase in particle diameter. The migration time reduces with increase in d for straight channel whereas it increases for backward facing stepped and constricted channel.

4.3.3.4 Dependence of constriction clearance

The effect of constriction clearance on lateral migration is analyzed here. The effect of three distinct constriction clearances 0.5, 0.6 and 0.7 on the lateral migration is analyzed by keeping Reynolds number (10.0) and particle diameter of (0.25) as constant. The

initial release position of particle is (5.0, 0.5). The particle trajectory for the different constriction clearances is given in figure 4.28.

The equilibrium position seems to be independent of constriction clearance. There should be two factors playing behind this scenario. One is that, as constriction clearance decreases the distance between wall and particle increases. Hence, the effect of wall lift on particle will become more influential and particle is driven closer to wall. However, this additional effect on wall induced lift can be neutralized by escalation in influence of shear lift due to improvement in fluid velocity in the constriction part which arises due to reduction in constriction clearance. So effectively both shear and wall lifts increase with decrease in constriction clearance. Thus, equilibrium position stays independent with change in constriction clearance. The lift force variation with particle linear position and time are shown in figure 4.29 a) and b).

The lift force approaches zero at longer horizontal distances from initial position for lower constriction clearances (figure 4.29 a)). It is stated before that both shear and wall lifts increase with expansion in constriction clearance. This will create imbalance in lift force and particle will travel more horizontal distance and take more time to acquire equilibrium position which is obvious from figure 4.29 a) and b). This characteristic is also visible from the plot of shortest equilibrium distance and time with constriction clearance (4.30 a) and b)). The shortest equilibrium distance and migration time tend to decrease with increase in constriction clearance as shown in figure 4.30 a) and b).

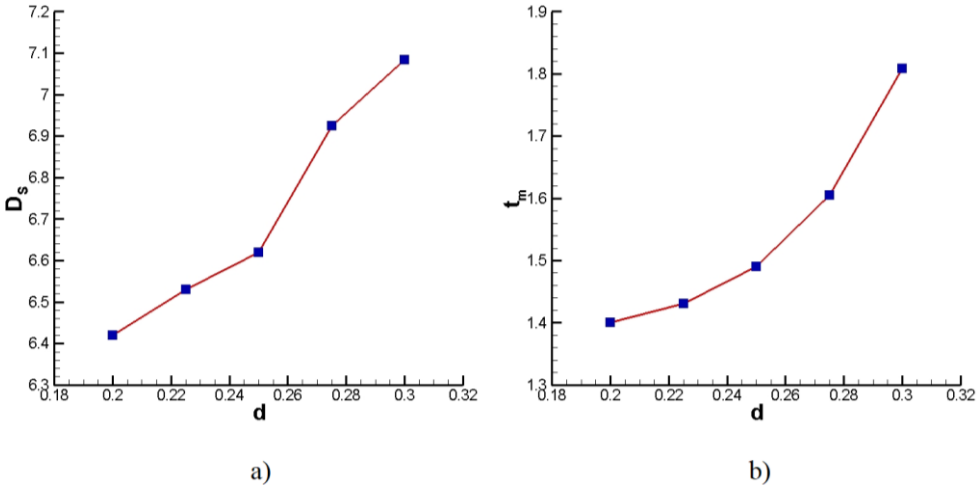

a) b)

Figure 4.27 a) Variation of shortest equilibrium distance with diameter of particle b) Variation of migration time with diameter of particle (Re=10, Cc=0.5)

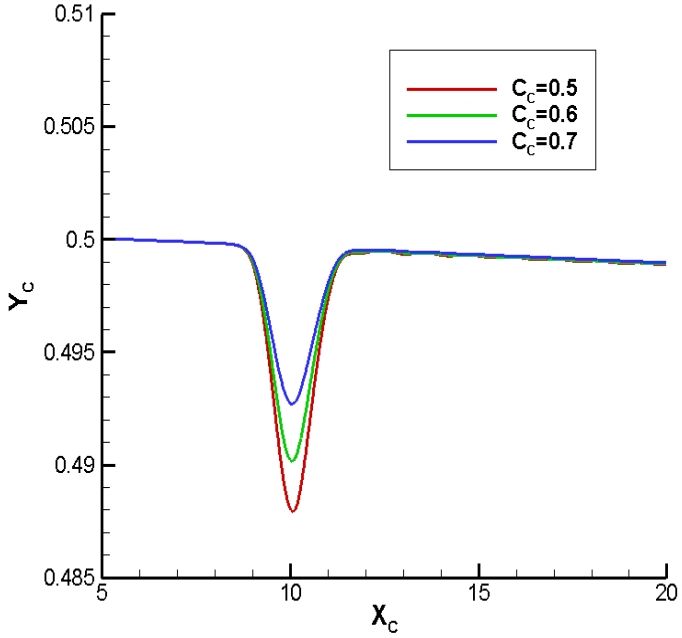

Figure 4.28 Particle trajectory for Cc =0.5, 0.6 and 0.7 (Re=10, d=0.25)

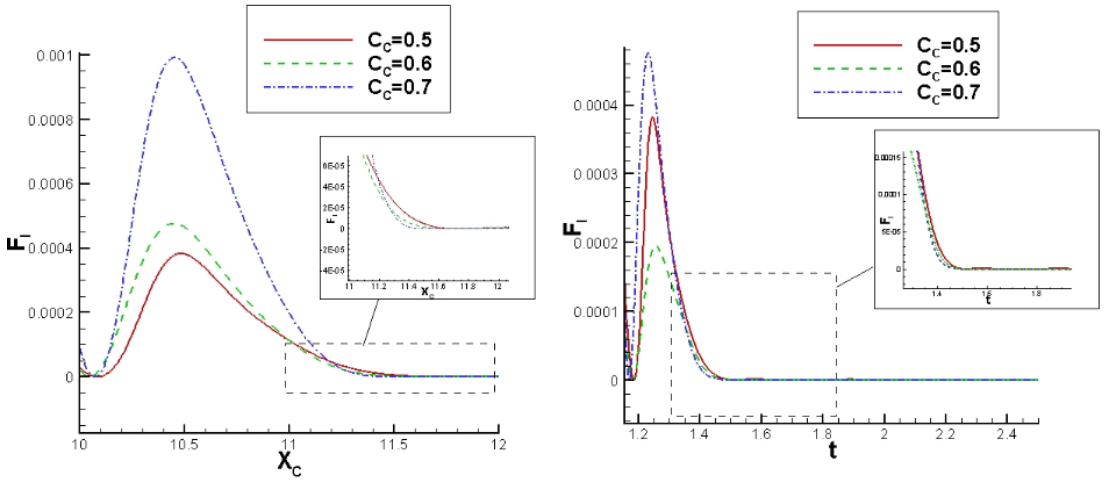

Figure 4.29 a) Characteristics of lift force with horizontal position of particle for different constriction clearances b) Characteristics of lift force with time for various constriction clearances (Re=10, d=0.25)

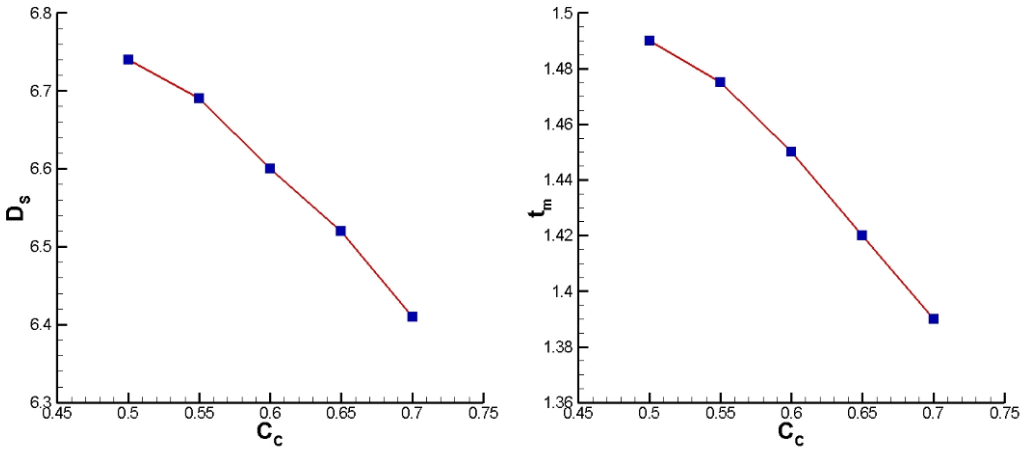

a) b)

Figure 4.30 a) Variation of shortest equilibrium distance (D_S) with constriction clearance (C_C) b) Variation of migration time (t_m) with constriction clearance (C_C) (Re=10, d=0.25)

4.3.3.5 Prediction model development for inertial migration in constricted channel

From the parametric study conducted on inertial migration of rigid neutrally buoyant cylindrical particle in a constricted channel, some key points are observed. The equilibrium position significantly changes with the change in particle initial release position and slightly varies with diameter. However, it stays unaffected with Reynolds number and constriction clearance. On the other part, shortest equilibrium distance and migration time depends upon Reynolds number, particle diameter and constriction clearance. Hence, it is understood that by changing Reynolds number, initial position, particle diameter and constriction clearance control or prediction of equilibrium position, shortest equilibrium distance and migration time can be achieved. Hence, considering all of these parameters a prediction model is made with the assistance of artificial neural network (ANN) algorithm for the forecast of equilibrium position, shortest equilibrium distance and migration time. MATLAB is used to create the prediction model. The multilayer architecture used is illustrated in figure 4.31.

The ANN model has four input layers and three output layers which is evident from figure 4.31. The number of hidden layers is chosen as 18 which is the optimum number which is determined by trial and error method. The number of neurons is taken on the

basis of minimum mean square error (MSE). The input values and observed output values are normalized before entering into the ANN (equation 3.18).

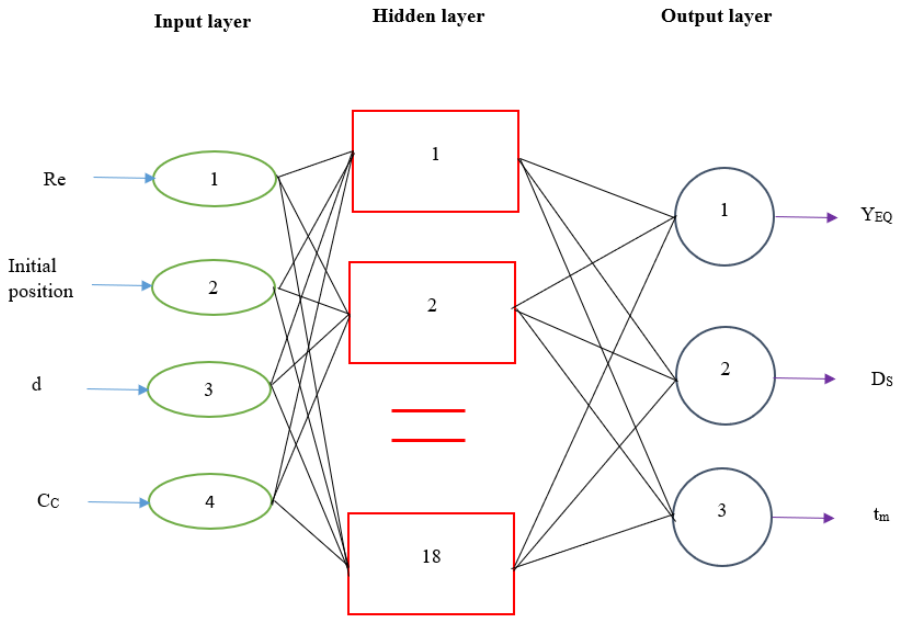

Figure 4.31 Architecture of ANN prediction model

The logarithmic transfer function is used for hidden layers whereas linear transfer function is opted for output layers (Kanchan and Maniyeri 2020a). A total of 108 simulation data are taken and entered into the ANN algorithm. This dataset is divided into two. The two third of the data is used for training and remaining part is utilized for testing. The performance of the ANN prediction model is shown in figure 4.32.

It is understood from figure 4.32 that the training process stops when MSE becomes steady. The behavior of predicted values of equilibrium position, migration time and shortest equilibrium distance are plotted against their corresponding observed values in figure 4.33.

The absolute value of variance is 0.990 which is almost close to 1. The predicted and observed values maintain a linear relationship y=ax+b (y denotes predicted and x represents observed quantities). Here the constants a and b are almost equal to 1 and 0 respectively. Hence, it can be said that ANN prediction model presented here has the best prediction capacity. Further in figure 4.34 a)-c) both the predicted and observed values are mapped against number of tests performed.

It is understood from figure 4.34 a)-c) that for all quantities the predicted and observed values are almost matching. This again proves prediction capability of created ANN model. The significant impact of IBM simulations and ANN model can help us to design optimal microfluidic channel configurations for effective separation of rigid particle under different conditions of fluid flow for various diameter range.

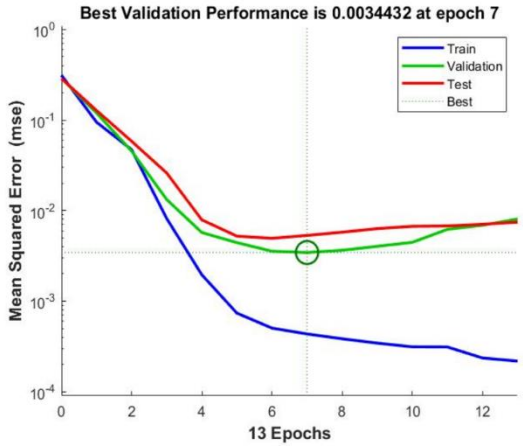

Figure 4.32 Performance plot of neural network training

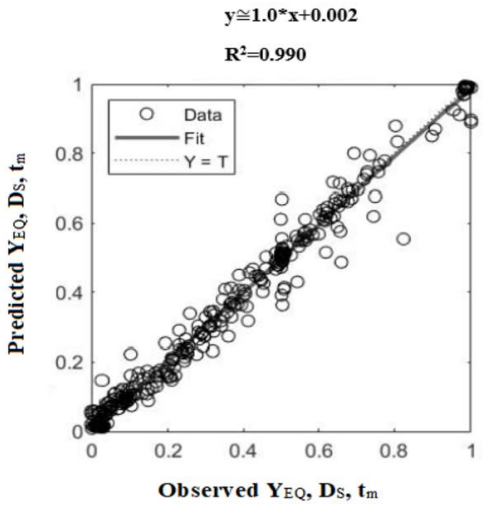

Figure 4.33 Regression plot obtained for both predicted and observed values of Y_{EQ}, t_m and D_S

4.3.3.6 Critical Reynolds number

The present numerical model is utilised to simulate particle migration in constricted channel for Reynolds numbers more than 100. It is noticed that up to some Reynolds number migration time and shortest equilibrium distance increases and after that particular Re, migration time and shortest equilibrium distance start to decline. This

special Reynolds number where migration time and shortest equilibrium distance reach their maximum value and then start to drop is termed as critical Reynolds number (Re_{cr}). As Reynolds number increases shear induced lift and opposing force provided by secondary flow increases but until the critical Reynolds number shear lift acts as dominant force. But for flow above critical Reynolds number the strength of secondary flow vortices overpowers the shear lift which in turn help particle to acquire equilibrium position faster and at a lower shortest distance compared to the case in below critical Reynolds number. In other words, migration time and shortest equilibrium distance tends to increase with raise in Reynolds number up to its critical value and then starts to fall off. So, it is important to determine the critical Reynolds number and study how it is affected by diameter and constriction clearance. The critical Reynolds number can play vital role in separation techniques which is aided by inertial migration. The effect of initial release position is not addressed since it is already understood from section 4.3.3.2 that migration time and shortest equilibrium distance are independent of initial position. Figure 4.35 a) and b) shows the variation in shortest equilibrium distance and migration time with Reynolds number ranging from 100 to 125 for different particle diameters (0.2-0.3). The constriction clearance and particle initial release position are kept as 0.5 and (5.0, 0.5) respectively in all cases.

It is evident from figure 4.35 a) and b) that both shortest equilibrium distance and migration time decreases gradually while Reynolds number changes from 100 to 125 for all diameters of particle. From section 4.3.3.1 it is found that shortest equilibrium distance and migration time increases with Reynolds number from 10 to 100. But after Reynolds number of 100 both start to reduce. So, in case of constricted channel with constriction clearance equal to 0.5 the critical Reynolds number (Re_{cr}) is 100 for all diameters of particle. But it is important to verify whether the critical Reynolds number changes with variation in constriction clearance or not. Figure 4.36 a) and b) shows the variation in shortest equilibrium distance and migration time with Reynolds number for different constriction clearance which vary from 0.5 to 0.7. The particle diameter and initial release position are kept same for all cases as 0.25 and (5.0, 0.5) respectively.

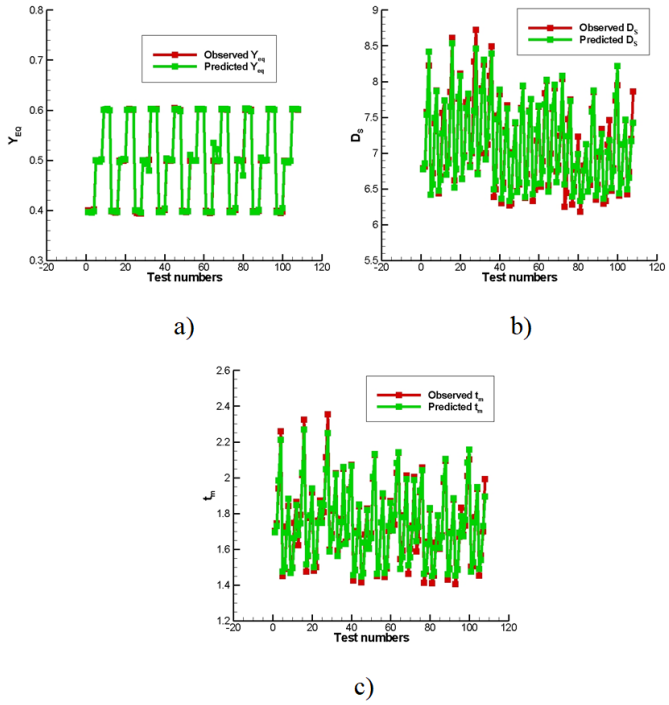

Figure 4.34 Comparison between predicted values and observed values a) equilibrium position Y_{EQ}, b) shortest equilibrium distance D_S, c) migration time t_m

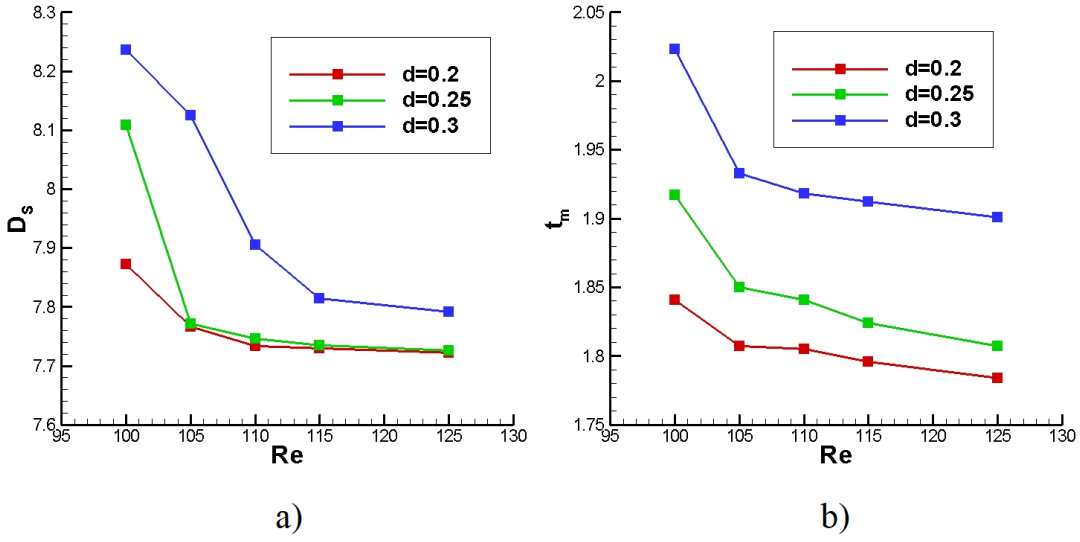

Figure 4.35 a) Variation of shortest equilibrium distance with Reynolds number for different diameters 0.2, 0.25 and 0.3 b) Variation of migration time with Re for different diameters 0.2, 0.25 and 0.3 (Cc=0.5)

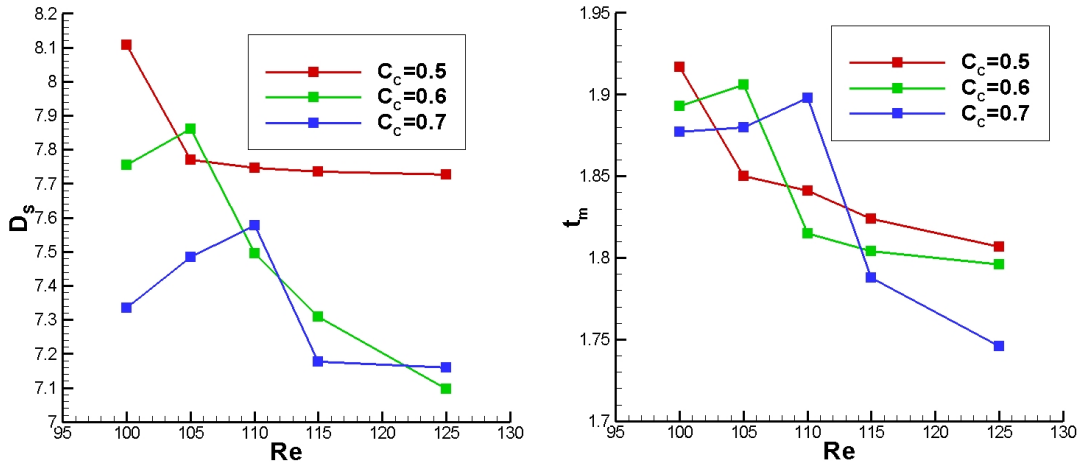

a) b)

Figure 4.36 a) Variation of shortest equilibrium distance with Re for different Cc 0.5, 0.6 and 0.7 b) Variation of migration time with Re for different Cc 0.5, 0.6 and 0.7 (d=0.25)

It is interesting to observe that as constriction clearance varies Reynolds number corresponding to the maximum value of shortest equilibrium distance and migration time changes. In other words, critical Reynolds number increases with raise in constriction clearance. The characteristic of critical Reynolds number is mapped against constriction clearance in figure 4.37.

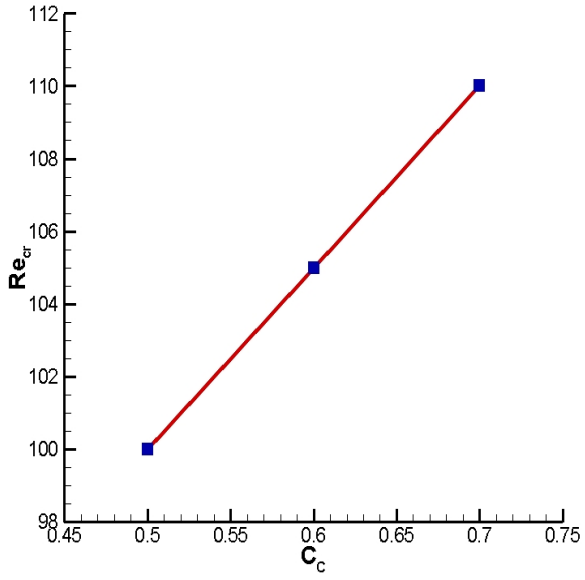

Figure 4.37 Variation of Re_{cr} with Cc (d=0.25)

The critical Reynolds number maintains a linear relationship with constriction clearance as observable can observe from figure 4.37. It can be stated that the critical Reynolds number does not vary significantly with particle diameter but have a linear relationship with constriction clearance. The behaviour of secondary flow vortices present near constricted part should be the cause playing behind this phenomenon. The particle diameter has no influence on size and strength of vortices hence the critical Reynolds number remains unchanged with its variation. However, when constriction clearance is reduced the size of secondary flow vortex enlarges. This will create higher opposing force to shear lift at lower Reynolds numbers. Hence for lower constriction clearance the opposing force put forward by the vortices dominate the shear induced lift at lower Reynolds number and it implies that the critical Reynolds number increases with enlargement of constriction clearance. Therefore, it is evident that for particle migration in constricted channel the critical Reynolds number will be same for all diameters but it varies linearly with change in constriction clearance in channel.

4.3.4 Comparison of inertial migration dynamics in different channel configurations

So far, the detailed parametric study on inertial migration of rigid particle in straight (3.3.1), backward facing stepped and constricted channels are carried out. Out of those, the common parameters were Reynolds number, particle diameter and initial position. The dependence of equilibrium position and migration time on these parameters are tabulated in table 4.5 a) and b).

The variation of equilibrium position and migration time with different parameters in various channel configurations are compared in table 4.5 a) and b). It is clear that, that the presence of additional structures such as constriction arcs and step make significant changes in inertial migration characteristics of particle in channel. The increase in Reynolds number drive equilibrium position towards lower wall in case of straight channel and vice versa in backward facing stepped channel. However, it does not have significant impact in case of constricted channel. This may be due to the presence of constriction arcs. The area of flow through constriction arcs reduces up to center and then increases in gradual pattern. This will cancel out the increase in lift forces due to rise in Reynolds number. On the other hand, migration time reduces with increase in Reynolds number for straight channel and vice versa for constricted channel. However,

it remains unchanged for backward facing stepped channel. This may be due to presence of backward facing step in one side of channel. The size of vortices near the step increases with Re and it will cancel the effect of increased shear induced lift and keep migration time constant. On the other hand, in case of constricted channel, vortices are present on both side of channel which act in opposite directions and it will reduce the magnitude of reverse lift forces against shear lift. Hence migration time can increase with Re in case of constricted channel.

The increase in particle diameter d drives equilibrium position towards channel center for all channel configurations. However, in case of constricted channel the variation is very low compared to straight and backward facing stepped channels. The presence of constriction arcs in both sides can reduce the amount of reversed lift forces and hence the variation of equilibrium position with diameter is reduced considerably. On the other hand, migration time decreases for straight channel with increase in particle diameter and it reduces for backward facing stepped and constricted channels. When step and constriction arcs come, the effect of wall induced lift will increase more. So, the balancing of lift forces will take more time and hence migration time increases with d.

The equilibrium position remains constant with variation in initial position in case of straight channel. On the other part, it changes in case of backward facing stepped, stepped and constricted channel. This is due to the presence of secondary flow vortices in non-straight channels. The effect of forces exerted by these vortices may alter in each position in channel. Hence equilibrium position changes according to initial position. It should be also noted that equilibrium position attained in constricted channel is almost near to initial position. The constriction arcs act in such a way that it balances the lift forces at a point close to initial lateral position. The migration time changes with initial position according to the distance travelled between initial and equilibrium positions in case of straight channel. However, it remains unaltered with initial position in case of backward facing stepped, stepped and constricted since the distance travelled by particle is almost same as inferred from trajectories.

Table 4.5 a) Equilibrium position variation for different channel configurations b) migration time variation for different channel configurations

a)

Channel Configuration	**Increase in Re**	**Increase in d**	**Change in Initial position**
Straight channel	Shifts towards lower wall	Shifts towards channel center	No variation
Backward facing stepped channel	Shifts towards channel center	Shifts towards channel center	Varies
Constricted channel	No variation	Shifts slightly towards channel center	Varies and close to initial position

b)

Channel Configuration	**Increase in Re**	**Increase in d**	**Change in Initial position**
Straight channel	Decreases	Decreases	Changes according to the distance between equilibrium position and initial position
Backward facing stepped channel	No variation	Increases	No variation
Constricted channel	Increases	Increases	No variation

CHAPTER 5. INERTIAL MIGRATION OF VARIOUS SHAPED PARTICLES

The current chapter tries to study inertial migration of various shaped particles such as circular, elliptical, rectangular, square and biconcave. Along with that, the inertial migration dynamics of both neutrally and non-neutrally buoyant particles are compared. The details are given in the following paragraphs.

5.1 Background

It is inferred from literature review in chapter 2 that most of the works in inertial migration focused on circular shaped particles. Very few works are reported on other shaped particles such as elliptical and rectangular ones. Hu et al. (2021) studied and compared the motion of neutrally buoyant elliptical and rectangular particles. Continuous oscillations in the particle trajectories were observed in both elliptical and rectangular ones. The elliptical particle trajectory and orientation in shear flow of Giesekus fluid was analysed by Liu et al. (2021). The formation of elliptical particle trains was studied by Hu et al. (2021) and it was observed that particles form a train with same center-to-center distance at same lateral position. It is a clear known fact that particles migrating in fluids exist in different shapes. For example, sugar fragments are mostly in rectangular or square shape. Also, RBC exist in a special shape called biconcave in some conditions. So, analysis of inertial migration of square, rectangular and biconcave particles will be an important one for process industries and biofluid dynamics.

Most of the previous research concentrated on neutrally buoyant particle migration. It is interesting to see the effect of the mass of the particle in the inertial migration dynamics and equilibrium position. Akhatov et al. (2008) implemented theoretical analysis on the migration of massive aerosol particles in straight channels. Qian et al. (2021) simulated the migration of aerosol particles whose densities were very much higher than the air through which they were moving. When the particles became neutrally non-buoyant, effect of buoyant force also came into play. Hence, along with shear and wall lift forces, the buoyancy force will also significantly affect the equilibrium position. The buoyancy force acts against the induced wall lift. However, the emergence of another force, called Saffman lift, acts as a reactive force against the

buoyancy force. The Saffman lift force depends on the relative velocity of the particle with respect to the fluid and it increases when the (particle to fluid) density ratio becomes higher. Hence, the equilibrium position shifts to the top wall when density ratio increases.

From previous works, it is understood that inertial migration of differently shaped particles such as elliptical, square, rectangular and biconcave needs will be of keen interest. Also, the effect of mass of particle in inertial migration dynamics should be also addressed. Taking these factors into consideration, the present chapter attempts to capture the equilibrium position and migration time of different shaped particles like circular, elliptical, square, rectangular and biconcave. The study also attempts to compare the inertial migration dynamics of various shaped particles for both neutrally and non-neutrally buoyant cases. In the following sections methodology (5.2) and results (5.3) are discussed.

5.2 Methodology

The detailed methodology (feedback forcing assisted IBM) and algorithm are explained in chapter 3 section 3.2. The only difference is the introduction of gravitational acceleration term in the equation of translational velocity to address the non-neutrally buoyant particle migration as given in equation in 5.1 (Feng and Michaelides 2004b, 2009b).

$$\mathbf{U}_p{}^{n+1} = \mathbf{U}_p{}^{n} + \frac{1}{m_p}[\sum(-\mathbf{F}(s,t)ds)]\Delta t + \frac{\rho_f}{\rho_p}\left(\mathbf{U}_p{}^{n} - \mathbf{U}_p{}^{n-1}\right) + (1 - \frac{\rho_f}{\rho_p})g\Delta t \quad (5.1)$$

Where, g is the gravitational acceleration.

5.3 Results and discussion

The migration of different shaped particles is simulated with the help of immersed boundary feedback forcing scheme. The channel size is kept constant throughout the simulation as 50x1. The Lagrangian and Eulerian grid sizes are 0.01 and 0.05 respectively. The values of α and β are -4000.0 and -40.0. The area of all shapes is kept as same for keeping the mass constant (as simulation is two-dimensional).

5.3.1 Migration of neutrally buoyant particle

The migration of circular, elliptical, square, rectangular and biconcave shaped particles is simulated and their migration trajectory is compared. The Reynolds number for each case is kept as 100 and the particle starts movement from (1.0, 0.15). The positions at times 0.0 and 15.0 (final) of different shaped particle are displayed in figure 5.1 a)-b), 5.2 a)-b), 5.3 a)-b), 5.4 a)-b) and 5.5 a)-b). The circular particle diameter is fixed as 0.25. The dimensions of all other particles are taken as keeping their surface area same as that of circular particle (to keep same mass various shaped particles).

All the particles start from same initial position and attain equilibrium position at different locations. From figure 5.3 and 5.4 it can be observed that, rectangular and square particles have tilted to a larger angle from initial position compared to that of elliptical and biconcave particle. It should be noted that, mass of all shapes is equal and hence surface area also. For same surface area, elliptical and biconcave particles have larger horizontal length compared to rectangular and square particles. Hence, these particles will tilt to smaller angles compared to square and rectangular.

The vorticity plot over rectangular and biconcave particles are shown in figure 5.6 a) and b). Vortex shedding can be observed in biconcave particle due to its sharp corners.

The trajectory of y coordinate of particles with time is exhibited in figure 5.7. From figure 5.7 it can be noticed that the y coordinate become constant after particular time for each particle. This lateral position (equilibrium position (Y_{EQ})) and migration time (t_m) are tabulated in table 5.1. It can be observed from figure 5.2 and 5.4 there is oscillation in the trajectory of elliptical and rectangular particles. This is due to the reason that distance between center and points on particle surface keep fluctuating for elliptical and rectangular ones. Hence, there will be oscillation in lift forces as the distance between the points on the surface of elliptical and rectangular particles and channel wall fluctuates compared to the other shapes. This will create oscillation in the particle trajectory.

The equilibrium positions of all particles stay almost in the range 0.2-0.25. The elliptical and rectangular particles attain equilibrium position closer to channel center whereas circular, square and biconcave have equilibrium positions close to lower wall. For circular and square particles, center-to-particle outer surface distance is almost

same while it fluctuates for elliptical and rectangular more. While rotating, the effect of wall induced lift will be more on elliptical and rectangular particles due to this fluctuation in radial distance. Hence, they will attain equilibrium position closer to channel center compared to circular and rectangular particles. However, biconcave is more irregular than elliptical and rectangular particles, but it attains equilibrium position closer to lower wall. This strange behavior may be due to the specialty of biconcave shape. The two dumbbells like structure present at both side of biconcave shape will alter the mass distribution of the shape while rotating. These will alter the center of mass on rotation each time. Hence the biconcave shaped particle will have to travel more distance in lateral downward direction to attain equilibrium position. Hence, the biconcave shaped particle attains equilibrium position closest to lower wall compared to other shapes. The migration time reduces from circular to rectangular. However, there is an abrupt increase in migration time for biconcave particle. This may be due to the reason that biconcave shape is more irregular compared to other shapes. Hence the distance between its points and the wall varies abruptly and hence wall induced lift also. This will lead to more time in balancing of the lift forces and hence migration time increases for biconcave shape.

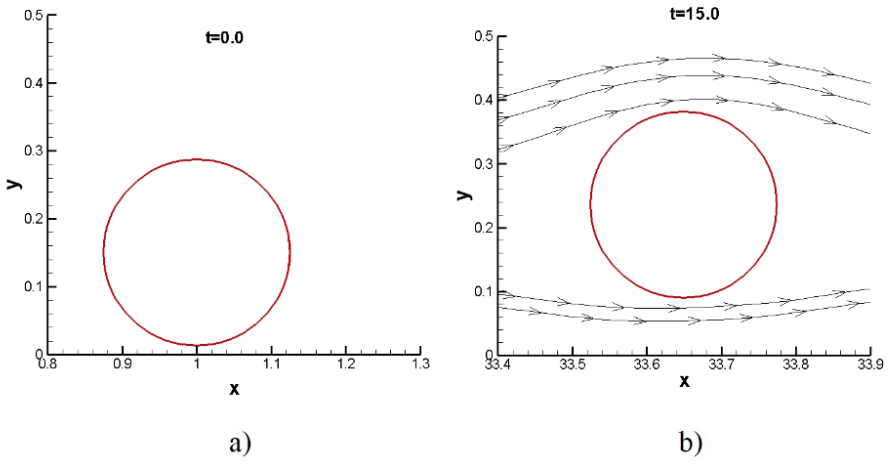

Figure 5.1 a) Initial position, b) final position of circular particle

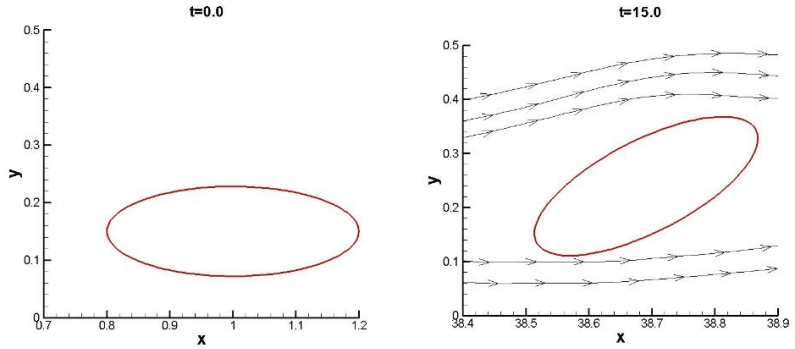

Figure 5.2 a) Initial position, b) final position of elliptical particle

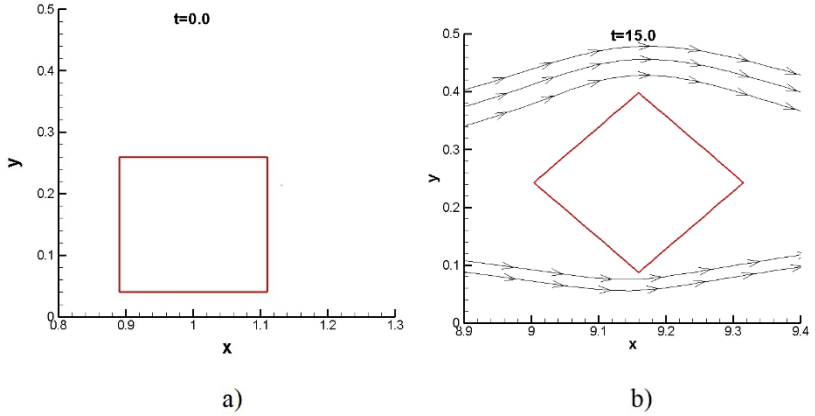

Figure 5.3 a) Initial position, b) final position of square particle

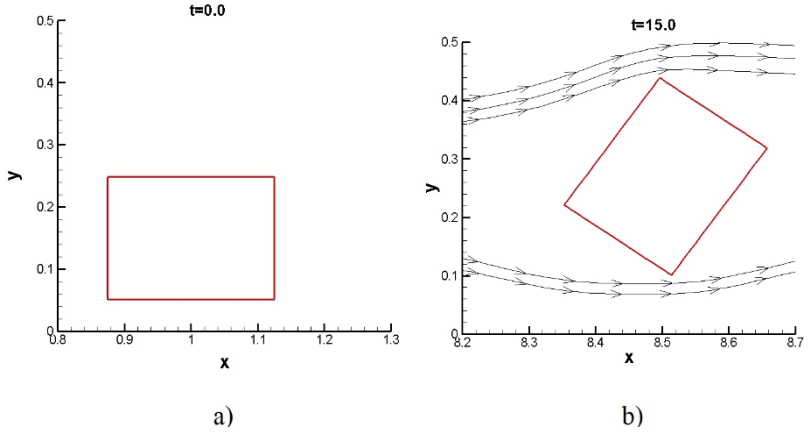

Figure 5.4 a) Initial position, b) final position of rectangular particle

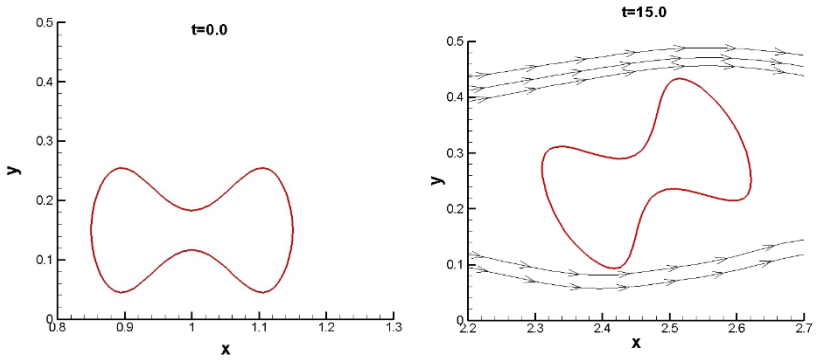

a) b)

Figure 5.5 a) Initial position, b) final position of biconcave particle

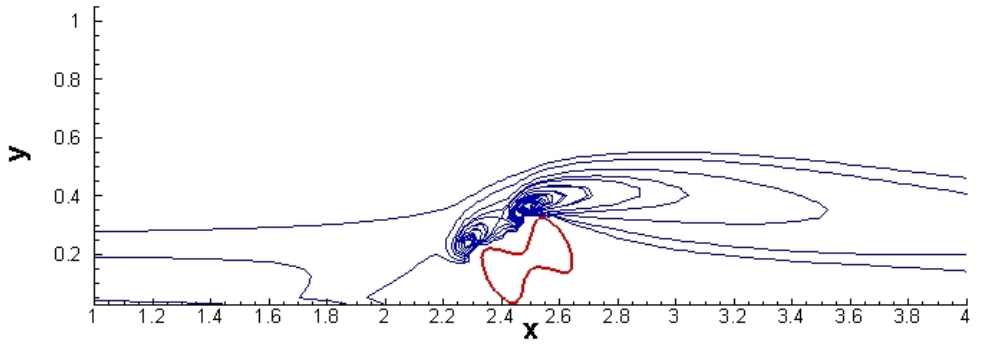

a)

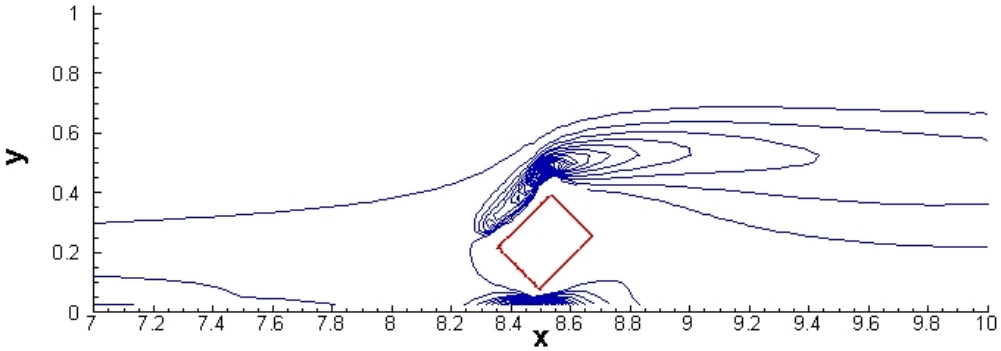

b)

Figure 5.6 Vorticity plot over a) Biconcave particle, b) rectangular particle

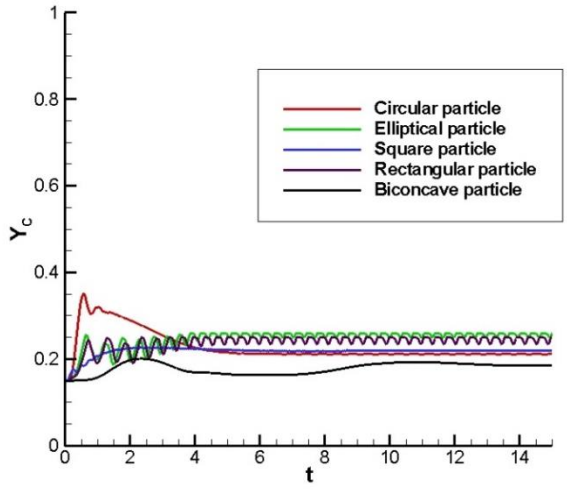

Figure 5.7 Particle trajectory of different shaped particle with time (Re=100.0, density ratio=1.0)

Table 5.1 Equilibrium position and migration time of different shaped particles

Shape of particle	**Y_{EQ}**	**t_m**
Circular	0.222	5.761
Elliptical	0.252	4.132
Square	0.219	3.664
Rectangular	0.240	1.741
Biconcave	0.186	13.379

5.3.2 Migration of non-neutrally buoyant particle

In the next step, the migration of different shaped particles are simulated by taking the ratio of density of particle to fluid as 100. All other parameters are kept same. The particle trajectory for different shaped particles are shown in figure 5.8.

The particle trajectory shows the same oscillation for elliptical and rectangular particles. The equilibrium position shifts towards lower wall when buoyancy force comes into picture. It should be also noted that the migration time of all particles are reduced and the equilibrium position is shifted towards lower wall compared to the neutrally buoyant cases as shown in table 5.2.

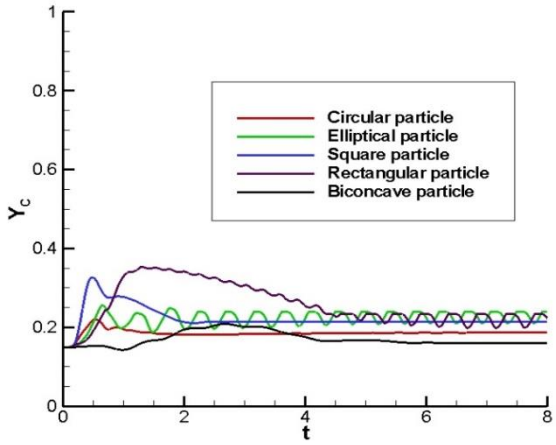

Figure 5.8 Particle trajectory of different shaped particle with time (Re=100.0, density ratio=100.0)

Table 5.2 Equilibrium position and migration time of different shaped particles (Re=100, density ratio=100)

Shape of particle	**Y_{EQ}**	**t_m**
Circular	0.181	2.283
Elliptical	0.216	2.138
Square	0.215	1.954
Rectangular	0.225	1.941
Biconcave	0.160	5.861

The equilibrium positions have been shifted downwards and the migration time is reduced considerably when particle has mass. The buoyancy force acts against the wall induced lift in the direction of lower wall. This will create a move in the equilibrium position towards lower wall. Also, due to this additional force, the balance of lift forces is reached at a faster rate which in turn, reduces the migration time.

CHAPTER 6. CONTROL FORCE AND INERTIAL MIGRATION IN POISEUILLE AND PULSATILE FLOWS

The current chapter deals with the study of an external axial force applied to control the equilibrium position. This control force is applied in such a way to obtain the equilibrium position in a desired location. The detailed explanations are given below.

6.1 Background

In the previous chapters, it has already been stated that the equilibrium position depends on flow velocity, particle size and channel dimensions. However, if it is possible to direct the particles towards an equilibrium position at a particular desired location in the channel, irrespective of all other flow parameters, then it can lead to significant advances in the design of separation devices. (Schaaf and Stark 2017) applied an axial force in the flow, in such a way that deformable particles attained equilibrium positions at the lower end of the channel. The same was later achieved for neutrally buoyant rigid particles (Prohm and Stark 2014). Prohm et al. (2014) utilised external torque to drive the particles and attain an equilibrium position at a particular location. The common characteristic in these works is that all researchers tried to apply the control force in such a manner that the particles attained an equilibrium position at the extreme ends of the channel. Also, the particles considered were neutrally buoyant. The centre of the channel is another important location where separation can take place. However, until now, no works have been reported on the application of control force to bring non-neutrally buoyant rigid particles to the channel centre in inertial migration.

A large part of currently reported studies is based on particle inertial migration in Poiseuille flow. However, in the field of biological fluid dynamics, pulsatile flow has significant importance. The heart pumps blood into the arteries according to this fluid flow pattern. Since blood contains several particles like red and white blood corpuscles and platelets, it is interesting to study particle migration in a pulsatile flow pattern. The particle migration in pulsatile flow was simulated by Huang et al.(Huang et al. 2021) using immersed boundary- lattice Boltzmann method (IB-LBM). It was interesting to observe that there was oscillation in the particle trajectory even after attaining the equilibrium position. It should be also noted that the application of control force for

bringing particle to a desired location in pulsatile flow will provide useful insights to the biological field.

Gaining motivation from the previous studies, the current chapter tries to study the effect of control force applied on inertial migration of massive particles in both Poiseuille and pulsatile flows. The relation between control force and parameters such as Reynolds number, particle diameter and density ratio are explored in both flow cases. Finally, a correlation between control force and parameters are made with the aid of linear regression algorithm. The methodology and detailed results and discussions are given below.

6.2 Methodology

A non-neutrally buoyant cylindrical particle is released in a straight channel with Poiseuille and pulsatile flows, as shown in the physical model (figure 6.1 a) and b)).

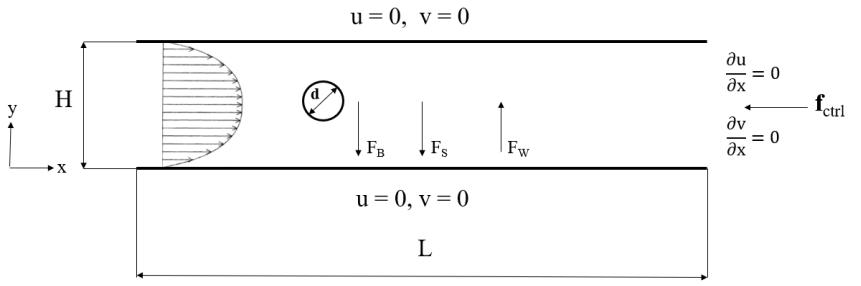

a)

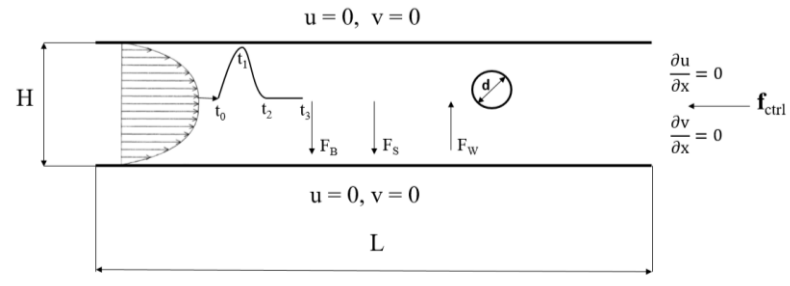

b)

Figure 6.1 Physical model a) Poiseuille flow, b) Pulsatile flow

The pulsatile flow from left side enters the channel and exit the outlet with zero gradient of velocity boundary conditions. The diameter of the particle is represented by d and a

control force $\mathbf{f}_{ctrl}$ is acting against the fluid flow. The control force is a pure fluid force. In the pulsatile fluid flow pattern (Huang et al. 2021) t_0, t_1, t_2 and t_3 are the time intervals corresponding to the initial, peak, end of half pulse and end of one complete pulse cycle velocities. The buoyant force and gravity acts in the negative y direction (downward y as shown in figure 6.1).

The associated N-S equation is given in equation (6.1).

$$\frac{\partial \mathbf{u}}{\partial t} + \mathbf{u}.\nabla\mathbf{u} = -\nabla p + \frac{1}{Re}\nabla^2\mathbf{u} + \mathbf{f}(\mathbf{x}, t) + \mathbf{f}_{ctrl} \quad (6.1)$$

The other equations and methodology are same which is shown in chapter 3.

6.3 Results and discussion

The effect of control force on inertial migration dynamics of massive cylindrical particle in both Poiseuille and pulsatile flows are explored and explained in the following sections.

6.3.1 Control force in Poiseuille flow

A computational model is developed for the simulation of single cylindrically shaped rigid massive particle inertial migration in a two-dimensional straight channel with Poiseuille flow. The considered particle has a significantly higher density than the fluid. The density ratio of the particle to fluid is denoted by ρ. A particle of diameter 0.25 and density ratio 100 is released in a Poiseuille flow channel of 50 x 1 dimensions. The initial position of the particle is (1.0, 0.15). Also, the control force is applied against the direction of flow. The particle trajectory for different magnitudes of control forces is shown in figure 6.2.

As the magnitude of control force increases, particle attains an equilibrium position nearer to the upper wall. The equilibrium position reaches the centre of the channel with a control force of -26.0, as can be seen in figure 6.2. When axial force is applied opposite to the flow, a reverse flow is generated in the initial stage. Due to the action of main and reverse flows, the shear induced lift acts in the direction of the upper wall. This will create dynamic lift over the particle. Hence, the particle attains equilibrium position nearer to the upper wall as the magnitude of control force increases. The

horizontal velocity contour for the zero axial force and -26.0 is shown in figure 6.3 a)-d), respectively.

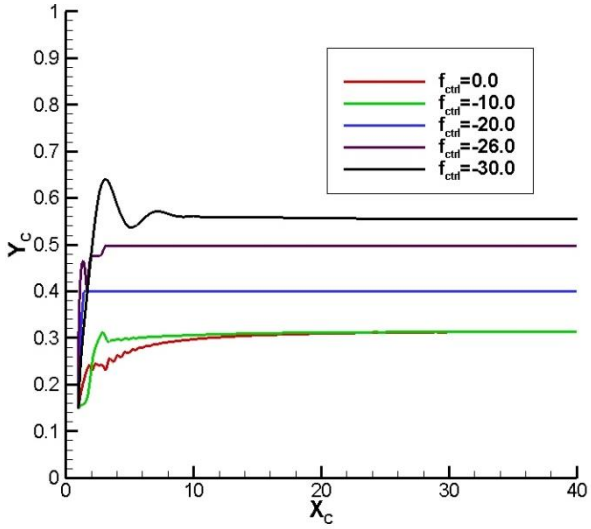

Figure 6.2 Particle trajectory for different magnitude of control forces (Re=10.0, d=0.25, ρ=100.0)

In the absence of external forces, the particle migrates with the fluid flow from left to right and attains an equilibrium position close to 0.31. However, when $\mathbf{f}_{ctrl}$ is applied (as a fluid force in the opposite direction to the flow), reverse flow occurs in the initial stages (t=0.1), as can be seen in figure 6.3 c). The action of the primary and reverse flows pushes the particle to the back of the left-hand side for some time and a dynamic lift is also created over the particle. This dynamic lift is created due to the bulk relative velocity between the fluid and the particle. This is known as the Saffman lift force ($\mathbf{F}_{SA}$) and its expression is given in equation (6.2) (Akhatov et al. 2008a).

$$\mathbf{F_{SA}} = 6.46\,(\tfrac{d}{2})^2\,(\mathbf{u}(\mathbf{x},t) - \mathbf{U}_P)\sqrt{\frac{1}{Re}\frac{\partial \mathbf{u}(x,t)}{\partial y}}\,\mathrm{sign}\left(\frac{\partial \mathbf{u}(x,t)}{\partial y}\right)e_y \qquad (6.2)$$

where e_y is the unit vector. Equation (6.2) shows that the Saffman lift force depends on the relative velocity of the fluid, with reference to the particle. When the control force is applied, reverse flow will reduce the velocity of the particle which, in turn, increases the relative velocity of the fluid, leading to a rise in the Saffman force. This will create additional lift, which drives the particle towards the centre of the channel. However, the channel flow becomes steady after some time and then the particle travels in the horizontal direction (figure 6.3 d)). Finally, the particle attains an equilibrium position.

The Saffman lift force, varying with time in the presence and absence of the control force, is shown in figure 6.4.

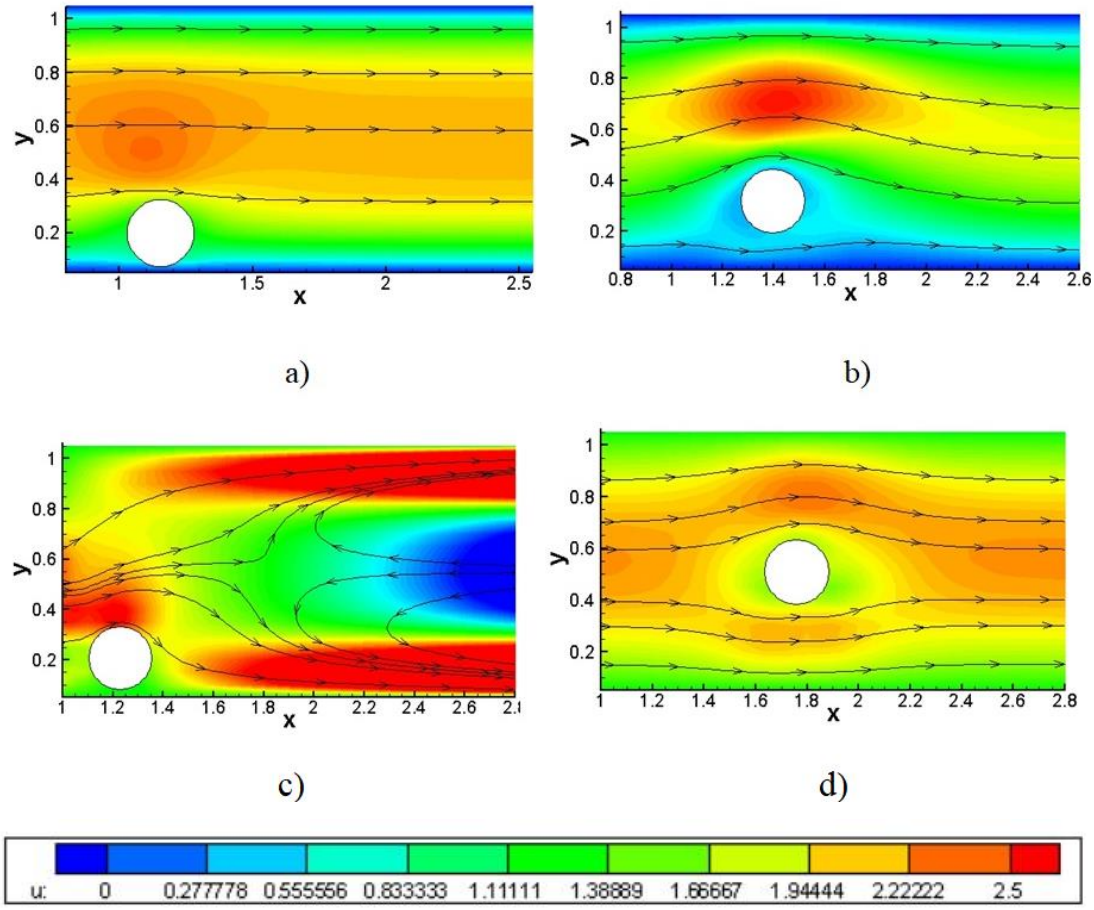

Figure 6.3 The u velocity contours for particle migration in the absence and presence of external controlling force a) t=0.1 without $\mathbf{f}_{ctrl}$ b) t=1.0 without $\mathbf{f}_{ctrl}$, c) t=0.1 with $\mathbf{f}_{ctrl}$ =-26.0, d) t=1.0 with $\mathbf{f}_{ctrl}$ =-26.0 (Re=10.0, d=0.25)

It is clear that the magnitude of the Saffman lift force is greater when an external control force is applied against the flow. However, it is interesting to see the variation of total lift force over the particle. The lift force is calculated from the y-component of the Eulerian force density, as given in chapter 4 (equation (4.6)). Figure 6.5 shows the lift force trajectory with particle lateral position.

The lift force reaches zero at YC=0.31, in the case of migrating particles where control force is absent. This means that the particle has reached its equilibrium position at that point. However, when control force is applied, the particle possesses zero lift force at YC=0.51 (close to the centre of the channel). From these results, it can be inferred that

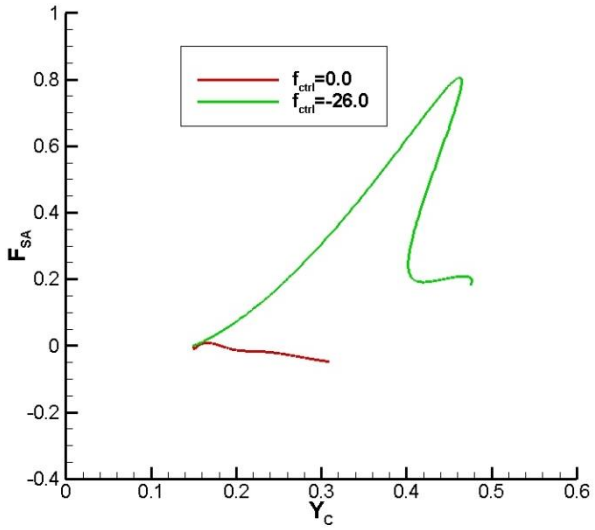

Figure 6.4 Saffman lift force trajectory with particle lateral position in the presence and absence of control force (Re=10, d=0.25)

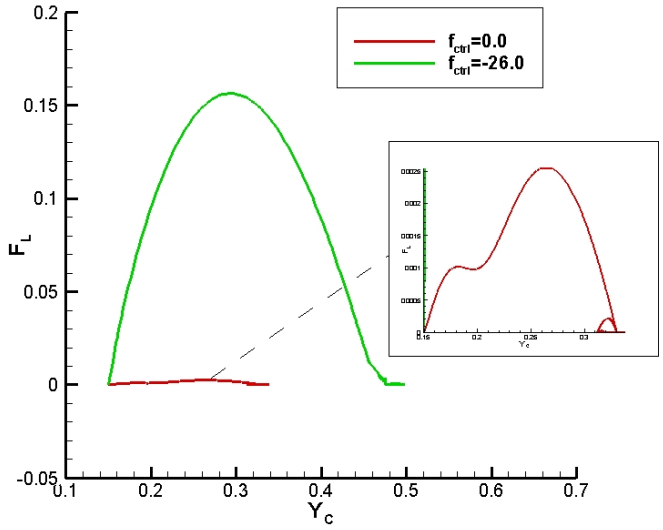

Figure 6.5 Lift force trajectory with particle lateral position

a migrating particle can attain equilibrium position at the channel centre, with the aid of an external control force. However, it is very important to study and analyse the influences of different parameters, such as the Reynolds number, particle diameter and (particle to fluid) density ratio, on the control force.

6.3.1.1 Control force and Reynolds number

The dependency of control force on the Reynolds number is studied in this section. Six Reynolds numbers (10.0, 20.0, 40.0, 60.0, 80.0 and 100.0) are selected for the parametric study. The particle diameter (d) and density ratio (ρ) are kept as 0.25 and 100.0. The trajectory of the particle centre for different Reynolds numbers, in the absence of control force, is shown in figure 6.6.

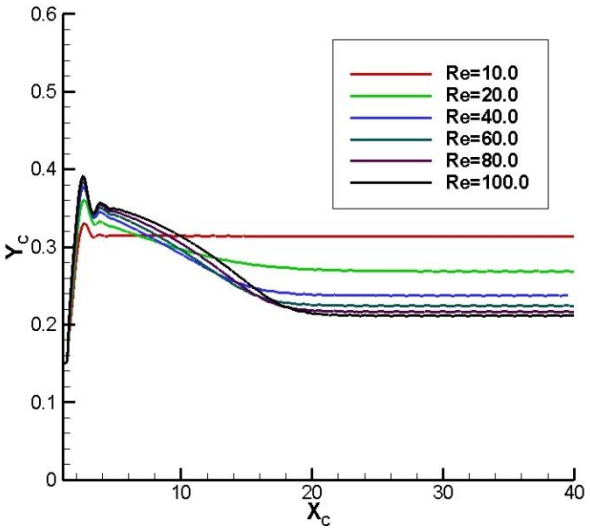

Figure 6.6 Particle centre trajectory with horizontal position for different Re in the absence of $\mathbf{f}_{ctrl}$ (d=0.25, ρ=100.0)

Figure 6.6 shows that the equilibrium position shifts to the lower wall with an increase in Reynolds number. The resistance between fluid layers reduces with an increase in Re, which will raise the slip velocity of the particle, with respect to fluid. This factor contributes to an increase in shear induced lift over the particle and increases with Reynolds number; the particle is driven adjacent to the lower wall. The control force is then applied (the magnitude of control force for each Reynolds number is shown in figure 6.7) to direct the particle towards an equilibrium position at the centre of the channel. The particle trajectory (with horizontal position) in the presence of control forces for each Reynolds number, is shown in figure 6.7.

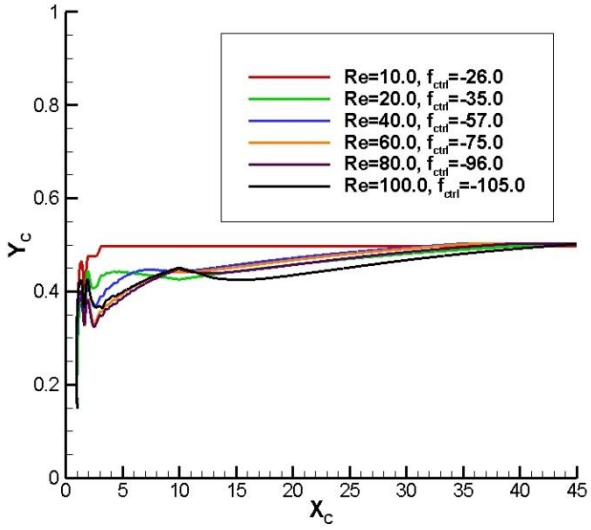

Figure 6.7 Particle centre trajectory in presence of $\mathbf{f}_{ctrl}$ with horizontal position (d=0.25, ρ=100.0)

When the control force is applied horizontally, the particle attains equilibrium position at the channel centre for all Reynolds numbers, as shown in figure 6.7. The migration time also varies in the presence of a control force and is presented in table 6.1.

As shown in table 3, migration time increases as the Reynolds number rises. Since shear induced lift increases with the Reynolds number, the balancing of lift forces will take more time with a rise in the Reynolds number and, therefore, migration time also increases. Table 6.1 also shows that the migration time becomes longer when a control force is applied to the flow. The Saffman lift force becomes larger when a control force is applied and, hence, migration time increases with the application of control force. However, magnitude of the applied control force is different for various Reynolds numbers. The magnitude of control force, for various Reynolds numbers, is plotted in figure 6.8.

Figure 6.8 shows that the magnitude of control force increases with an increase in Reynolds number; the sign of control force is taken to be negative, since it is applied in the opposite flow direction. As Re increases, the effect of induced shear lift force increases and drags the equilibrium position nearer to the lower wall. Hence, the magnitude of applied control force has to be raised to overcome the effect of an increase

in induced shear lift force. This can be attributed to the reason behind the large values of control force required for higher Re.

Table 6.1 Migration time (t_m) for different Re in the absence and presence of $\mathbf{f}_{ctrl}$ (d=0.25, ρ=100.0)

Re	**t_m (Absence of f_{ctrl})**	**t_m (Presence of f_{ctrl})**
10	0.62	0.73
20	6.856	8.531
40	7.073	8.876
60	7.231	9.971
80	7.606	10.025
100	8.096	11.628

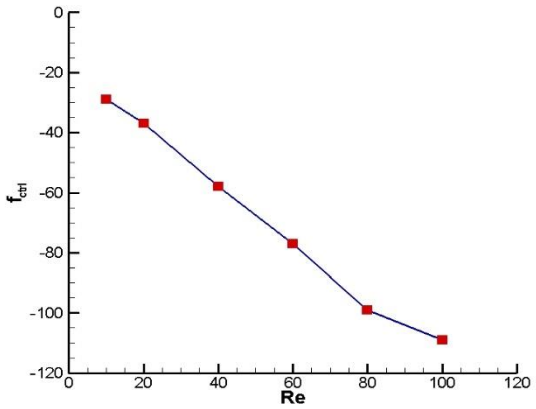

Figure 6.8 The variation of control force ($\mathbf{f}_{ctrl}$) with Re (d=0.25, ρ=100.0)

6.3.1.2 Control force and particle diameter

Here, the influence of particle diameter on control force is studied. Three distinct particle diameters are chosen: 0.2, 0.25 and 0.3. The density ratio and Reynolds number are kept the same (100.0 and 10.0, respectively). The particle trajectory is plotted with horizontal position in figure 6.9.

The equilibrium position of particle shifts to the centre of channel with an increase in particle diameter, as can be seen in figure 6.9. For large particle diameters, the space between outer surface of particle and lower wall decreases. This will enhance the effect of induced wall lift over the particle. Hence, the equilibrium position is driven to the channel centre with an increase in particle diameter. In the next stage, a control force is applied to shift the equilibrium position of particle to the centre of channel and the updated particle trajectories are shown in figure 6.10 (the magnitude of the control force is also shown).

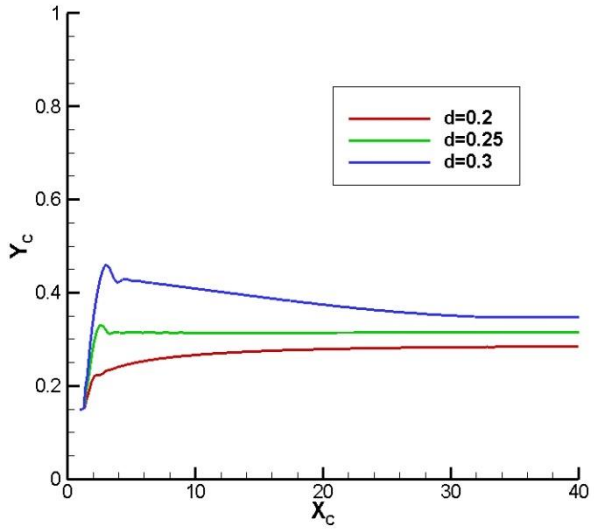

Figure 6.9 Particle trajectory in the absence of control force for different diameters with horizontal position of particle centre (ρ=100.0, Re=10.0)

Figure 6.10 shows that the equilibrium position is shifted towards the channel centre. It should be noted that the equilibrium position is reached at 48.5 for particle diameter of 0.3 which is closer to the outlet in a 50x1 domain. Hence, to show the particle trajectory after equilibrium position, a channel domain of 60x1 is used for this simulation. Table 6.2 presents the migration time in the presence and absence of a control force.

The migration time first reduces and then increases, as the particle diameter increases. This behaviour may be due to two factors. The enhancement in wall-induced lift, due to increased diameter, speeds up the process of lift force balancing and results in reduced migration time. However, a further rise in the diameter causes velocity of the

particle to reduce, since it is inversely proportional to mass of particle. This will increase travel time of the particle and lead to higher migration times. It is also observed that, application of a control force increases migration time. The variation in magnitude of the control force with particle diameter is represented in figure 6.11.

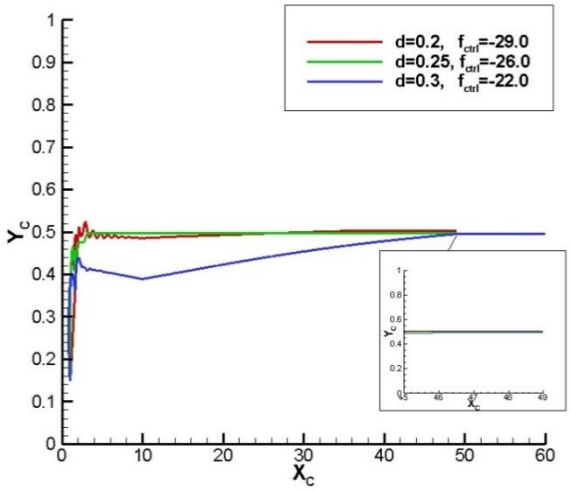

Figure 6.10 Particle trajectory for different diameters in the presence of $\mathbf{f}_{ctrl}$ with horizontal position (Re=10.0, ρ=100.0)

The magnitude of control force required for the attainment of equilibrium position at the channel centre reduces with an increase in particle diameter and the space between lower wall and particle outer surface reduces, since the height of the channel remains constant throughout. This will contribute to an increase in induced wall lift force over the particle which in turn, will push the equilibrium position towards channel centre. Hence, the magnitude of control force required will be at a maximum at the lowest particle diameter.

Table 6.2 Migration time (t_m) for different d in the absence and presence of $\mathbf{f}_{ctrl}$ (Re=10.0, ρ=100.0)

d	**t_m (Absence of f_{ctrl})**	**t_m (Presence of f_{ctrl})**
0.2	4.812	7.94
0.25	0.62	0.73
0.3	7.073	11.921

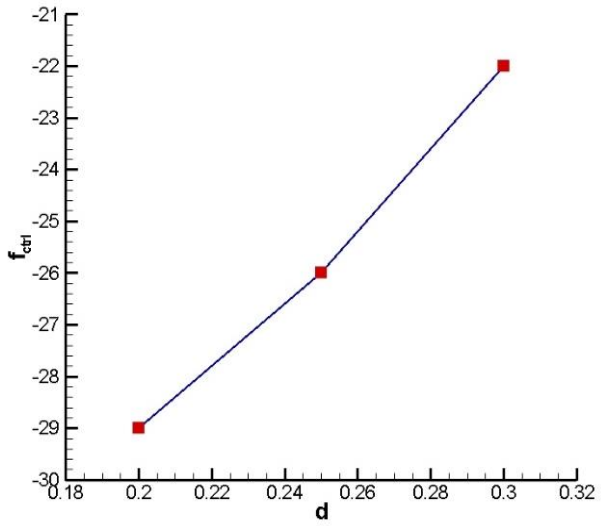

Figure 6.11 The control force variation with d (Re=10.0, ρ=100.0)

6.3.1.3 Control force and density ratio

In the next stage, the influence of density ratio on control force is considered. Three different density ratios (100.0, 200.0 and 500.0) are taken while the particle diameter and Reynolds number are kept constant at 0.25 and 10.0. Figure 6.12 depict the particle trajectory.

The equilibrium position shifts towards the lower wall when the density ratio increases from 100.0 to 200.0. However, it approaches the channel centre when the density ratio is 500.0. The buoyancy force is in the direction of shear induced lift and, when the density ratio increases, equilibrium position should be dragged towards the lower wall. However, when the density ratio goes beyond a particular value, Saffman lift force will increase and will act against shear induced lift. This may be due to increase in relative velocity between the fluid and particle with increase in density ratio (equation (6.2)). Therefore, this phenomenon occurs. Control force is then applied opposite to the flow and the resulting particle trajectories are shown in figure 6.13 and the required control force is also shown. Figure 6.13 shows that particle equilibrium position is shifted to the channel centre with the application of a control force. The migration times are given in table 6.3.

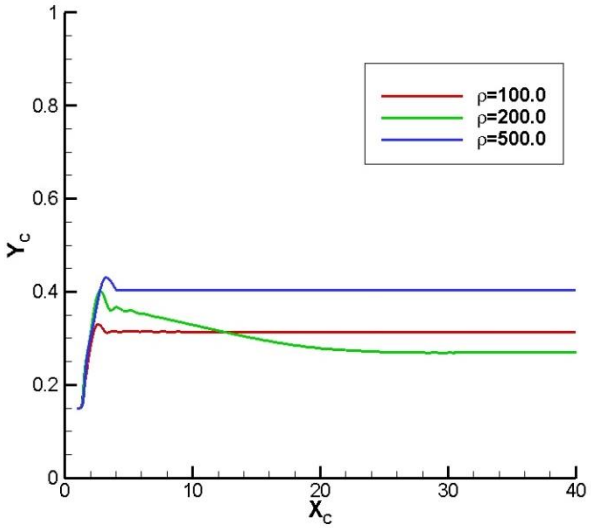

Figure 6.12 Particle trajectory in the absence of control force for different density ratios with horizontal position of particle centre (d=0.25, Re=10.0)

The migration time first increases and then decreases with an increase in density ratio. This may be due to the increase in Saffman lift force and its significant effect on the balancing of lift forces which will, in turn, reduce the migration time. The migration time in the presence of a control force, for density ratios of 200.0 and 500.0, is less than that in the absence of a control force. The effect of Saffman lift force may be the reason behind this. As the density ratio increases, Saffman lift also escalates. This will reduce the time it takes to balance the shear induced lift, which will further reduce the migration time. The magnitudes of control force for different density ratios are shown in figure 6.14. (More data points have been added, in order to check the trend).

The behaviour of control force, with changes in density ratio, is of prime significance. The control force first increases and then decreases with a rise in density ratio. In the absence of a control force, the equilibrium position first shifts towards the lower wall with an increase in density ratio. This may be due to the rise in buoyant force. However, an increase in density ratio will decrease the particle velocity and this will increase the Saffman lift force (equation (6.2)). Therefore, beyond a particular density ratio, equilibrium position will shift towards the channel centre. Therefore, the control force first increases and then decreases, with an increase in density ratio.

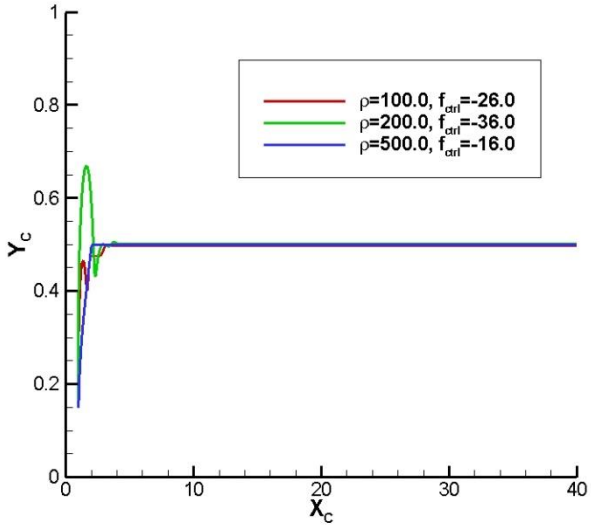

Figure 6.13 Particle trajectory in the presence of control force for different density ratios with horizontal position of particle centre, (d=0.25, Re=10.0)

Table 6.3 Migration time (t_m) for different ρ in absence and presence of $\mathbf{f}_{ctrl}$ (Re=10.0, d=0.25)

ρ	**t_m (Absence of f_{ctrl})**	**t_m (Presence of f_{ctrl})**
100.0	0.62	0.73
200.0	7.536	2.61
500.0	1.5	0.52

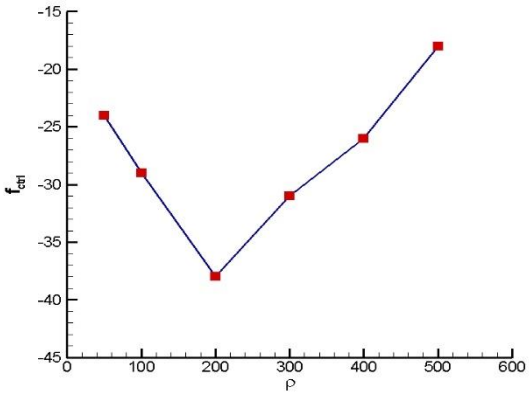

Figure 6.14 Trajectory of control force with density ratio (Re=10.0, d=0.25)

6.3.1.4 Development of prediction model for control force in Poiseuille flow

In the previous sections, control force and its dependence on parameters like Reynolds number, particle diameter and density ratio are discussed. Based on the parametric study, it is decided to build a prediction model for control force. There are three inputs (particle diameter, Reynolds number and density ratio) and one output (control force). To construct such a model, a good number of prediction models, such as artificial neural network (ANN), linear regression (LR), k- nearest neighbour (kNN) etc are available. Linear regression (LR) is considered to be the simplest and easiest to implement scheme.

Linear regression is normally applied to single input-output pairs. If output is y and input is x then LR gives the formula y=px+q, where q is the intercept and p is the slope. However, in the current problem, there are three inputs and one output. The sample diagram of the linear regression model is shown in figure 6.15.

Since there are three inputs in the current case, the natural log of all variables is used as the input to the model. r is the intercept and a, b and c are the coefficients of the inputs, respectively. The relationship between control force and inputs is given by:

$$\log_e \mathbf{f}_{ctrl} = r + a \log_e Re + b \log_e d + c \log_e \rho \tag{6.3}$$

This can be made into a correlation by taking an exponential of both sides of equation (6.4):

$$\mathbf{f}_{ctrl} = r\, Re^a\, d^b\, \rho^c \tag{6.4}$$

As per the parametric study, six Reynolds numbers (10.0-100.0), three diameters (0.25-0.30) and three density ratios (100.0-500.0) are taken into consideration. A total of 54 simulation data are given as inputs to the LR model. The LR model is constructed using machine learning and Python programming language. The coefficients and intercept values are obtained and the correlation obtained is shown in equation (6.5).

$$\mathbf{f}_{ctrl} = 10.076\, Re^{0.673}\, d^{-0.196}\, \rho^{-0.185} \tag{6.5}$$

The variation between predicted and observed values over number of tests is shown in figure 6.16.

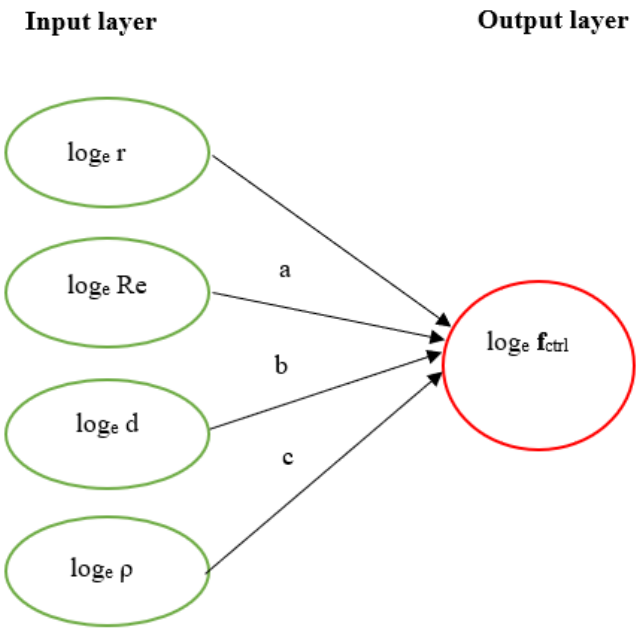

Figure 6.15 Network diagram of linear regression

The predicted values agree with the observed ones. Also, the R square value is greater than 0.9. This shows good prediction capability of the correlation made from the LR model. The correlation is tested on another set of data in the same range. The simulation is further carried out for a set of three Reynolds numbers (30.0, 50.0 and 70.0), density ratios (150.0, 250.0 and 450.0) and particle diameters (0.22, 0.24 and 0.28), which lies in the same range of data used to derive the correlation. The observed and predicted values of control force for the above set of 27 tests are plotted in figure 6.17.

The values of observed and predicted control forces are in agreement. This shows that equation (6.5) can be utilised to predict the magnitude of control force required to shift particle equilibrium position towards the channel centre. It should be noted that, for the above correlation to be applied, particle diameter, density ratio and Reynolds number should be in the range of (0.2-0.3), (100.0-500.0) and (10.0-100.0), respectively. The inertial migration of particles takes place predominantly in the Reynolds number range 1.0-100.0 (Razavi Bazaz et al. 2020). Hence, this correlation can be applied for calculating the magnitude of control force in future applications.

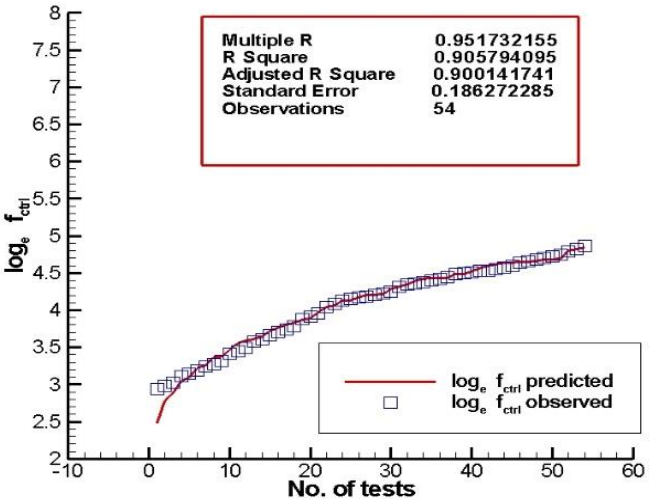

Figure 6.16 The variation of predicted and observed values of $\log_e \mathbf{f}_{ctrl}$

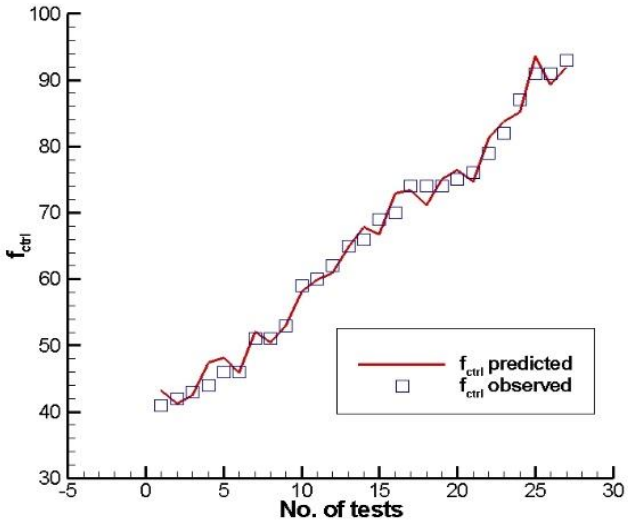

Figure 6.17 The predicted and observed values of control force (test of correlation)

6.3.2 Control force in pulsatile flow

In the next stage, the effect of control force on migration of massive particle in pulsatile flow is explored. Here, non-neutrally buoyant particle (diameter=0.25) migration in a 50.0x1.0 channel is simulated. A control force ($\mathbf{f}_{ctrl}$) is applied against the channel flow. The particle trajectory for different magnitudes of control forces is shown in figure

6.18. The density ratio of particle to fluid (ρ) is 100.0. The frequency of oscillation (υ) is taken as 2.5π.

The particle is released from a position of (1.0, 0.4) and attains equilibrium position at 0.459 (y-position) in the absence of control force. Meanwhile, when the magnitude of control force increases, particle equilibrium position moves up to the upper wall. It is clear from figure 6.18 that particle equilibrium position is brought to the channel centre when a control force of -20.0 is applied. When control force is applied against the flow, a dynamic lift is created over the particle. The u velocity contour for the particle in presence and absence of control force (-20.0) can be observed in figure 6.19 a)-d).

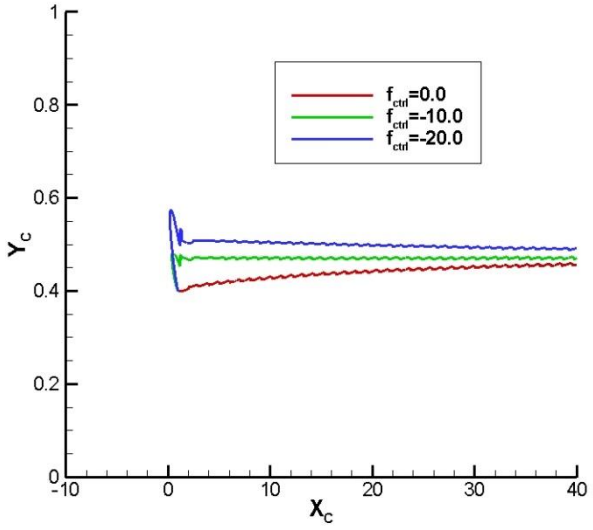

Figure 6.18 Particle trajectory for different control forces (Re=10.0, d=0.25, ρ=100.0, υ=2.5π)

The particle starts from (1.0, 0.4) and attains equilibrium position at 0.459 in the absence of control force, which is noticeable from figure 6.19 a) and b). However, when control force of -20.0 is applied, initially reverse flow happens against the particle (figure 6.19 c)). But the flow becomes fully developed and steady after some time (figure 6.19 d)). However, equilibrium position is shifted to the channel centre. This can be due to the presence of Saffman lift force (F_{SA}). The F_{SA} depends upon the relative velocity of fluid with particle. Hence, when control force acts against the flow, velocity of particle gets reduced and in turn the relative velocity of fluid increases. This will

contribute to the rise in F_{SA}. This is evident in the F_{SA} diagram with lateral particle position in the presence and absence of control force (-20.0) (figure.6.20).

The maximum value of F_{SA} is very much higher in the presence of the control force than in the absence of the same. It should also be noted that the oscillation of the force trajectory is due to the pulsatile nature of the flow. It is also interesting to see the variation of total lift force (F_L) over the particle. (figure 6.21).

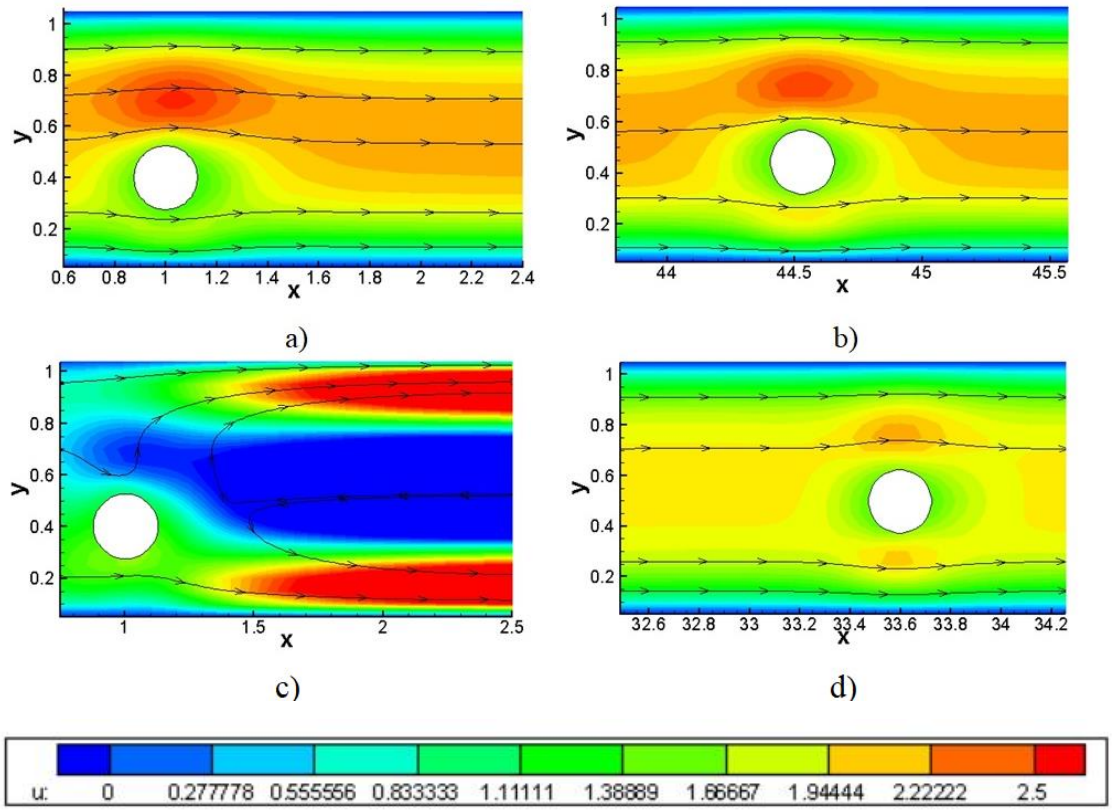

Figure 6.19 The u velocity contours for particle migration in both absence and presence of external controlling force a) t=0.1 without $\mathbf{f}_{ctrl}$ b) t=15.0 without $\mathbf{f}_{ctrl}$, c) t=0.1 with $\mathbf{f}_{ctrl}$ =-20.0, d) t=15.0 with $\mathbf{f}_{ctrl}$ =-20.0 (Re=10.0, d=0.25, $\upsilon=2.5\pi$)

The lift force first attains peak and then becomes zero, as shown in figure 6.21. It means that at equilibrium position lift forces are balanced and their sum becomes zero. When control force is applied, the maximum value of lift force escalates until it becomes zero at the channel centre.

It is known that the parameters of inertial migration, such as equilibrium position and migration time, are highly dependent on flow Reynolds number, density ratio and

particle diameter. Since the flow is pulsatile the effect of frequency of oscillation is also should be analysed. Hence, it is important to examine the influence of these parameters on control force also. Accordingly, parametric study on control force is carried out in the following subsections.

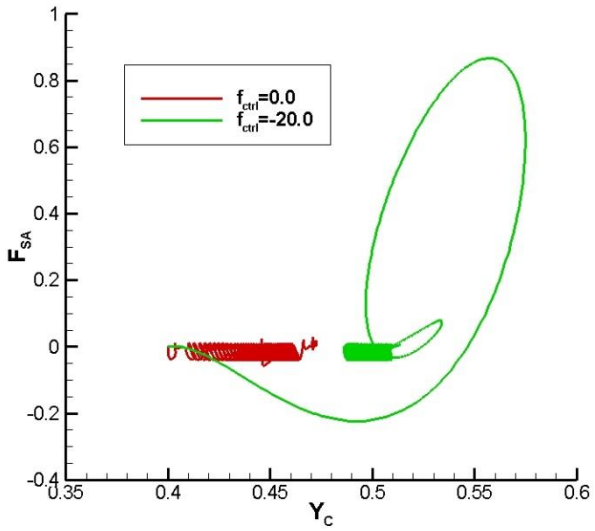

Figure 6.20 Saffman lift force variation with particle lateral position in presence and absence of control force (Re=10.0, d=0.25, υ=2.5π)

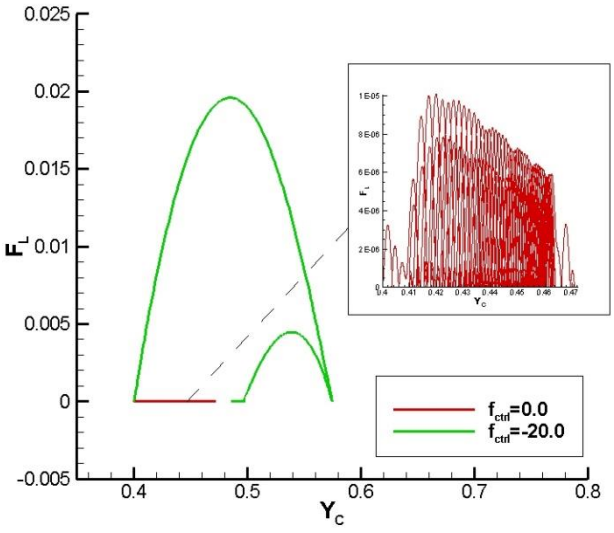

Figure 6.21 Lift force trajectory with particle lateral position

6.3.2.1. Effect of Reynolds number on control force

The effect of Reynolds number on control force is analysed here. For six different Reynolds numbers: 10.0, 20.0, 40.0, 60.0, 80.0 and 100.0 control force are applied in such a way that the equilibrium position of particle is transferred to the center of channel. The diameter, density ratio and frequency are kept constant at 0.25, 100.0 and 2.5π for all cases. The particle trajectory with horizontal position and time in the absence of control force is shown in figure 6.22.

It is clear from figure 6.22 that the equilibrium position is moving towards the lower wall as Reynolds number increases. Now, control force is applied to direct the equilibrium position towards the channel centre, and the updated particle trajectories are plotted in figure 6.23. The control force magnitude is also mentioned in figure 6.23.

It is already stated that the equilibrium position shifts towards the lower wall with an increase in Reynolds number. Hence, a higher magnitude of control force is needed to shift the equilibrium position towards the channel centre. Figure 6.24 shows the same pattern with magnitude of control force mapped to the Reynolds number.In table 6.4 migration time in the presence and absence of control force is shown.

The migration time increases with Reynolds number. The increase in shear induced lift, may be the reason behind this behaviour. The increase in Saffman lift force with the application of control force will also increase the migration time, which is noticeable from table 6.4.

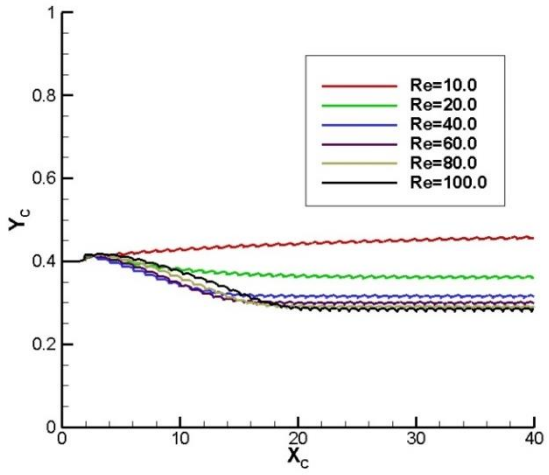

Figure 6.22 Particle center trajectory with horizontal position in absence of $\mathbf{f}_{ctrl}$ (d=0.25, ρ=100.0, υ=2.5π)

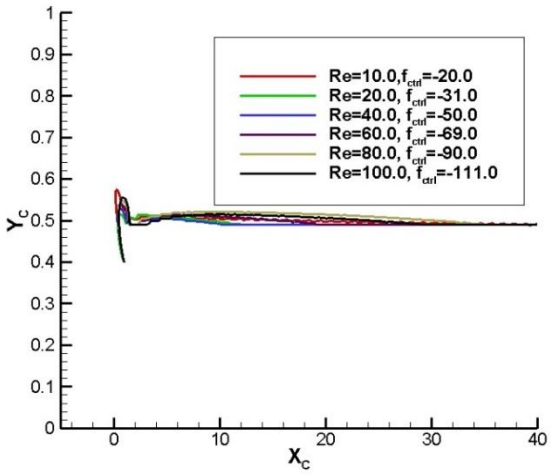

Figure 6.23 Particle centre trajectory in presence of $\mathbf{f}_{ctrl}$ with horizontal (d=0.25, ρ=100.0, υ=2.5π)

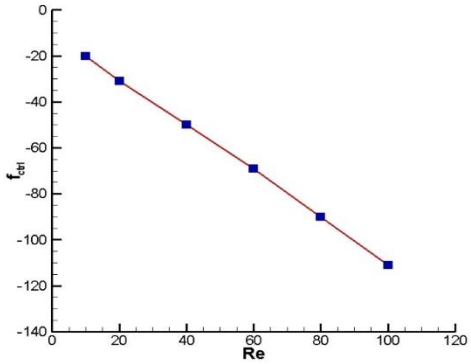

Figure 6.24 The variation of control force ($\mathbf{f}_{ctrl}$) with Re (d=0.25, ρ=100.0, υ=2.5π)

Table 6.4 Migration time (t_m) for different Re in absence and presence of $\mathbf{f}_{ctrl}$ (d=0.25, ρ=100.0, υ=2.5π)

Re	**t_m (Absence of f_{ctrl})**	**t_m (Presence of f_{ctrl})**
10	12.496	19.64
20	13.41	20.08
40	14.286	20.69
60	14.784	21.42
80	15.643	21.59
100	16.24	21.76

6.3.2.2. Effect of particle diameter on control force

In this section, the behaviour of control force with particle diameter is studied. The diameters considered are 0.2, 0.25 and 0.3 while Reynolds number, density ratio and frequency are kept as 10.0, 100.0 and 2.5π respectively. The movement of particle centre for various diameters is shown in figure 6.25 (in the absence of control Force).

The equilibrium position shifts towards channel centre with increase in diameter of particle, as it is observed from figure 6.25. In the subsequent simulation, control force is applied in such a way that equilibrium position is being brought to the channel centre and the corresponding particle trajectories are shown in figure 6.26.

The magnitude of control force applied reduces with an increase in particle diameter, as it is observable from figure 6.26. The magnitude of control force is plotted against particle diameter in figure 6.27.

From figure 6.25, it is clear that the equilibrium position moves nearer to the channel centre with an increase in particle diameter. Hence, the magnitude of control force reduces with the rise in particle diameter, which is visible from figure 6.27. The migration time for different diameters in the presence and absence of control force is shown in table 6.5.

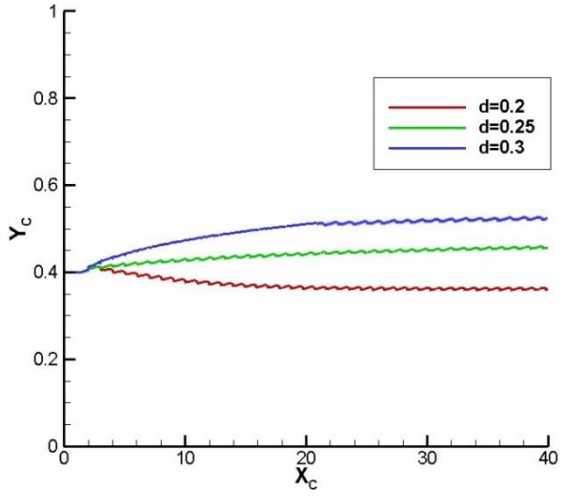

Figure 6.25 Particle trajectory in absence of control force for different diameters of particle with horizontal position of centre of particle (ρ=100.0, Re=10.0, υ=2.5π)

The migration time increases with the particle diameter. The enhanced wall induced lift due to increase in diameter will make the particle to take more time to balance the lift forces and hence, migration time increases. With control force migration time will again increase, as seen from Table 6.5. However, for a diameter of 0.3, magnitude of control force applied is zero and hence migration time remains the same.

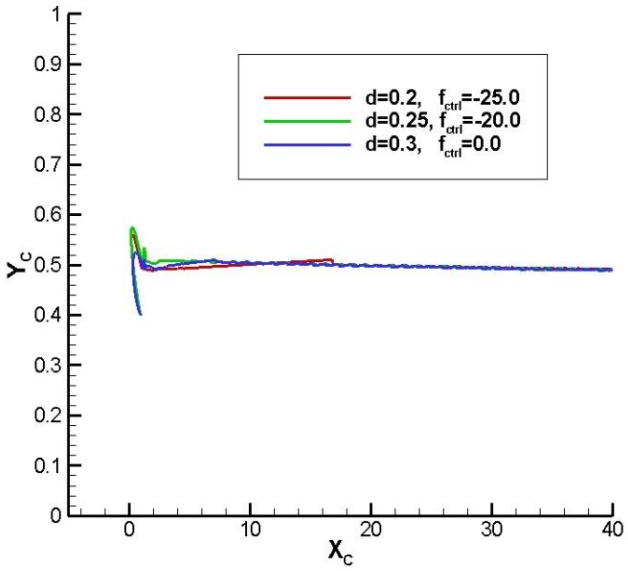

Figure 6.26 Particle trajectory in presence of control force for different diameters of particle with horizontal position of centre of particle (ρ=100.0, Re=10.0, υ=2.5π)

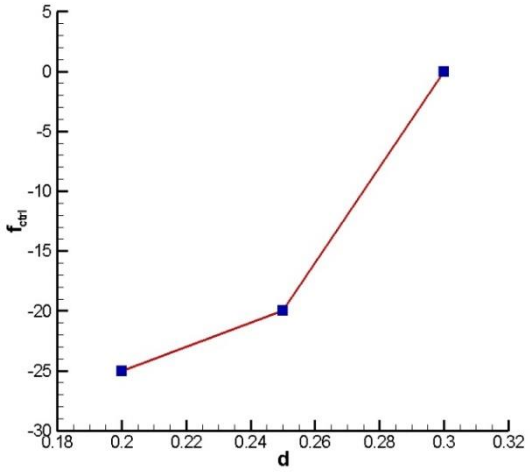

Figure 6.27 The variation of control force with d (ρ=100.0, Re=10.0, υ=2.5π)

Table 6.5 Migration time (t_m) for different d in absence and presence of $\mathbf{f}_{ctrl}$ (Re=10.0, ρ=100.0, υ=2.5π)

d	t_m (Absence of f_{ctrl})	t_m (Presence of f_{ctrl})
0.2	10.012	11.62
0.25	12.496	19.64
0.3	15.14	15.14

6.3.2.3. Effect of density ratio on control force

The dependence of control force on density ratio is addressed in this section. The density ratio of particle to fluid is changed to 100.0, 300.0 and 500.0 while, particle diameter, Reynolds number and frequency are kept same at 0.25, 10.0 and 2.5π respectively. The trajectory of particle in the absence of control force is shown in figure 6.28.

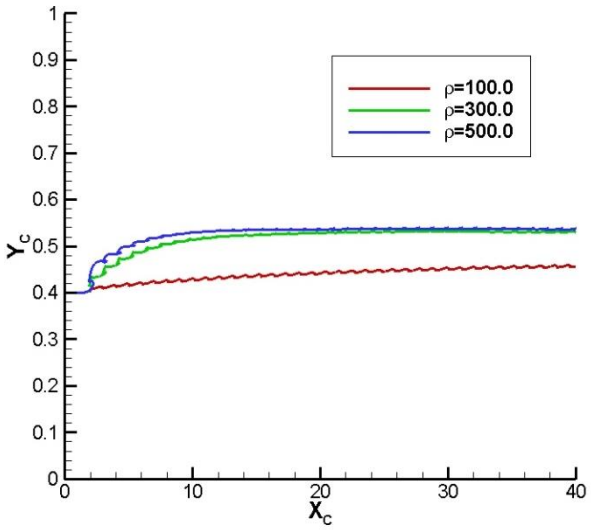

Figure 6.28 Particle trajectory in absence of control force for different density ratios of particle to fluid with horizontal position of centre of particle, (d=0.25, Re=10.0, υ=2.5π)

Equilibrium position shifts towards the upper wall with a rise in density ratio. Now, control force is applied and the resulting particle trajectories are shown in figure 6.29.

Magnitude of control force reduces and then increases (changes its direction) with rise in density ratio. The equilibrium position is observed to be closer to the top wall for a higher density ratio of 500.0 (figure 6.28). Hence, the magnitude of control force applied has to be increased to shift the equilibrium position towards the channel centre as it is clear from figure 6.29. Also, it has to change its direction. The magnitude of control force is mapped in figure 6.30.

It is also interesting to study the effect of control force and density ratio on migration time, which can be seen in table 6.6.

In the absence of control force, migration time increases with a rise in density ratio. This may be due to escalation in Saffman lift force due to the increased density ratio. This will cause the particle to take more time to balance all the lift forces. When control force is applied, the migration time increases for density ratios of 100.0 and 500.0. Since no control force is required for a density ratio of 300.0, migration time stays the same for that particular case.

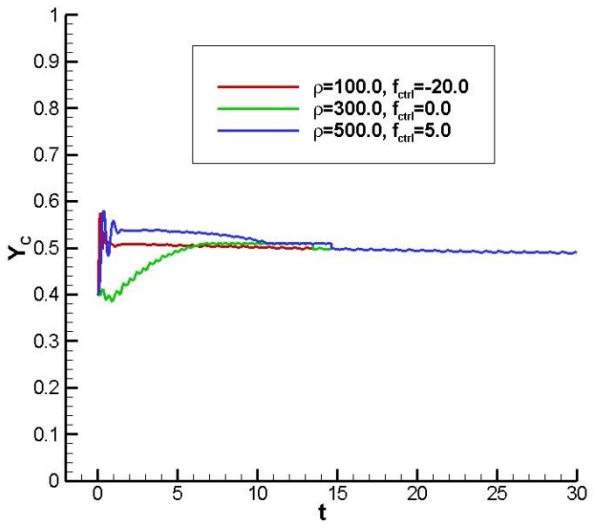

Figure 6.29 Particle trajectory in presence of control force for different density ratios of particle to fluid with horizontal position of centre of particle (d=0.25, Re=10.0, $\upsilon=2.5\pi$)

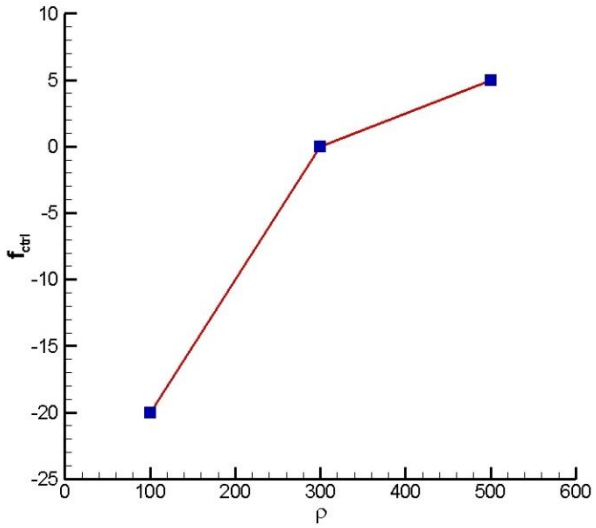

Figure 6.30 Variation of control force with density ratio (d=0.25, Re=10.0, υ=2.5π)

Table 6.6 Migration time (t_m) for different ρ in absence and presence of $\mathbf{f}_{ctrl}$ (Re=10.0, d=0.25, υ=2.5π)

ρ	**t_m (Absence of f_{ctrl})**	**t_m (Presence of f_{ctrl})**
100.0	12.496	19.64
300.0	13.49	13.49
500.0	14.64	16.42

6.3.2.4. Effect of frequency on control force

This section deals with the characteristics of control force with frequency of oscillation. Here, the frequency is varied as 2.0π, 2.5π and 3.0π and other parameters such as Reynolds number, density ratio and diameter are set at 10.0, 100.0 and 0.25 respectively. The resulting particle trajectories in absence of control force is shown in figure 6.31.

The equilibrium position gets shifted towards lower wall as frequency increases. The increase in frequency reduces the time period between peek and minimum velocities of flow. Hence, the peak velocity is attained faster and hence the shear induced lift will increase. This will drive the particle towards lower wall as shown in figure 6.30. Moving on, the control force is applied to drive the equilibrium position towards channel centre and the resulting trajectories are shown in figure 6.32.

The magnitude of control force increases with frequency of oscillation as it is depicted from figure 6.32. The equilibrium position goes closer to lower wall with increase in frequency (figure 6.31) and hence the magnitude control force has to be increased accordingly to drive it to channel centre. The magnitude of variation of control force with frequency can be observed in figure 6.33.

The variation of migration time in absence and presence of control force with frequency is given in table 6.7. The migration time reduces with increase in frequency. The flow velocity attains peek value in faster rate with higher frequency. Hence, migration time reduces with increase in frequency.

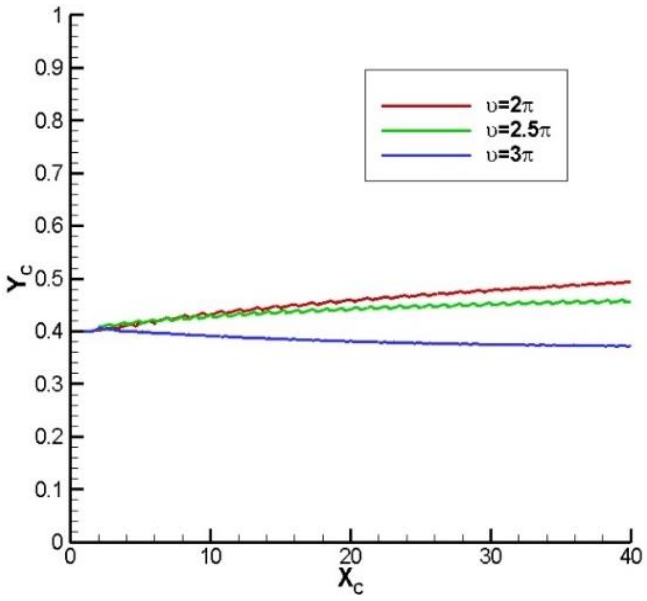

Figure 6.31 Particle trajectory for different frequencies of oscillation in the absence of control force (Re=10.0, d=0.25, ρ=100.0)

6.3.2.5 Prediction model for control force in pulsatile flow

In this stage, a prediction model is developed for the control force in pulsatile flow using linear regression algorithm. The algorithm is already discussed in section 6.3.1.4. The Reynolds number, diameter, density ratio and frequency of oscillation are taken as the inputs. A set of 162 simulations are carried out and the resulting correlation is shown in equation 6.6.

$$\mathbf{f_{ctrl} = 0.0141\ Re^{1.129}\ d^{-1.262}\ \rho^{-0.271}\ \upsilon^{1.526}} \qquad (6.6)$$

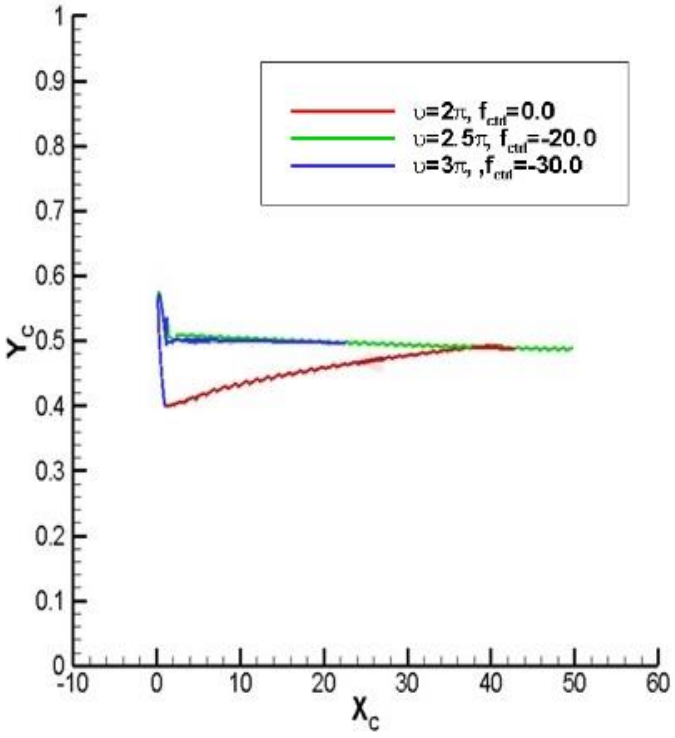

Figure 6.32 Particle trajectory for different frequencies of oscillation in presence of control force (Re=10.0, d=0.25, ρ=100.0)

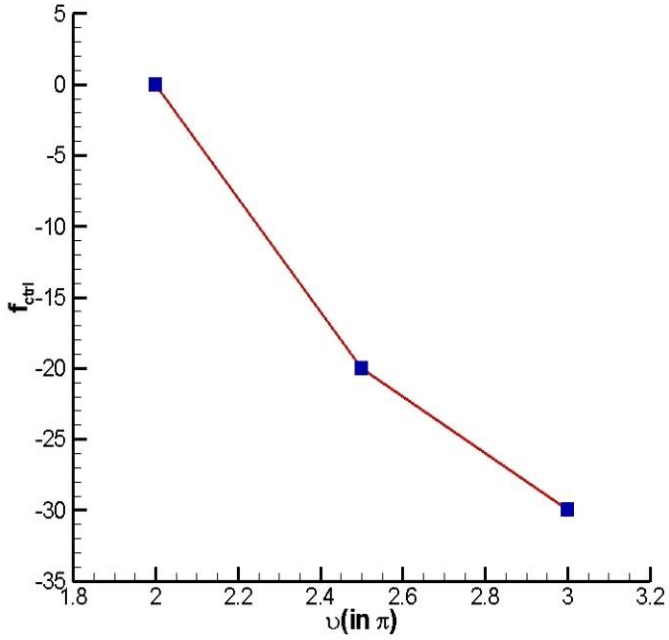

Figure 6.33 Variation of control force with frequency (d=0.25, Re=10.0, ρ=100.0)

Table 6.7 Migration time (t_m) for different υ in absence and presence of $\mathbf{f}_{ctrl}$ (Re=10.0, d=0.25, ρ=100.0)

υ	t_m (Absence of f_{ctrl})	t_m (Presence of f_{ctrl})
2.0π	25.64	25.64
2.5π	12.496	19.64
3.0π	8.62	12.56

The observed and predicted values of natural log of control force are plotted in figure 6.34. The R square value is obtained as 0.96 which is close to 1.0. This proves effective prediction capability of the correlation. The simulation is further carried out for a set of three Reynolds numbers (30.0, 50.0 and 70.0), density ratios (150.0, 250.0 and 450.0), particle diameters (0.22, 0.24 and 0.28) and frequencies (2.2π, 2.4π and 2.6π) which lies in the same range of data used to derive the correlation. The observed and predicted values of control force for the above set of 81 tests are plotted in figure 6.35.

The predicted values are matching with the observed ones. This proves good prediction capability of the correlation.

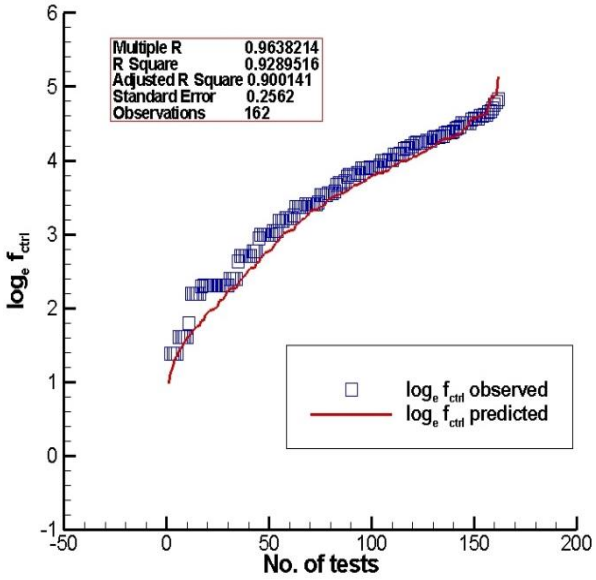

Figure 6.34 The variation of predicted and observed values of loge $\mathbf{f}_{ctrl}$ in pulsatile flow

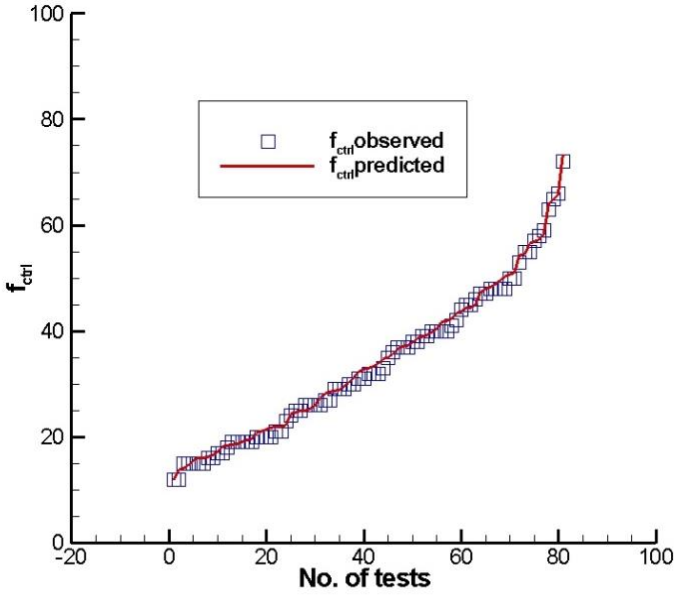

Figure 6.35 The predicted and observed values of control force in pulsatile flow (test of correlation)

CHAPTER 7. INERTIAL MIGRATION OF MULTIPLE PARTICLES

The current chapter deals with inertial migration of multiple particles in Poiseuille flow. Inertial migration of two particles in a straight channel is simulated and analysed first, followed by migration of two particles in stepped channel. Finally, movement of three rigid particles in a slit channel is studied. The details are presented in the following sections.

7.1 Background

The previous chapters study about inertial migration of single particle in different channel configurations. It should be noted that, very few studies have been reported on lateral migration of multiple particles. Pan & Glowinski (2002) studied about two particle migration in straight channel and they found out the equilibrium position of both particles. The formation of elliptical particle trains in a straight channel was simulated by Hu et al. (2021). It was found that the particles migrate to same equilibrium position and form trains irrespective of initial position in straight channel.

By referring to previous works, current chapter attempts to study the inertial migration dynamics of two particles in a straight channel. The effect of centre-to-centre distance and initial orientation on inertial migration dynamics are discussed along with this. In the next stage, computational model is extended to analyse two particle migration in stepped channel. Finally, the migration dynamics of three particles in a slit channel is discussed. The importance of slit channel is that it is used for many biological applications such as protein transfusion.

7.2 Methodology

The rigid particles migrating in Poiseuille flow in straight, stepped and slit channel are illustrated in the physical models given below.

In figure 7.1 b) the length and depth of rectangular step is denoted by L_C and H_C. In figure 7.1 c) the gap of slit is denoted by slit clearance (S_g) and angle of slit is represented as Ɵ. Here step and slit are modelled as additional immersed boundaries. Accordingly, the Lagrangian force densities are computed by using feedback forcing scheme as shown in equation (7.1) and (7.2).

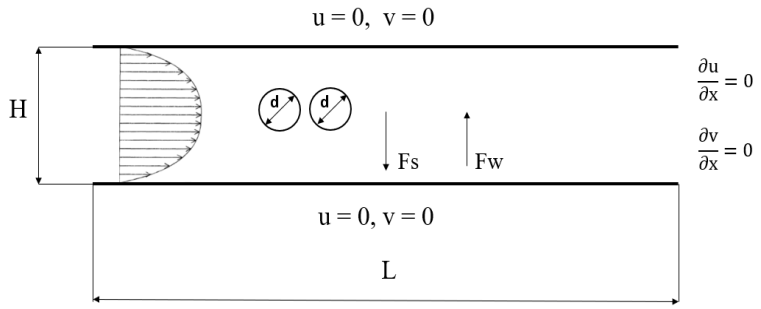

a)

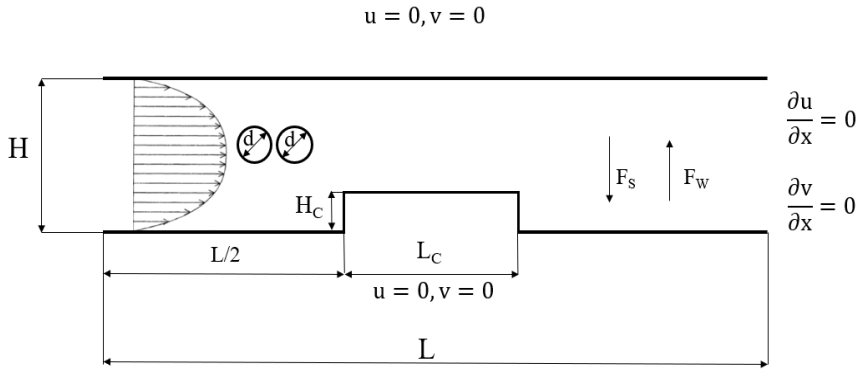

b)

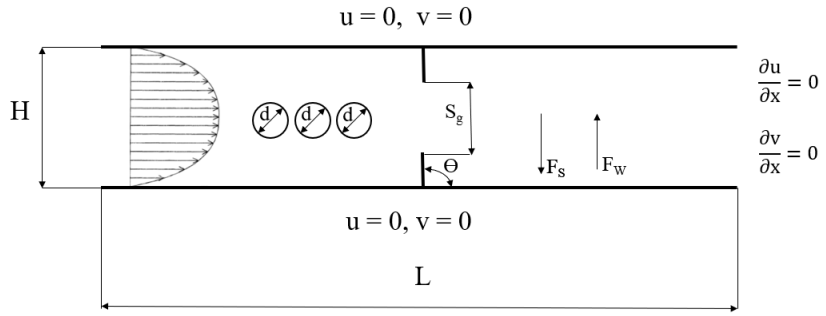

c)

Figure 7.1 Physical models of multiple particles in different channels a) two particles in straight channel, b) two particles in stepped channel and c) three particles in slit channel

$$\mathbf{F}_{P,K}(s,t) = \alpha \int (\mathbf{U}_{ibP,K} - \mathbf{U}_{P,K})\Delta t + \beta(\mathbf{U}_{ibP,K} - \mathbf{U}_{P,K}) \qquad (7.1)$$

$$\mathbf{F}_S(s,t) = \alpha \int (\mathbf{U}_{ibS} - \mathbf{U}_S)\Delta t + \beta(\mathbf{U}_{ibS} - \mathbf{U}_S) \quad (7.2)$$

The subscripts P, K (K=1, 2, 3) and S represents the particle, particle number and structure (step or slit) present in the channel respectively. The immersed boundary velocity is computed by equations (7.3) and (7.4).

$$\mathbf{U}_{ibP,K}(s, t) = \int \mathbf{u}(\mathbf{x}, t)\, \delta(\mathbf{x} - \mathbf{X}_{P,K}(s, t))\, d\mathbf{x} \quad (7.3)$$

$$\mathbf{U}_{ibS}(s, t) = \int \mathbf{u}(\mathbf{x}, t)\, \delta(\mathbf{x} - \mathbf{X}_S(s, t))\, d\mathbf{x} \quad (7.4)$$

The particle velocity $\mathbf{U}_{P,K}$ consist of both angular ($\mathbf{\Omega}_K$) and translational ($\mathbf{U}_K$) components as shown in equation (7.5). Since the step and slits rods are fixed, $\mathbf{U}_S$=0.

$$\mathbf{U}_{P,K} = \mathbf{U}_K + \mathbf{\Omega}_K (\mathbf{X}_{P,K} - X_{C,K}) \quad (7.5)$$

Other equations and algorithm are same as explained in chapter 3.

7.3 Results and discussion

The results associated with the simulation of inertial migration of two particles in straight and stepped channels are discussed in this section. Along with that the migration dynamics of three particles in slit channel is also discussed. The details are given below.

7.3.1 Inertial migration of two particles in straight channel

Two rigid particles are released in Poiseuille flow in a straight channel of length 50 and height 1. The centers of particles are placed 0.5 apart. The particles are released from initial positions (1.0, 0.25) and (1.5, 0.25). The initial and final positions of particles are shown in figure 7.2 a) and b). The Reynolds number and particle diameter are fixed as 10.0 and 0.2. The density ratio of particles is kept same as 100.0.

The particles move and attain equilibrium position at 0.271. This will be evident from figure 7.3 where the particle trajectory is plotted. The particle 1* indicates the trajectory when single particle is released in straight channel, keeping all other parameters same.

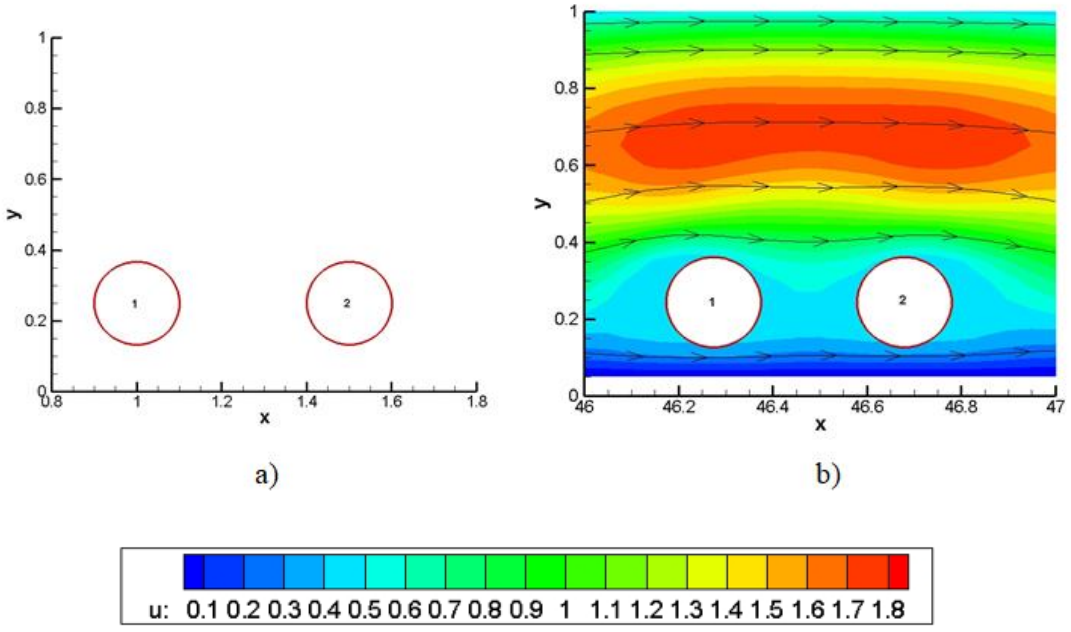

Figure 7.2 Initial and final positions of particles with u velocity contour a) Initial position, b) Final position (Re=10.0, d=0.2)

From the particle trajectory it is understood that the equilibrium positions of particles when two particles are released is almost same. However, it is shifted towards channel centre compared to the equilibrium position attained by single particle released in straight channel. This is due to both hydrodynamic and mutual flow vortex interaction between the two particles. The secondary flow vortices in the downstream side of particle 1 and upstream side of particle 2 interacts and this will create an additional force over the particles which will act against the shear induced lift. Hence, the equilibrium position is shifted towards channel centre for two particle case due to the combined action of these vortices and wall induced lift against shear induced lift.

It is also important to check the variation of centre-to-centre distance (D_C) (calculated as algebraic distance between the position of centres of both particles $D_C = \sqrt{(X_{C,1} - X_{C,2})^2 + (Y_{C,1} - Y_{C,2})^2}$, where subscripts 1 and 2 denotes particle 1 and 2 respectively) with time and it is shown in figure 7.4.

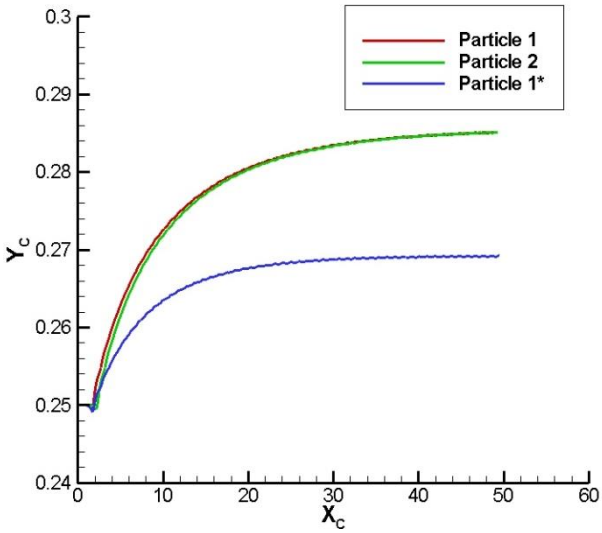

Figure 7.3 Particle trajectory

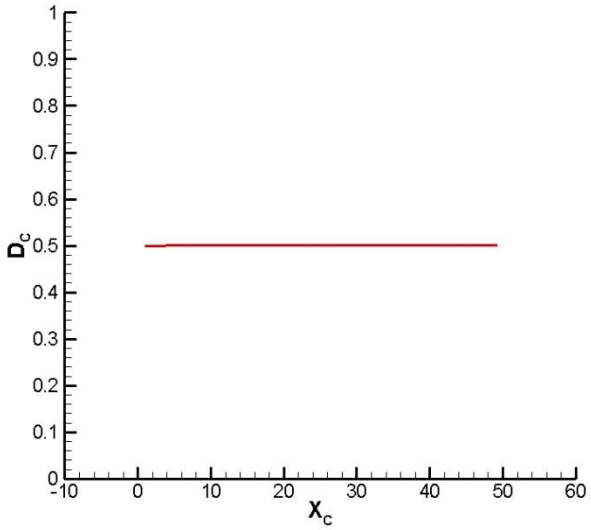

Figure 7.4 Variation of D_C with X_C

Centre-to-centre distance remains almost constant with horizontal trajectory. This may be due to the fact that both the particles are released from same initial lateral position. In case of Poiseuille flow, same lateral position has equal flow velocity and hence both particles will experience same velocity. Hence, centre-to-centre distance will remain constant throughout. However, it is important to check these trends in different scenarios. The initial centre-to-centre distance and initial orientation of particles are varied and checked. The results are presented in the following subsections.

7.3.1.1 Effect of initial centre-to-centre distance

The initial centre-to-centre distance (D_{Ci}) is varied as 0.5, 0.75 and 1.0 and its effects on equilibrium position, migration time and final centre-to-centre distance is studied in this section. The Reynolds number and particle diameter are kept same as 10.0 and 0.2. The resulting particle trajectory is shown in figure 7.5.

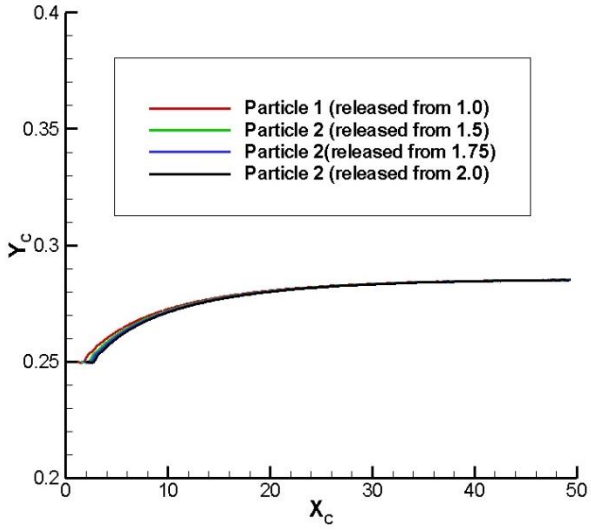

Figure 7.5 Particle trajectory for different D_{Ci}

It can be seen from figure 7.5 that the particles migrate to same equilibrium position with change in initial centre-to-centre distance. This may be due to the fact that the equilibrium position is independent of initial position. Moving on, the variation of final centre-to-centre distance for different initial centre-to-centre distance is plotted in figure 7.6.

It is observed from figure 7.6 that the centre-to-centre distance remains constant throughout for all three cases. The particles are released from same lateral position and hence both particles will experience same velocity of flow. Hence, centre-to-centre distance will remain constant

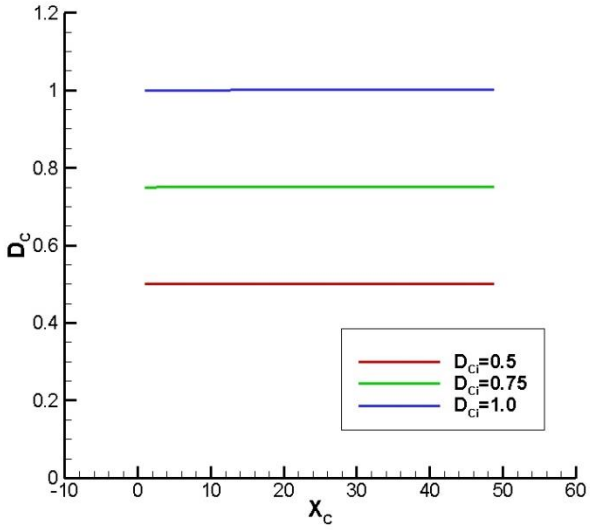

Figure 7.6 Variation D_C with time for different D_{Ci}

. The migration time for all initial centre-to-centre distance is shown in table 7.1.

Table 7.1 Migration time for different D_{Ci}

D_{Ci}	Migration time for particle 1	Migration time for particle 2
0.5	11.582	11.287
0.75	11.582	11.373
1.0	11.582	11.381

The migration time for particle 2 increases slightly with initial centre-to-centre distance. This may be due to the interaction of flow vortices between the two particles. The interaction of flow vortices will give rise to a reverse lift force against the shear induced lift. The combined effect of wall and this reverse lift force will cancel out shear induced lift at a faster rate. However, when initial centre-to-centre distance between particles increases, the interaction of flow vortices will become weak. Hence, the strength of reverse lift force also reduces. So, the balancing of lift forces will take more time when initial centre-to-centre distance increases.

7.3.1.2 Effect of initial orientation

In this section, the effect of initial orientation on inertial migration dynamics of two particles is analysed. Three types of initial orientations are discussed here and they are horizontal, vertical and offset. In all cases the initial centre-to-centre distance is kept as 0.5. The schematic of orientations is given in figure 7.7 a)-c).

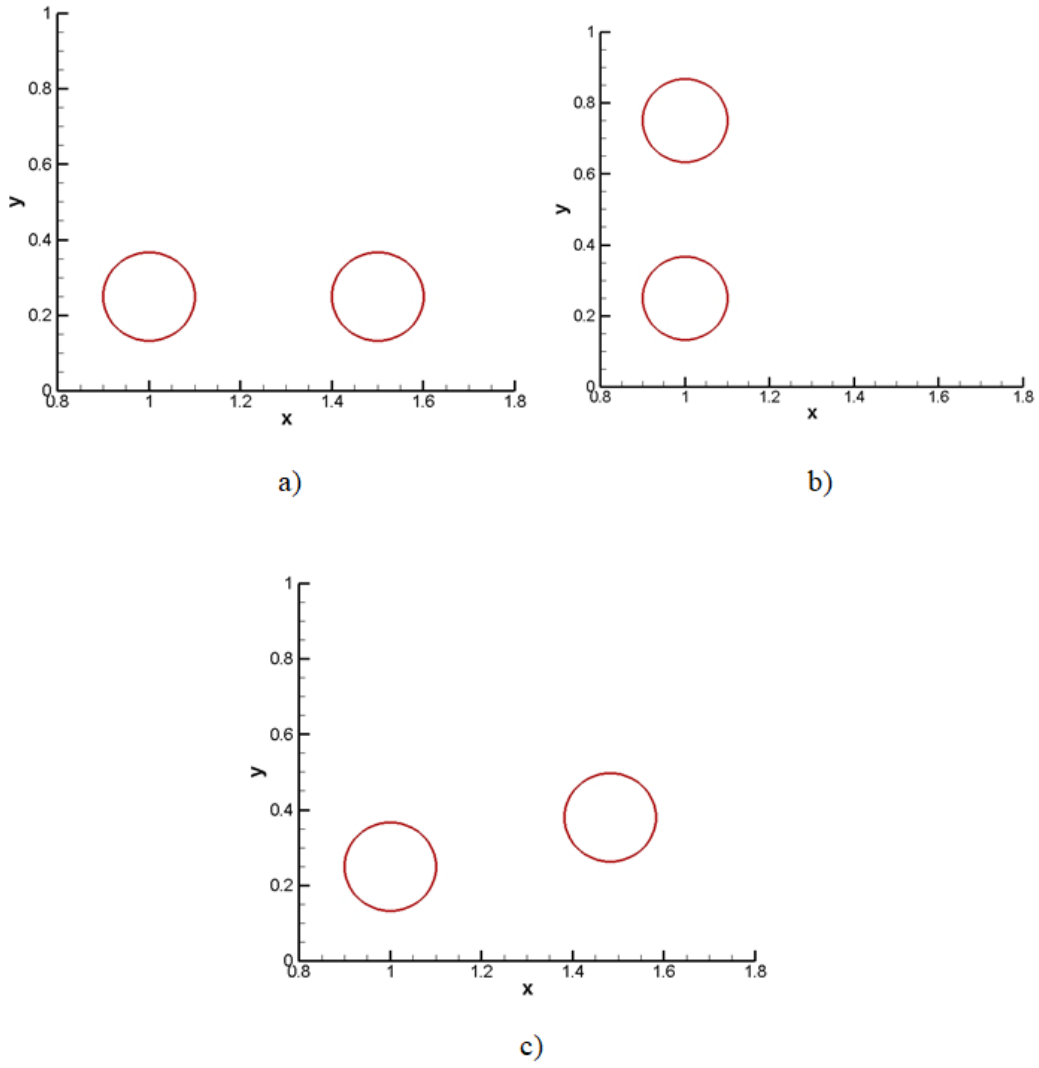

Figure 7.7 Initial orientation of particles a) horizontal, b) vertical, c) offset

The particle trajectory for all cases are shown in figure 7.8 a)-c). From figure 7.8 it can be observed that only particle 2 in vertical orientation attains a different equilibrium position close to top wall. This is due to the fact that particle 2 in vertical orientation is released closer to top wall. Hence, it attains equilibrium position close to top wall. Now, the variation of centre-to-centre distance with time for each orientation is analysed in figure 7.9.

The centre-to-centre distance variation is very high in case of offset than other two conditions. The particle 2 in offset condition is released close to channel centre and hence it will have higher velocity and cover more distance compared to particle 1. It may be the reason behind the variation in centre-to-centre distance in case of offset condition compared to horizontal and vertical. Moving on, the effect of migration time is discussed for different initial orientations in table 7.2.

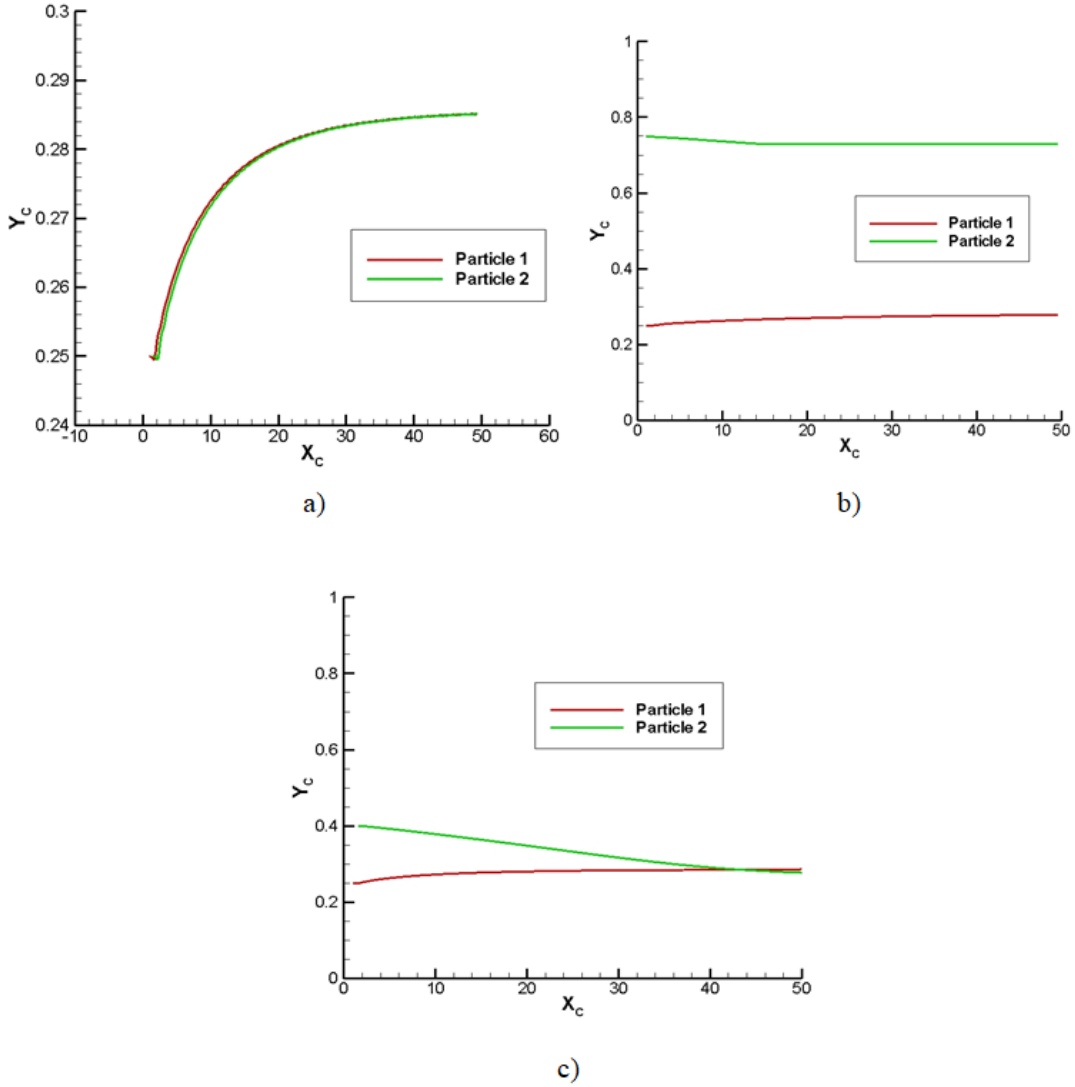

Figure 7.8 Particle trajectory for different initial orientations a) Horizontal, b) Vertical and c) Offset

The migration time is very high for particle 2 in offset condition. The particle 2 in offset condition is released initially closer to channel centre where the velocity is higher compared to initial position of particle 1. Hence, it will move faster in horizontal

direction. However, it will take more time to reach the equilibrium position since the distance between initial and equilibrium position is higher compared to particle 1.

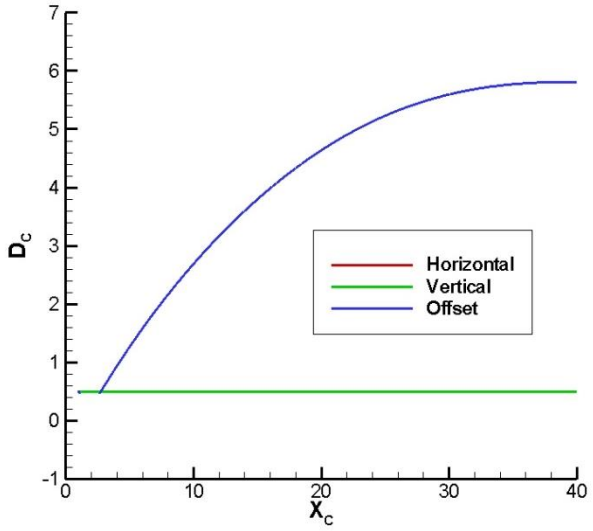

Figure 7.9 Variation of D_C with time for different initial orientation

Table 7.2 Migration time for different Initial orientations

Initial orientation	Migration time for particle 1	Migration time for particle 2
Horizontal	11.582	11.287
Vertical	11.582	11.585
Offset	11.582	18.698

7.3.2 Inertial migration of two particles in stepped channel

In this stage, inertial migration of two particles of diameter 0.2 each released from (5.0, 0.6) and (5.5, 0.6) in a stepped channel (dimension 20x1) is studied. The height and length of step are 0.25 and 2 respectively. The Reynolds number is 50.0. The position of particle at three different time instances are shown in figure 7.10 a) –b). The density ratio of particle is 100.0.

The particles travel over the step and then attain the equilibrium position. Moving on, the study is carried out for three different density ratios (ρ) and depths of step (H_C). The results are discussed in the following subsections.

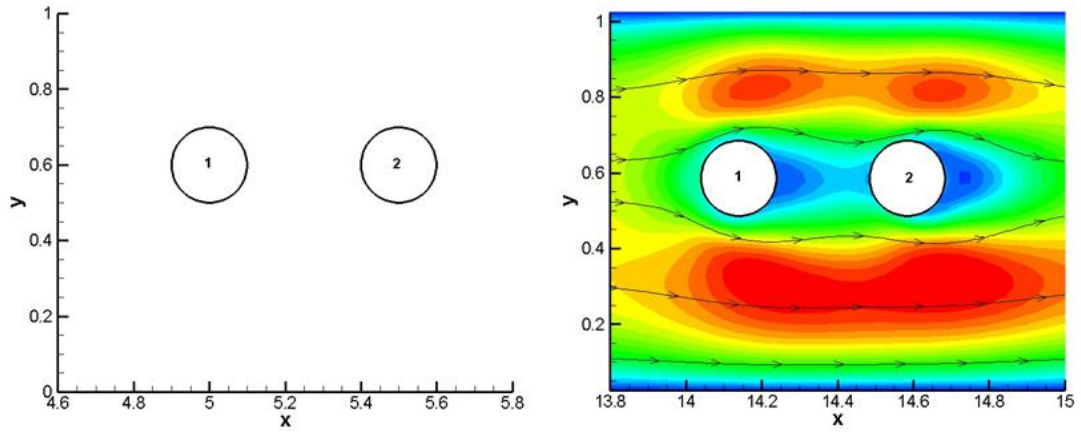

Figure 7.10 a) Initial position of particles ((5.0, 0.6) and (5.5, 0.6) b) Final position of particles with u velocity contour ((14.15, 0.586), (14.61, 0.586)) (Re=50.0, d=0.2, ρ=100.0, H_C=0.25)

7.3.2.1 Influence of density ratio

Two particles having same density as that of the carrying fluid are released from initial positions (5.0, 0.6) and (5.5, 0.6) respectively. The particle diameter and Reynolds number are kept constant as 0.2 and 50.0 respectively. The depth of the step is kept same as 0.25. The particles trajectory for different density ratios with time are shown in 7.11 a)-b).

The particles attain equilibrium position after passing the step. It can be noticed that the equilibrium position is almost same for density ratios of 1.0 and 100.0. However, it moves towards lower wall for a density ratio of 500. It is known that, the buoyant force acts against wall induced lift. Hence, when the density ratio is very high, the buoyant force become very high and by the virtue of that effect, equilibrium position is brought closer to lower wall. Now the migration time is mapped against density ratio for the two particles in figure 7.12.

The migration time increases almost linearly for both particles. The increase in buoyant force will make the particle to take more time for balancing all lift forces. Hence the migration time rises with increase in density ratio. For more clarity, the migration time is tabulated in table 7.3.

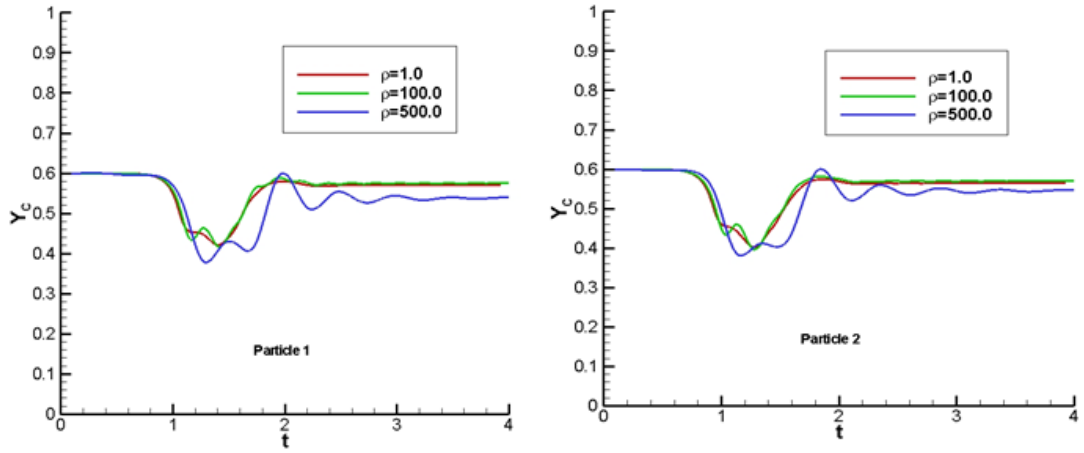

Figure 7.11 a) Particle 1 trajectory against time b) Particle 2 trajectory against time for different density ratios (Re=50.0, d=0.2 H_C=0.25)

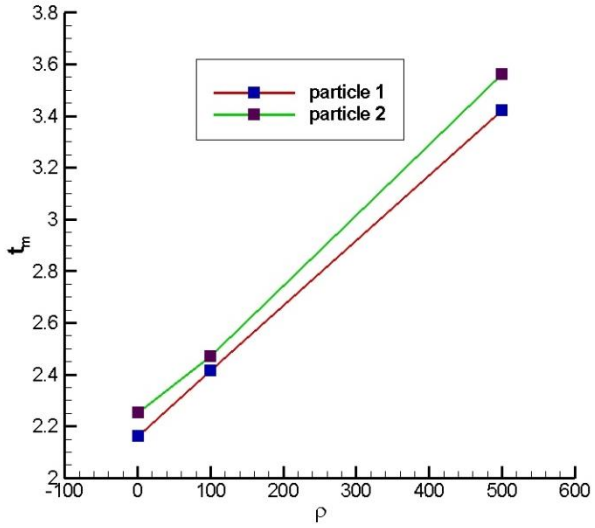

Figure 7.12 Variation of migration time with density ratio (Re=50.0, d=0.2, H_C=0.25)

Table 7.3 Variation of migration time with density ratio (Re=50.0, d=0.2, HC=0.25)

Density ratio (ρ)	Migration time (t_m) of particle 1	Migration time (t_m) of particle 2
1.0	2.162	2.252
100.0	2.416	2.469
500.0	3.423	3.561

7.3.2.2 Influence of depth of step

In this subsection, the effect of depth of step on the migration time and equilibrium position is studied. The depth of step is varied as 0.15, 0.2 and 0.25. On the other hand, the other parameters such as density ratio, Reynolds number and diameter of particle remain constant as 100.0, 50.0 and 0.2. The variation of lateral position of both particles with time for different depths is visualised in figure 7.13 a)-b).

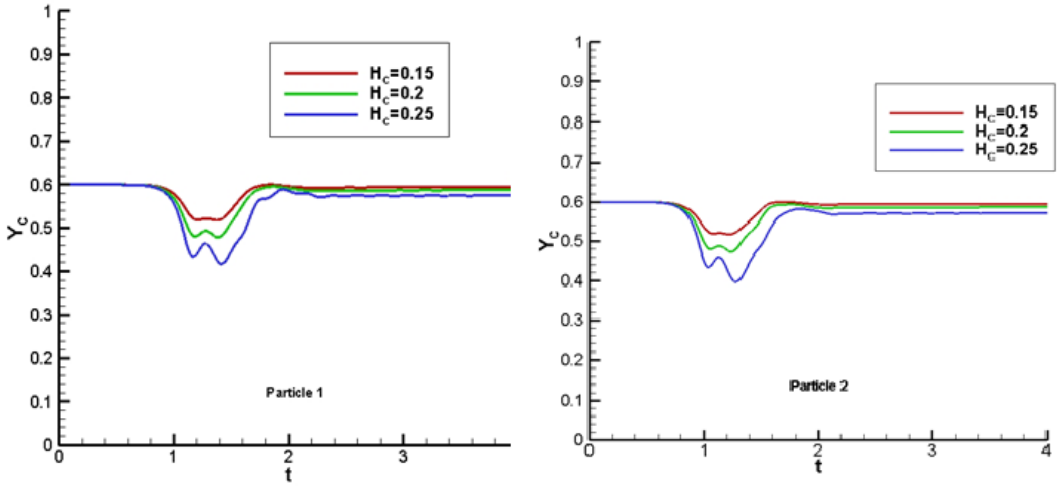

a) b)

Figure 7.13 a) Particle 1 trajectory against time b) Particle 2 trajectory against time for different depths of step (Re=50.0, d=0.2 ρ=100.0)

With the increase in depth of step, the size of the secondary flow vortices near the step increases. This will increase the shear force of fluid applied over the particle and in turn, the shear lift will have larger advantage over induced wall lift. Hence, equilibrium position shifts towards lower wall with increase in depth of step. The characteristics of migration time with depth of step is shown in figure 7.14.

The migration time increases with rise in depth of step. The enlargement in size of secondary flow vortices with increase in depth of step, will increase the time for balancing of forces. This may be the reason for the behaviour. The variation of migration time with depth of step is tabulated in table 7.4 as follows. The depth corresponding to the lowest migration time here is 0.15. Hence, it can be said as the critical depth of step for the present problem.

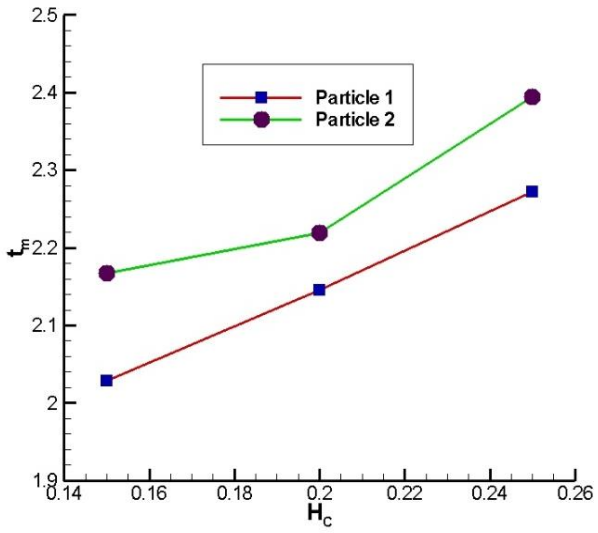

Figure 7.14 Variation of migration time with depth of step (Re=50.0, d=0.2, ρ=100.0)

Table 7.4 Variation of migration time with depth of step (Re=50.0, d=0.2, ρ=100.0)

Depth of step (H_C)	Migration time (t_m) of particle 1	Migration time (t_m) of particle 2
0.15	2.029	2.167
0.2	2.145	2.219
0.25	2.272	2.394

7.3.3 Inertial migration of three particles in a slit channel

The inertial migration of three rigid particles in a slit channel is simulated and analysed in this section. The slit channel is a type of microchannel which is used for biological processes such as protein transfusion, gene therapy and DNA sequencing. A straight channel of 20x1 dimension and a slit is placed at the centre of it is considered. The particle diameters, Reynolds numbers and density ratio are kept as 0.2, 50.0 and 100.0. The time taken by the particles to surpass the slit is termed as residence time. The determination of this residence time can lead light to slit channel design in many biological processes in future. Also, it is important to determine whether the particles pass through the slit without collision. The three particles are separated by centre-to-centre distance of 0.5 and are released from (5.0, 0.5), (5.5, 0.5) and (6.0, 0.5)

respectively. The initial and final positions of particles are shown in figure 7.15. The slit clearance is 0.5 and the slit angle π/2.

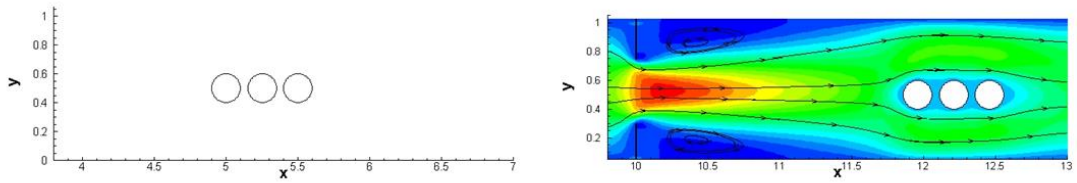

Figure 7.15 a) Initial positions of three particles b) final position of particles with u velocity contour (d=0.2, Re=50.0, S_g=0.5 and Θ= π/2, ρ=100.0)

The particles move past the slit and attain the equilibrium position. It is more evident from figure 7.16 where particle lateral trajectories are mapped against horizontal position and time.

The particle trajectory become parallel to horizontal axis after it passes the slit placed at 10.0 and attain equilibrium position. However, the equilibrium positions coincide for all three particles. This may be due to the same size and initial lateral release position of all the particles. From figure 7.16 b) it is clear that the particles pass the slit at different times. The particle which is placed very close to the slit (particle 3) passes the slit at the earliest. The time taken to pass the slit is called residence time (t_r). It is important to analyse the effect of different parameters such as slit clearance, slit angle, initial position, initial orientation of particles on residence time. Also, it is crucial to check whether all the particles pass through the slit with change in the above-mentioned parameters.

7.3.3.1 Effect of slit clearance

The slit clearance is varied in this section while other parameters such as Reynolds number (50.0), particle diameter (0.2), density ratio (100.0) and slit angle (π/2) are kept constant. The particle trajectory with time is shown in figure 5 for different S_g (0.4, 0.5 and 0.6). For the sake of better explanation, only the trajectory of particle 3 in each case is plotted. The particle trajectory with time is shown in figure 7.17.

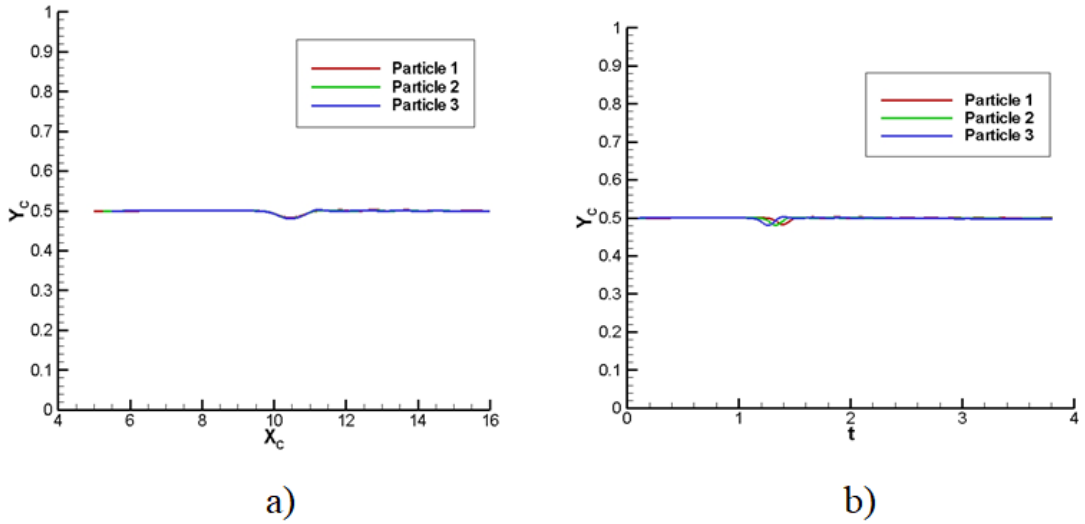

Figure 7.16 Variation of lateral positions of particles with a) horizontal position b) time (Re=50.0, d=0.2, S_g =0.5, Θ=π/2, ρ=100.0)

The equilibrium position of particles stays unaltered with variation in slit clearance. The reduction in slit clearance increases the velocity at the channel centre and it should normally increase the effect of shear induced lift which drive the particle equilibrium position towards either wall. However, the size of flow vortex plays an important role here. The strength and size of flow vortex increases with shortening of the slit clearance. Hence, this will act as a reverse force against the shear induced lift and hence the additional effect of increased velocity gets cancelled. This may be the reason for the unchanged equilibrium position. It is also noticeable from figure 7.17 that the particles take lower time to pass the slit for lower slit clearances. The size of the secondary flow vortex increases with reduction in slit clearance. Hence, the larger flow vortex deflects the particle in horizontal direction and hence the residence time decreases. The same behaviour can be observed from table 7.5 where the residence time for different slit clearances are tabulated. It should be also noted that, all the particles pass the slit without collision for all the slit gaps. When the slit gap was reduced to 0.3, the particles collided with the slit.

7.3.3.2 Effect of slit angle

Here, the effect of different slit angle on the equilibrium position and residence time are analysed. three different slit angles such as π/4, π/2 and 3π/4 are selected for the study. In all three cases the particle diameter, Reynolds number, density ratio and slit

clearance are kept same (0.2, 50.0, 100.0 and 0.5 respectively). The particle trajectory with time for different slit angle is shown in figure 7.18.

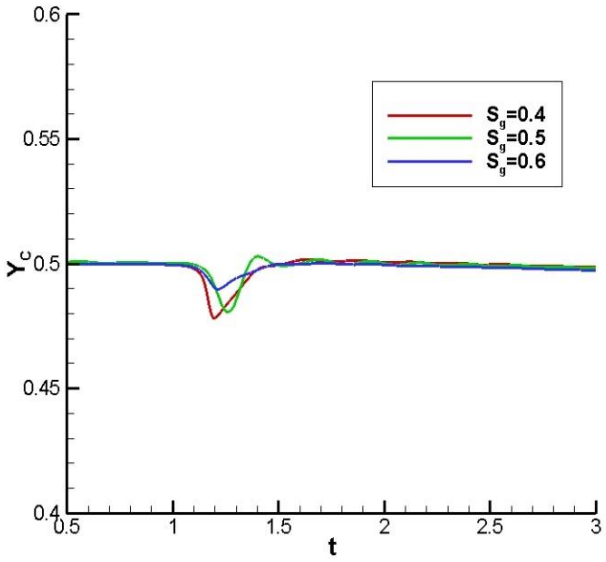

Figure 7.17 Particle trajectory with time for different S_g (Re=50.0, d=0.2, ρ=100.0 and Θ=π/2)

Table 7.5 Residence time (t_r) for different S_g) (Re=50.0, d=0.2, Θ=π/2)

S_g	t_r
0.4	1.476
0.5	1.518
0.6	1.567

The equilibrium position stays unaffected with slit angle. As the slit angle increases from π/4 to π/2 the size of secondary flow vortex increases. This will deflect the particle away from the wall. However, the same effect is cancelled by the increase in flow velocity with change in slit angle from π/4 to π/2. When the slit angle is 3π/4 then the conditions are similar to that of π/4. The residence time is minimum for slit angle of π/2 since the flow velocity is highest and the vortex sizes are largest. To confirm the same, the residence time is tabulated in table 7.6. The collision did not happen for any of the three cases.

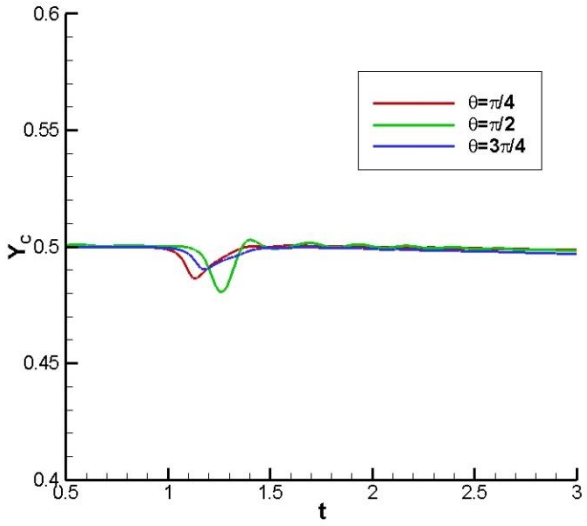

Figure 7.18 Particle trajectory with time for different Θ (Re=50.0, d= 0.2, S_g=0.5, ρ=100.0)

Table 7.6 Residence time (t_r) for different Θ (Re=50.0, d=0.2, S_g=0.5)

Θ	**t_r**
π/4	1.583
π/2	1.518
3.0π/4	1.579

7.3.3.3 Effect of initial position

The effect of initial position is discussed in this section. The particles are released from three different initial positions 0.4, 0.5 and 0.6. The Reynolds number, particle diameter, density ratio, slit clearance and slit angle are kept constant as 50.0, 0.2, 100.0, 0.5 and π/2. The particle trajectory with time for each initial position is shown in figure 7.19.

The particles pass through the slit and attain equilibrium position closer to the initial position of release. This may be due to the presence of secondary flow vortices near the slit. Now, the residence time is calculated for each initial position and presented in table 7.7.

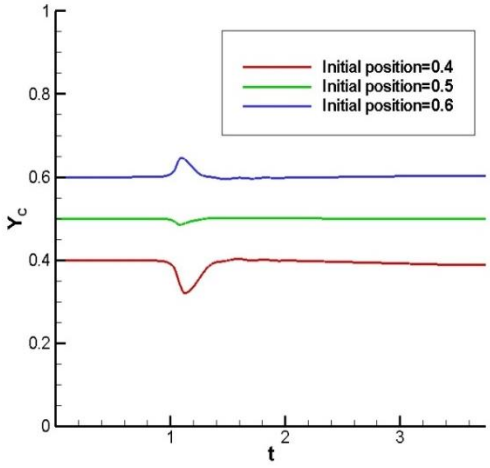

Figure 7.19 Particle trajectory with time for different initial positions (Re=50.0, d= 0.2, S_g=0.5, ρ=100.0 and Θ=π/2)

Table 7.7 Residence time (t_r) for different initial position (Re=50.0, d=0.2, S_g=0.5 and Θ=π/2)

Initial position	**t_r**
0.4	1.569
0.5	1.518
0.6	1.571

The residence time is lowest for an initial position of 0.5. The effect of flow vortices is lowest when particles are released from 0.5 (centre of channel). Hence, it can pass the slit without much disturbance and the residence time will be lower compared to other initial positions.

7.3.3.4 Initial orientation and inertial migration

In this section, the effect of initial orientation is discussed. The horizontal arrangement is already discussed in the previous sections. Now the triangular arrangement is created by keeping the centre-to-centre distance same for particle 1 and 2 and particle 2 and 3. The particle 1, 2 and 3 are released initially from (5.0, 0.5), (5.5, 0.6) and (6.0, 0.5) respectively as shown in 7.20 a). The intermediate (while passing through slit) and final positions of particles are shown in figure 7.20 b)-c).

All the particles pass through the slit without colliding. The particle trajectory with time can be visible in figure 7.21.

The initial orientation does not have much impact on residence time of particle 3 since the centre-to-centre distance between particle 3 and 2 remains constant. Hence, the residence time of particle 2 is checked for both conditions and plotted in figure 7.22.

From figure 7.22 it is clear that residence time is higher for particle 2 in triangle orientation than that of horizontal. The particle 2 in horizontal orientation is at channel centre and hence it will experience more flow velocity than particle 2 in triangle orientation. Hence, residence time will be lower for particle 2 in horizontal condition. The values of residence time for both conditions are tabulated in table 7.8.

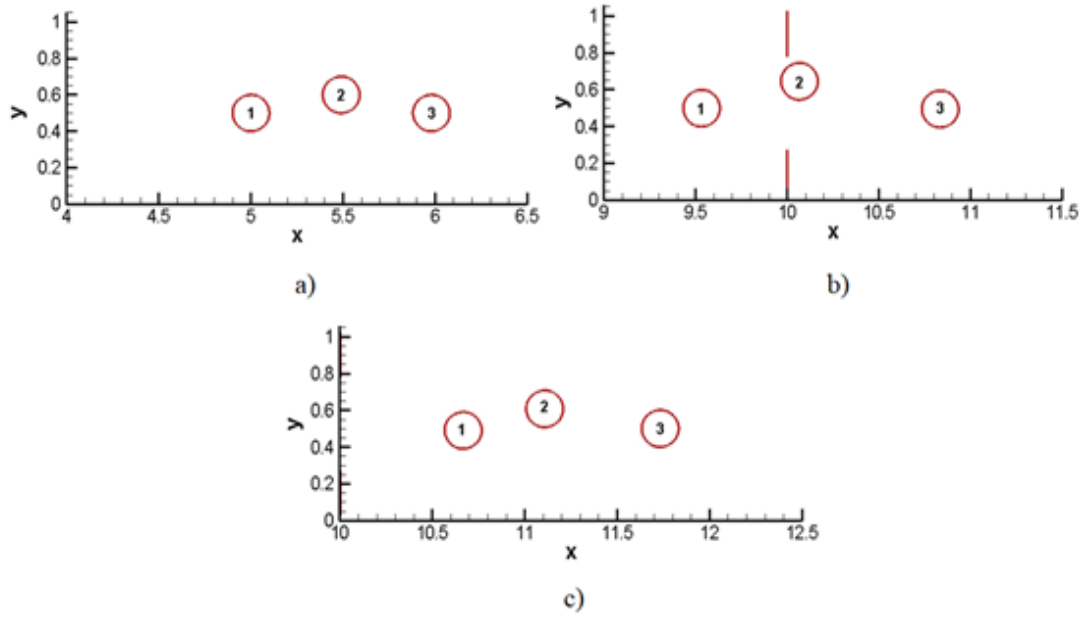

Figure 7.20 Particle positions when migrating through slit for triangle orientation a) initial, b) when passing through slit and c) final position

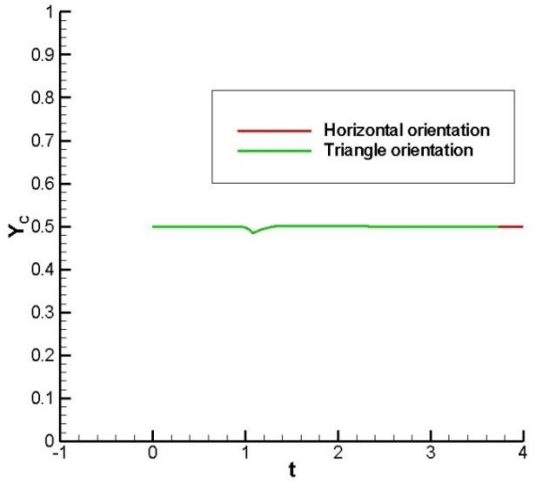

Figure 7.21 Particle 3 trajectory with time for different orientations (Re=50.0, d= 0.2, S_g=0.5, ρ=100.0 and Θ=π/2)

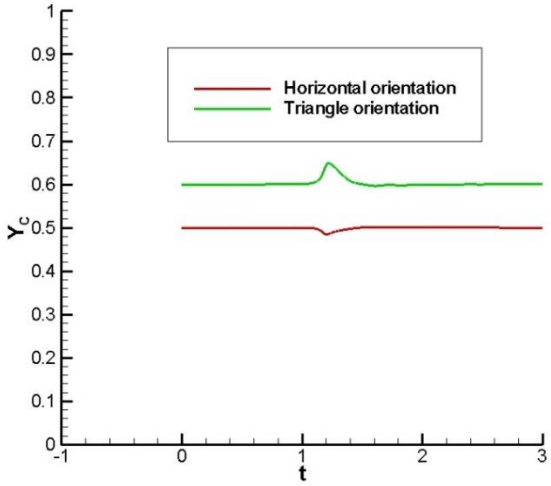

Figure 7.22 Particle 2 trajectory with time for different orientations (Re=50.0, d= 0.2, S_g=0.5, ρ=100.0 and Θ=π/2)

Table 7.8 Residence time (t_r) of particle 2 for different initial orientation (Re=50.0, d=0.2, S_g=0.5 and Θ=π/2)

Initial orientation	**t_r**
Horizontal	1.518
Triangle	1.685

CHAPTER 8. CONCLUSIONS

The prime objective of the current study is to build two-dimensional computational models based on feedback forcing immersed boundary finite volume method to investigate the inertial migration dynamics of single and multiple rigid particles in different fluid flow conditions and channel configurations. The same has been done and the details are explained in Chapters 3 to 7. A summary of each chapters is provided below.

8.1 Inertial migration of particle in straight channel

The study shown in chapter 3 is the development and analysis of inertial migration of single cylindrical particle in straight channel. The inertial migration in flow types such as Poiseuille and shear flow are compared in this chapter.

- A staggered Cartesian grid system is used and semi-implicit fractional step-based algorithm is incorporated in the model to solve the fluid flow equations. The particle is observed to attain equilibrium position around 0.6 times the height of the channel in case of Poiseuille flow whereas the same is found to be at the centre of channel in shear flow. Further, detailed parametric study is carried out in both flow cases to analyse the effect of Re, initial position of release, diameter of particle and height of channel on the equilibrium position.
- It is found that, the particle equilibrium position shifts towards bottom wall in case of Poiseuille flow with increase in Re and channel height and reduction in diameter. However, the initial position of release of particle have negligible effect on the equilibrium position.
- Also, it is found that, the migration time decreases with increase in Re and diameter of particle but decreases with the height of channel. In case of shear flow, the equilibrium position is found to be very near to the centre of the channel and it is independent of diameter. However, equilibrium position shift towards top wall with increase in channel height.
- The variation in Re and initial position of release do not have significant effect on equilibrium position. The time taken to reach the equilibrium position reduces with increase in Re and channel height and reduction in particle diameter.

- Finally, the inertial migration in Poiseuille and shear flow in straight channel are compared and it is found that the migration time is lesser for shear flow. Further, prediction model is constructed with the help of simulation data and artificial neural network (ANN) algorithm for predicting the equilibrium position and migration time of the cylindrical particle in Poiseuille flow. The predicted values and simulation data are in good agreement demonstrating the prediction capability of the ANN model. This model can help in designing a well-suited separation device in future.

8.2 Inertial migration of particle in non-straight channels

Chapter 4 analyses inertial migration of rigid cylindrical particle in non-straight channels. Inertial migration dynamics in three type of channel configurations such as backward facing stepped, stepped and constricted channel are simulated.

- The particle equilibrium position in case of backward facing stepped channel is observed between centre and 0.6 times height of the channel. Detailed parametric study is carried out further on the migration of particle in backward facing stepped channel including the effect of blockage ratio.
- It is observed that the particle equilibrium position shifts towards the upper wall with increase in Re, diameter of particle and blockage ratio. Unlike in the cases of Poiseuille flow and shear flow the equilibrium position depends upon the initial position of release of particle while migrating in a backward facing stepped channel flow.
- As the lateral distance from the initial position to the vortices increases, the equilibrium position shifts towards the upper wall. It is also found that the migration time decreases with reduction in diameter and blockage ratio whereas it remains unchanged with variation in Re.

In the next stage, the immersed boundary method (IBM) computational model is extended to study the inertial migration of single rigid neutrally buoyant cylindrical particle in stepped channel. The influence of initial position of release of particle, height and length of contraction portion on inertial migration is studied.

- The particle equilibrium position shifts off-centre with respect to its initial release position and it moves towards the upper wall with respect to the reduction in height of contraction portion. This may be due to the increase in velocity of flow when height of contraction portion is lowered.
- The shear induced lift becomes higher and become more dominant over wall induced lift when velocity of flow increases and hence the equilibrium position shifts slightly towards the upper wall. However, the migration time reduces with increase in length of contraction portion.

The inertial migration in constricted channel is simulated in the next stage.

- It is noticed that the particle passes the constriction region and acquire the equilibrium position almost close to the initial release position. The effect of various parameters like Reynolds number, diameter and initial release position of particle and constriction clearance on equilibrium position, shortest equilibrium distance and migration time are analysed.
- As Reynolds number increases from 10 to 100 both shortest equilibrium distance and migration time increases while equilibrium position stays unchanged. The increase in diameter also causes raise in shortest equilibrium distance and migration time. On the flip side, the raise in constriction clearance tends to decrease the shortest equilibrium distance and migration time.
- The parametric study reveals that equilibrium position is crucially affected by the initial release position and slightly by change in particle diameter. The inertial migration characteristics in straight, backward facing stepped and constricted channel are compared in the next section.
- By the utilization of the simulation data, an ANN model is developed for the effective prediction of equilibrium position, shortest equilibrium distance and migration time. The input parameters given are Reynolds number, diameter and initial release position of particle and constriction clearance in the channel. Predicted values and observed data coincided at all test numbers and it indicates that effective forecast of output values is accomplished with the ANN model.
- Further, to search for the existence of a critical Reynolds number the simulation of particle migration is done for Reynolds number 100 to 125. The shortest

equilibrium distance and migration time are found first to increase up to a critical Reynolds number and then drops.

- The behaviour of critical Reynolds number with particle diameter and constriction clearance is analysed. It is noticed that the particle diameter has no effect on the critical Reynolds number. On the other part, the critical Reynolds number varies linearly with constriction clearance.

8.3 Inertial migration of various shaped particles

The inertial migration dynamics of different shaped particles such as circular, elliptical, square, rectangular and biconcave shaped particles are studied in chapter 5.

- The particles released in a channel of 50x1 dimension seem to attain the equilibrium position in the range of 0.18-0.25.
- The biconcave shape attains equilibrium position closest to lower wall and elliptical particle has an oscillation in its trajectory. This may be due to the irregularity in biconcave shape and high aspect ratio of elliptical particle.
- In the next stage the same simulations are repeated for particles of density ratio 100. As density ratio is increased the buoyant force come into picture which shifts the equilibrium position towards lower wall and reduces migration time considerably.
- It should be also noted that the migration time of biconcave shaped particle is highest compared to other shapes in both neutrally and non-neutrally buoyant cases. This may be due to the irregularity in the biconcave shape compared to other particles.

8.4 Control force and inertial migration

The possibility of driving the equilibrium position towards a desired location with the application of a control force is explored in two flow conditions (Poiseuille and pulsatile) in chapter 6.

- An additional axial force is applied against the fluid flow for the attainment of the equilibrium position of a particle at the centre. With the implementation of

a suitable control force, particle attained its equilibrium position at the channel centre, regardless of its diameter, Reynolds number and density ratio.

- However, it is observed that the magnitude of the control force is significantly dependent on the Reynolds number, particle diameter and density ratio. Hence, thorough parametric study is performed to capture the characteristics of control force with the above-mentioned parameters.
- It should be noted that the magnitude of control force required to shift the equilibrium position to the channel centre, increases with a rise in Reynolds number and reduces with an increase in particle diameter. This may be due to the enhancement in shear induced lift when the Reynolds number is increased. Also, the wall induced lift is raised with an increase in particle diameter, demanding less force for larger particles.
- When density ratio is varied, the magnitude of the control force first increases and then decreases. This may be due to the increase in Saffman lift force when the density ratio reaches a certain value.
- Inspired by detailed parametric study, prediction model is constructed with the help of linear regression techniques. A correlation between control force and parameters like the Reynolds number, particle diameter and density ratio are created. The predicted values are found to be match with the simulation results.

Moving on, the effect of control force on inertial migration dynamics are explored in a pulsatile flow. A thorough parametric study is performed to analyse the relationship between control force and diameter of particle, Reynolds number and density ratio.

- It is observed that magnitude of control force increases with Reynolds number. This increase may be used to overcome additional enhancement in the shear induced lift due to the increase in Reynolds number.

- It is noted that particle with larger diameter requires lower control force. This is due to the fact that equilibrium position shifts nearer to the channel center as the diameter enlarges.

- The magnitude of required control force reduces to zero when the density ratio increases from 100.0 to 300.0 and the same increases again for a density ratio of 500.0. The variation in Saffman lift force may be the reason behind this.
- Based on parametric study, a prediction model for control force is constructed with the aid of linear regression techniques. The predicted values are found to be almost equal to the observed values. The current findings on control force can further be utilized to determine the magnitude of control force to bring the particle towards other positions. It can be also extended to study the control force characteristics in non-straight channels and three-dimensional domains.

8.5 Inertial migration of multiple particles

Chapter 7 deals with inertial migration of multiple particles. The migration of two rigid cylindrical particles in straight channel is simulated first which is followed by two particle migration in stepped channel. Finally, inertial migration of three particles in slit channel is studied.

- Two particles of same diameter are released in straight channel of dimension 50x1 with 0.5 center-to-center distance. It is observed that both the particles attain equilibrium position around 0.281.
- It is observed that, the particles attain equilibrium position closer to channel center than compared to that in inertial migration of single particle of same size. This may be due to the generation of a lift force due to the interaction of vortices between the two particles. This reverse lift force will act against the shear induced lift to drive the equilibrium position towards channel center.
- To explore further, the effect of initial center-to-center distance and initial orientation of particles on equilibrium position, center-to-center distance and migration time are studied.
- The equilibrium position stays unaffected with change in initial center-to-center distance. The center-to-center distance also remains unchanged with change in initial center-to-center distance.
- The particles are released from same lateral position and hence it will experience same velocity. This may be the reason behind this behavior.

- On the other hand, migration time of particle 2 rises with initial center-to-center distance. As initial center-to-center distance increases, the effect of reverse lift force created due to vortices interaction decreases. Hence, particle 2 will move slower as initial center-to-center distance gets higher. Hence, migration time will be higher for higher initial center-to-center distance.
- In the next stage, the effect of initial orientation on inertial migration dynamics is examined. Three type of initial orientations such as horizontal, vertical and offset are simulated.
- For, vertical condition, particle 2 will attain equilibrium position closer to top wall since it is closer to top wall. The center-to-center distance remains constant for horizontal and vertical conditions. However, it increases and attain a constant value for offset condition. The velocity of flow is higher for position of particle 2 in offset condition as it is closer to channel center. Hence, particle 2 will move faster and hence, center-to-center distance will also increase. The migration time is higher for particle 2 in offset condition. This happens because particle 2 is closer to channel center in offset condition and it will take time to reach equilibrium position closer to lower wall compared to other conditions.

Further, inertial migration of two particles in a stepped channel is simulated. The particles are released and get pass over the step and attain the equilibrium position then.

- The influence of density ratio and depth of step on the migration time and equilibrium position are studied in the following stage. The equilibrium position is attained near lower wall for very high-density ratio. Also, the migration time increases with escalation in density ratio. The buoyant force may be the reason behind this.
- On the other hand, larger depth of step creates more disturbance to the flow which will result in stronger flow vortices. This will contribute to the shear induced lift and in progress, the equilibrium position moves towards lower wall. Also, the rise in size of vortices enhances the particle to take more time for balancing of lift forces. Hence the migration time increase with rise in depth of step. The migration time is the lowest for a depth of 0.15. Hence, the critical depth of migration is 0.15 for the present study.

Moving on, three-particle migration in a slit channel is examined. Three particles pass through the slit and then acquire equilibrium position. The influence of slit clearance, slit angle, initial position and orientation on dynamics of inertial migration is studied in the next section.

- The equilibrium position seems to change with initial position and initial triangle orientation and it stays unaffected with slit clearance and slit angle. However, the residence time (time taken by particle to move pass the slit) increases with slit clearance. The larger flow vortex generated with reduced slit clearance will deflect the particle more and it will reduce the residence time.
- The residence time is lowest for a slit angle of $\pi/2$. The largest vortex is generated for the same angle and it may be the reason for this characteristic. The residence time is also found to be lowest for initial position of release of 0.5. The maximum flow velocity is at the centre of channel and hence, particles will move faster when they are released from channel lateral centre.
- When the initial orientation is changed from horizontal to triangle, particle 2 moves away from channel centre. Hence, it will experience less velocity compared to the horizontal condition and will need more residence time. The current results can be further extended to study the migration of different multiple biological particles in straight and non-straight channels.

The present study is carried out in two-dimensional domain and it is a main limitation of the study. Also, the behavior of bulk particles is not explored in this study. However, the present model can be improved and utilized for three-dimensional and studies involving number of particles more than three.

REFERENCES

Abbas, M., Magaud, P., Gao, Y., and Geoffroy, S. (2014). Migration of finite sized particles in a laminar square channel flow from low to high Reynolds numbers. *Physics of Fluids*, 26(12).

Aidun, C. K., and Clausen, J. R. (2010a). Lattice-Boltzmann method for complex flows. *Annual Review of Fluid Mechanics*, 42, 439–472.

Akhatov, I. S., Hoey, J. M., Swenson, O. F., and Schulz, D. L. (2008). Aerosol focusing in micro-capillaries: Theory and experiment. *Journal of Aerosol Science*, 39(8), 691–709.

Alizad Banaei, A., Loiseau, J. C., Lashgari, I., and Brandt, L. (2017). Numerical simulations of elastic capsules with nucleus in shear flow. *European Journal of Computational Mechanics*, 26(1–2), 131–153.

Asmolov, E. S. (1999). The inertial lift on a spherical particle in a plane Poiseuille flow at large channel Reynolds number. *Journal of Fluid Mechanics*, 381, 63-87.

Bazaz, S. R, Mashhadian, A., Ehsani, A., Saha, S. C., Krüger, T., and Ebrahimi Warkiani, M. (2020). Computational inertial microfluidics: A review. *Lab on a Chip*, 20(6), 1023–1048.

Biswas, G., Breuer, M., and Durst, F. (2004). Backward-facing step flows for various expansion ratios at low and moderate Reynolds numbers. *Journal of Fluids Engineering, Transactions of the ASME*, 126(3), 362–374.

Carlo, D. D., Edd, J. F., Humphry, K. J., Stone, H. A., and Toner, M. (2009). Particle segregation and dynamics in confined flows. *Physical Review Letters*, 102(9), 1–4.

Choi, C. R., and Kim, C. N. (2010). Inertial migration and multiple equilibrium positions of a neutrally buoyant spherical particle in Poiseuille flow. *Korean Journal of Chemical Engineering*, 27(4), 1076-1086.

Chun, B., and Ladd, A. J. C. (2006). Inertial migration of neutrally buoyant particles in a square duct: An investigation of multiple equilibrium positions. *Physics of Fluids*, 18(3).

Feng, Z. G., and Michaelides, E. E. (2004). The immersed boundary-lattice Boltzmann method for solving fluid-particles interaction problems. *Journal of Computational Physics*, 195(2), 602–628.

Feng, Z. G., and Michaelides, E. E. (2009). Robust treatment of no-slip boundary condition and velocity updating for the lattice-Boltzmann simulation of particulate flows. *Computers and Fluids*, 38(2), 370–381.

Fox, A. J., Schneider, J. W., and Khair, A. S. (2020). Inertial bifurcation of the equilibrium position of a neutrally-buoyant circular cylinder in shear flow between parallel walls. *Physical Review Research*, 2(1), 1–7.

Frank, M., Anderson, D., Weeks, E. R., and Morris, J. F. (2003). Particle migration in pressure-driven flow of a Brownian suspension. *Journal of Fluid Mechanics*, 493, 363–378.

Ghosh, S., and Stockie, J. M. (2015). Numerical simulations of particle sedimentation using the immersed boundary method. *Communications in Computational Physics*, 18(2), 380–416.

Ho A N, B. P., and Leal, D. L. G. (1976). Migration of rigid spheres in a two-dimensional unidirectional shear flow of a second-order fluid. *Journal of Fluid Mechanics*, 76(4), 783-799.

Ho, B. P., and Leal, L. G. (1974). Inertial migration of rigid spheres in two-dimensional unidirectional flows. *Journal of Fluid Mechanics*, 65(2), 365-400.

Hood, K., Lee, S., and Roper, M. (2015). Inertial migration of a rigid sphere in three-dimensional Poiseuille flow. *Journal of Fluid Mechanics*, 765, 452–479.

Huang, L., Du, J., and Zhu, Z. (2021). Neutrally buoyant particle migration in Poiseuille flow driven by pulsatile velocity. *Micromachines*, 12, 1075.

Huang, P. Y., Feng, J., Hu, H. H., and Joseph, D. D. (1997). Direct simulation of the motion of solid particles in Couette and Poiseuille flows of viscoelastic fluids. *Journal of Fluid Mechanics*, 343, 73–94.

Huang, W. X., Shin, S. J., and Sung, H. J. (2007). Simulation of flexible filaments in a uniform flow by the immersed boundary method. *Journal of Computational Physics*, 226(2), 2206–2228.

Huang, W. X., and Sung, H. J. (2009). An immersed boundary method for fluid-flexible structure interaction. *Computer Methods in Applied Mechanics and Engineering*, 198(33–36), 2650–2661.

Hu, H. H., Joseph, D. D., and Crochet, M. J. (1992). Direct simulation of fluid particle motions I. *Theoretical and Computational Fluid Dynamics*, 3, 285-306.

Hu, X., Lin, J., Guo, Y., and Ku, X. (2021). Inertial focusing of elliptical particles and formation of self-organizing trains in a channel flow. *Physics of Fluids*, 33(1), 013310.

Hu, X., Lin, J., Guo, Y., and Ku, X. (2021). Motion and equilibrium position of elliptical and rectangular particles in a channel flow of a power-law fluid. *Powder Technology*, 377, 585–596.

Inamuro, T., Maeba, K., and Ogino, F. (2000). Flow between parallel walls containing the lines of neutrally buoyant circular cylinders. *International Journal of Multiphase Flow*, 26(12), 1981–2004.

Jiang, D., Tang, W., Xiang, N., and Ni, Z. (2016). Numerical simulation of particle focusing in a symmetrical serpentine microchannel. *RSC Advances*, 6(62), 57647–57657.

Kanchan, M., and Maniyeri, R. (2019). Numerical analysis of the buckling and recuperation dynamics of flexible filament using an immersed boundary framework. *International Journal of Heat Fluid Flow*, 77, 256–277.

Kanchan, M., and Maniyeri, R. (2020). Numerical simulation and prediction model development of multiple flexible filaments in viscous shear flow using immersed boundary method and artificial neural network techniques. *Fluid Dynamics Research*, 52(4), 045507.

Kanchan, M., and Maniyeri, R. (2020). Numerical simulation of buckling and asymmetric behavior of flexible filament using temporal second-order immersed

boundary method. *International Journal of Numerical Methods for Heat Fluid Flow*, 30(3), 1047–1095.

Kanchan, M., and Maniyeri, R. (2020). Fluid-Structure Interaction Study and Flowrate Prediction Past a Flexible Membrane Using Immersed Boundary Method and Artificial Neural Network Techniques. *Journal of Fluids Engineering, Transactions of the ASME*, 142(5), 051501.

Kim, B., Chang, C. B., Park, S. G., and Sung, H. J. (2015). Inertial migration of a 3D elastic capsule in a plane Poiseuille flow. *International Journal of Heat and Fluid Flow*, 54, 87–96.

Kim, B., Huang, W. X., Shin, S. J., and Sung, H. J. (2012). Flexible ring flapping in a uniform flow. *Journal of Fluid Mechanics*, 707, 129–149.

Koh, J., Kim, J., Shin, J. H., and Lee, W. (2014). Fabrication and integration of microprism mirrors for high-speed three-dimensional measurement in inertial microfluidic system. *Applied Physics Letters*, 105(11), 0–5.

Ladd, A. J. (1994). Numerical Simulations of Particulate Suspensions Via a Discretized Boltzmann Equation. Part 1. Theoretical Foundation. *Journal of Fluid Mechanics*, 271, 285–309.

Lai, M. C., and Peskin, C. S. (2000). An immersed boundary method with formal second-order accuracy and reduced numerical viscosity. *Journal of Computational Physics*, 160(2), 705–719.

Lashgari, I., Ardekani, M. N., Banerjee, I., Russom, A., and Brandt, L. (2017). Inertial migration of spherical and oblate particles in straight ducts. *Journal of Fluid Mechanics*, 819, 540–561.

Lin, J., Liang, X., and Zhang, S. (2011). Fiber orientation distribution in turbulent fiber suspensions flowing through an axisymmetric contraction. *Canadian Journal of Chemical Engineering*, 89(6), 1416–1425.

Lin, J., Zhang, S., and Olson, J. A. (2007). Computing orientation distribution and rheology of turbulent fiber suspensions flowing through a contraction. *Engineering Computations*, 24(1), 52–76.

Liu, B., Lin, J., Ku, X., and Yu, Z. (2021). Particle trajectory and orientation evolution of ellipsoidal particles in bounded shear flow of Giesekus fluids. *Korea Australia Rheology Journal*, 33(4), 343–355.

Liu, C., Hu, G., Jiang, X., and Sun, J. (2015). Inertial focusing of spherical particles in rectangular microchannels over a wide range of Reynolds numbers. *Lab on a Chip*, 15(4), 1168–1177.

Liu, Y., Li, Q., and Nie, D. (2018). Two-dimensional numerical study on the migration of particle in a serpentine channel. *Journal of Nanotechnology*, 2018, 2615404.

Mach, A., J., and Carlo, D. (2010). Continuous scalable blood filtration device using inertial microfluidics. *Biotechnology and Bioengineering*, 107(2), 302-311.

Maniyeri, R., and Kang, S. (2012). Numerical study on the rotation of an elastic rod in a viscous fluid using an immersed boundary method. *Journal of Mechanical Science and Technology*, 26(5), 1515–1522.

Maniyeri, R., and Kang, S. (2014). Numerical study on bacterial flagellar bundling and tumbling in a viscous fluid using an immersed boundary method. *Applied Mathematical Modelling*, 38(14), 3567–3590.

Maniyeri, R., Suh, Y. K., Kang, S., and Kim, M. J. (2012). Numerical study on the propulsion of a bacterial flagellum in a viscous fluid using an immersed boundary method. *Computers and Fluids*, 62, 13–24.

Mao, W., and Alexeev, A. (2011). Hydrodynamic sorting of microparticles by size in ridged microchannels. *Physics of Fluids*, 23(5), 1–5.

Matas, J. P., Morris, J. F., and Guazzelli, É. (2004). Inertial migration of rigid spherical particles in Poiseuille flow. *Journal of Fluid Mechanics*, 515, 171–195.

Matas, J. P., Morris, J. F., and Guazzelli, É. (2009). Lateral force on a rigid sphere in large-inertia laminar pipe flow. *Journal of Fluid Mechanics*, 621, 59–67.

Mittal, R., and Bhardwaj, R. (2022). Immersed boundary methods for thermofluids problems, *Annual Review of Heat Transfer*, 24, 33-70.

Navidbakhsh, M., and Rezazadeh, M. (2012). An immersed boundary-lattice Boltzmann model for simulation of malaria-infected red blood cell in micro-channel. *Scientia Iranica*, 19(5), 1329–1336.

Pan, T. W., and Glowinski, R. (2002). Direct simulation of the motion of neutrally buoyant circular cylinders in plane Poiseuille flow. *Journal of Computational Physics*, 181(1), 260–279.

Park, S. G., Chang, C. B., Huang, W. X., and Sung, H. J. (2014). Simulation of swimming oblate jellyfish with a paddling-based locomotion. *Journal of Fluid Mechanics*, 748, 731–755.

Park, S. G., Kim, B., Lee, J., Huang, W. X., and Sung, H. J. (2015). Dynamics of prolate jellyfish with a jet-based locomotion. *Journal of Fluids and Structures*, 57, 331–343.

Peskin, C. S. (1977). Numerical analysis of blood flow in the heart. *Journal of Computational Physics*, 25(3), 220-252.

Peskin, C. S. (2002). The immersed boundary method. *Acta Numerica*, 11, 479–517.

Pitt, R. E., Sherwin, S. J., and Theofilis, V. (2005). BiGlobal stability analysis of steady flow in constricted channel geometries. *International Journal for Numerical Methods in Fluids*, 47(10–11), 1229–1235.

Prohm, C., and Stark, H. (2014). Feedback control of inertial microfluidics using axial control forces. *Lab on a Chip*, 14(12), 2115–2123.

Prohm, C., Zöller, N., and Stark, H. (2014). Controlling inertial focussing using rotational motion. *European Physical Journal E*, 37(5), 36.

Qian, S., Jiang, M., and Liu, Z. (2021). Inertial migration of aerosol particles in three-dimensional microfluidic channels. *Particuology*, 55, 23–34.

Rubinow, S. I., and Keller, J. B. (1961). The transverse force on a spinning sphere moving in a viscous fluid. *Journal of Fluid Mechanics*, 11(3), 447-459

Schaaf, C., and Stark, H. (2017). Inertial migration and axial control of deformable capsules. *Soft Matter*, 13(19), 3544–3555.

Schonberg A N, J. A., and Hinch, D. E. J. (1989). Inertial migration of a sphere in Poiseuille flow. *Journal of Fluid Mechanics*, 203, 517-524.

Segre, G., and Silberberg, A. (1962). Behaviour of macroscopic rigid spheres in Poiseuille flow Part 1. Determination of local concentration by statistical analysis of particle passages through crossed light beams. *Journal of Fluid Mechanics*, 14(1), 115-135.

Shin, S. J., Huang, W. X., and Sung, H. J. (2008). Assessment of regularized delta functions and feedback forcing schemes for an immersed boundary method. *International Journal for Numerical Methods in Fluids*, 58(3), 263–286.

Shin, S. J., and Sung, H. J. (2010). Three-dimensional simulation of a valveless pump. *International Journal of Heat and Fluid Flow*, 31(5), 942–951.

Shin, S. J., and Sung, H. J. (2012). Dynamics of an elastic capsule in moderate Reynolds number Poiseuille flow. *International Journal of Heat and Fluid Flow*, 36, 167–177.

Sollier, E., Amini, H., Go, D. E., Sandoz, P. A., Owsley, K., and Carlo, D. D. (2015). Inertial microfluidic programming of microparticle-laden flows for solution transfer around cells and particles. *Microfluidics and Nanofluidics*, 19(1), 53–65.

Song, C., Shin, S. J., Sung, H. J., and Chang, K. S. (2011). Dynamic fluid-structure interaction of an elastic capsule in a viscous shear flow at moderate Reynolds number. *Journal of Fluids and Structures*, 27(3), 438–455.

Su, J., Chen, X., and Hu, G. (2018). Inertial migrations of cylindrical particles in rectangular microchannels: Variations of equilibrium positions and equivalent diameters. *Physics of Fluids*, 30(3), 032007.

Sun, D. K., and Bo, Z. (2015). Numerical simulation of hydrodynamic focusing of particles in straight channel flows with the immersed boundary-lattice Boltzmann method. *International Journal of Heat and Mass Transfer*, 80, 139–149.

Tam, C. K. W., and Hyman, W. A. (1973). Transverse motion of an elastic sphere in a shear field. *Journal of Fluid Mechanics*, 59(1), 177-185.

Tang, W., Zhu, S., Jiang, D., Zhu, L., Yang, J., and Xiang, N. (2020). Channel innovations for inertial microfluidics. *Lab on a Chip*, 20(19), 3485–3502.

Tohme, T., Magaud, P., and Baldas, L. (2021). Transport of Non-Spherical Particles in Square Microchannel Flows: A Review. *Micromachines*, 12, 277.

Uddin, E., Huang, W. X., and Sung, H. J. (2015). Actively flapping tandem flexible flags in a viscous flow. *Journal of Fluid Mechanics*, 780, 120–142.

Vahidkhah, K., Balogh, P., and Bagchi, P. (2016). Flow of red blood cells in stenosed microvessels. *Scientific Reports*, 6, 28194.

Warkiani, M. E., Guan, G., Luan, K. B., Lee, W. C., Bhagat, A. A. S., Kant Chaudhuri, P., Tan, D. S. W., Lim, W. T., Lee, S. C., Chen, P. C. Y., Lim, C. T., and Han, J. (2014). Slanted spiral microfluidics for the ultra-fast, label-free isolation of circulating tumor cells. *Lab on a Chip*, 14(1), 128–137.

Wu, L., Guan, G., Hou, H. W., Bhagat, A. A. S., and Han, J. (2012). Separation of leukocytes from blood using spiral channel with trapezoid cross-section. *Analytical Chemistry*, 84(21), 9324–9331.

Yang, B. H., Wang, J., Joseph, D. D., Hu, H. H., Pan, T. W., and Glowinski, R. (2005). Migration of a sphere in tube flow. *Journal of Fluid Mechanics*, 540, 109–131.

Yuan, C., Pan, Z., and Wu, H. (2018). Inertial migration of single particle in a square microchannel over wide ranges of Re and particle sizes. *Microfluidics and Nanofluidics*, 22(9), 10.

Zhang, J., Yan, S., Yuan, D., Alici, G., Nguyen, N. T., Ebrahimi Warkiani, M., and Li, W. (2016). Fundamentals and applications of inertial microfluidics: A review. *Lab on a Chip*, 16(1), 10–34.

Zhou, J., and Papautsky, I. (2013). Fundamentals of inertial focusing in microchannels. *Lab on a Chip*, 13(6), 1121–1132.

Zhou, J., Peng, Z., and Papautsky, I. (2020). Mapping inertial migration in the cross section of a microfluidic channel with high-speed imaging. *Microsystems and Nanoengineering.*, 6(1).

List of Publications based on Ph.D. Research Work

The thesis outlined "Numerical study on inertial migration of particles in microchannels" is a result of the research work carried out at the Department of Mechanical Engineering, National Institute of Technology Karnataka between July 2018 and May 2023. The research during this period has resulted in the following publications and conference proceedings.

Sl. No.	Title of Paper	Authors (in the same order as in the paper. Underline the Research Scholar's name)	Name of the Journal/ Conference, Vol., No., Pages	Month and Year of publication	Category
1	Lateral migration of cylindrical particle in a constricted microchannel—A numerical study	Manjappatta Pazhiyottumana Neeraj, Ranjith Maniyeri	The Canadian Journal of Chemical Engineering, 101 (3), pp-1680-1699	May 2022	1
2	Control force and inertial mi gration in Poiseuille flow: a computational study	Manjappatta Pazhiyottumana Neeraj, Ranjith Maniyeri	Particulate Science and Technology, https://doi.org/10.1080/02726351.2022.2163730	Jan 2023	1
3	Lateral migration of various shaped particles – A computational study	Manjappatta Pazhiyottumana Neeraj, Ranjith Maniyeri	Chemical Engineering and Technology https://doi.org/10.1002/ceat.202200499	Jan 2023	1

4	Numerical study and prediction model development of inertial migration of cylindrical particle in channel flow using immersed boundary and artificial neural network methods	Manjappatta Pazhiyottumana Neeraj, Ranjith Maniyeri	Theoretical Foundations of Chemical Engineering Under review	Under review	1
5	Inertial migration and control force in pulsatile flow- a computational study	Manjappatta Pazhiyottumana Neeraj, Ranjith Maniyeri	Indian Chemical Engineer Accepted	Accepted	1
6	Mixing in Oscillating Lid Driven Cavity- A Numerical Study	Manjappatta Pazhiyottumana Neeraj, Ranjith Maniyeri	46th National Conference on Fluid Mechanics and Fluid Power (FMFP-2019), PSGCT	Dec 2019	3
7	Numerical simulation of flow over oscillating cylinder using feedback forcing based immersed boundary finite volume method	Manjappatta Pazhiyottumana Neeraj, Ranjith Maniyeri	International Conference on Numerical Heat Transfer and Fluid Flow (NHTFF-2020), NITW	Jan 2020	3
8	Numerical Study on Inertial Migration of a Cylindrical Particle in Straight Channel Using Feedback Forcing	Manjappatta Pazhiyottumana Neeraj, Ranjith Maniyeri, Sangmo Kang	65th CONGRESS OF Indian Society of Theoretical and Applied Mechanics, GITAM university, Hyderabad	Dec 2020	3

	Based Immersed Boundary Method				
9	Numerical Study on Inertial Migration of Single Rigid Neutrally Buoyant Cylindrical Particle in Shear Flow Using Feedback Forcing Based Immersed Boundary Method	Manjappatta Pazhiyottumana Neeraj, Ranjith Maniyeri, Sangmo Kang	8th International and 47th National Conference on Fluid Mechanics and Fluid Power (FMFP), IITG	Dec 2020	3
10	Inertial Migration of Cylindrical Particle In Stepped Channel- A Numerical Study	Manjappatta Pazhiyottumana Neeraj, Ranjith Maniyeri, Sangmo Kang	National e-conference On Recent Trends in Fluid Dynamics Research (RTFDR-21), Organized by Department of Chemical Engineering, NITR	April 2021	3
11	Numerical simulation of inertial migration of elliptical particle using immersed boundary method	Manjappatta Pazhiyottumana Neeraj, Ranjith Maniyeri	48th National Conference on Fluid Mechanics and Fluid Power (FMFP) BITS Pilani, Pilani Campus, RJ, India.	Dec 2021	3
12	Immersed Boundary Method Based Numerical Study on Lateral Migration of Various Shaped Particles	Manjappatta Pazhiyottumana Neeraj, Ranjith Maniyeri	1st International Conference in Fluid Thermal and Energy Systems, NIT Calicut, Kerala, India	June 2022	3

13	Numerical Study of Two Particle Migration in a Stepped Channel	Manjappatta Pazhiyottumana Neeraj, Ranjith Maniyeri	International Conference on Material Science and Computational Engineering (ICMCE 2022), , Baselios Mathews College, Kollam, Kerala, India	November 2022	3
14	Lateral migration of three particles through a slit- An immersed boundary computational analysis	Manjappatta Pazhiyottumana Neeraj, Ranjith Maniyeri	9th International and 49th National Conference on Fluid Mechanics and Fluid Power (FMFP), IITR	December 2022	3

*Category: 1: Journal paper, full paper reviewed 2: Journal paper, Abstract reviews 3: Conference/Symposium paper, full paper reviewed 4: Conference/Symposium paper, abstract reviewed 5: Others (including papers in Workshops, NITK Research Bulletins, Short notes etc.)

Neeraj M P
Research Scholar
Name & Signature, with Date

15/01/2024

Dr. Ranjith M
Research Guide
Name & Signature, with Date

BIODATA

NAME: NEERAJ M P

D.O.B: 10-08-1993

Mobile: +919846861498

Email: neerajbhavadas@gmail.com

ADDRESS: Saketham, Paruthipra, Shornur, Kerala-679121

QUALIFICATION:

Examination	Board/Institute	Year	Percentage/ CGPA
Ph. D (course work)	NITK, Surathkal	2019	8.25
M. Tech (Thermal Science)	CET Trivandrum	2016-18	87.9%
B. Tech (Mechanical Engg)	JECC, Cheruthuruthy	2011-15	72.9%
XII	Kerala State Board	2009-11	87.33%
SSLC	Kerala State Board	2009	85%

WORK EXPERIENCE:

Sr. No	Name of the company	Designation	Description	From	To
1	Instrumentation Limited Palakkad, Kerala	Engineering Graduate Apprentice	Design and sizing of control valves, Manufacturing coordination	December 2015	July 2016

ACHIEVEMENTS:

1. Received best paper award in FMFP 2021 and ICMCE 2022 conferences.